ANALYSIS OF MONOTONE AND NON-MONOTONE TRAVELING WAVES IN A SYSTEM FOR SOCIAL OUTBURSTS

Caroline Yang

A dissertation submitted to the faculty at the University of North Carolina at Chapel Hill in partial fulfillment of the requirements for the degree of Doctor of Philosophy in the Department of Mathematics in the College of Arts and Sciences.

Chapel Hill
2018

Approved by:

Nancy Rodríguez

Henri Berestycki

Christopher Jones

Jeremy Marzuola

Katherine Newhall

ABSTRACT

Caroline Yang: Analysis of Monotone and Non-monotone Traveling Waves
in a System for Social Outbursts
(Under the direction of Nancy Rodríguez)

Rioting events in the last several years in the United States, such as the Ferguson riots of 2014 and the Baltimore riots of 2015, captured the attention of the entire nation and have increased scrutiny of racial and social tension. The strength and duration of these riots leads to a question: is there a mathematical model that can reproduce the spread and intensity of rioting behavior observed over time and space in events like these? The goal of this work is to prove the existence and stability of traveling wave solutions to a model for the spread of rioting and social outbursts given by a reaction-diffusion system which captures the relationship between two variables: intensity of rioting behavior and social tension. This model was first introduced by Berestycki, Nadal, and Rodríguez in 2015.

To prove the existence and stability of the traveling wave solutions, we use existence and stability theory for monotone systems. In the case of parameter values that yield a non-monotone system, we establish the stability of traveling wave solutions by proving that the spectrum of the linear operator is not located in the closed, deleted, right half plane. We analyze the spectrum of the linear operator by finding the essential spectrum, placing a bound on the location of the point spectrum, and numerically searching for point spectra within this bounded region using the Evans function.

In addition to proofs for the existence and stability of these traveling wave solutions, we provide a thorough exploration of different parameter regimes for the system, including an analysis of the stability of stationary points for the spatially homogeneous system, numerical approximations of traveling wave solutions and their wave speeds, and an analysis of the asymptotic behavior of traveling wave solutions for particular parameter sets.

To my parents, Raymond and Ann Yang, and to my fiancé, Michael Zimmerman. If I put into words the love and respect I have for you three, it would fill the pages of this manuscript 1000 times over.

ACKNOWLEDGEMENTS

I would first like to thank my advisor, Nancy Rodríguez, for her guidance, insight, patience, and support over the past three years. Her passion for mathematics is clear, and she is an amazing model of work-life balance...I seriously do not know how she does it all. I am very grateful for her taking me on as a student and supporting my work through NSF Award 1516778. This work would not have been possible without her and my other committee members: Henri Berestycki, Chris Jones, Jeremy Marzuola, and Katie Newhall. Thank you all for your encouragement and support and for your enthusiasm for teaching and mathematics.

Thank you also to all the UNC faculty I had as professors; you broadened my horizons, challenged me, and made me think. I would like to also give a special thank you to Laurie Straube, Betty Davidson, and Sara Kross for answering every administrative question I ever had and to Linda Green for mentoring me and for the many interesting conversations we had about teaching.

I would also like to say an enormous thank you to my Durham friends and to all the friends I made at UNC: to Diana Bear for *literally* everything; to Andrew and Marie for their insight, their optimism, and their love; to Perrywinkle and Manuch for their conversations about math, graduate school, and relationships, and for always making me laugh with their hilarious hijinks; to Francesca for being my almost constant companion during our first two years; to Charles for always competing with me and for our mutual venting sessions; to all the other awesome, open, kind, and funny friends I've met here (Marc Besson, Colin Guider, Sam Heroy, Zeliha Kilic, Jacob Perry, Ian Phillip, Andrew Prudhom, Kate Rodrigues, Sean Rogers, Alexis Sparko, and Sterling Swygert), thank you for your friendship over the past five years.

Finally, I would like to thank my parents, Raymond and Ann Yang, and my fiancé, Michael Zimmerman, for giving me more love and support than any one person could hope for in a lifetime. To my parents: thank you for teaching me the importance of education and for listening to me and giving me advice through all the highs and lows of the past 34 years. You still inspire me with your bravery, your kindness, your sense of adventure, and your wisdom. To Michael: life is just better

with you. Period. Thank you for everything you have done to make the past year and a half so memorable and happy, and I am looking forward to many more like it!

TABLE OF CONTENTS

LIST OF FIGURES

LIST OF TABLES

CHAPTER 1

Introduction

In 2005, the deaths of two Paris teenagers sparked weeks of rioting in the Paris suburbs and in various cities throughout the country. The severity and duration of the rioting was such that France eventually declared itself to be in a state of emergency. Although over ten years have passed since these events, social unrest remains an important issue both in France (as evidenced by the recent 2017 riots) as well as the world at large [1, 2, 3, 4, 5, 6].

Prolonged periods of rioting and social unrest are often preceded by an initial triggering event [7, 8, 4, 9]. This is certainly true in the case of the 2005 France riots. Our interest lies in creating a mathematical model that can effectively describe the geographical spread and intensity of rioting behavior as time progresses after this initial triggering event.

A dataset accompanying the 2005 France riots contains the number of instances of rioting behavior (i.e., burning of cars, attacks on police, etc. [10]) in each of the 96 departments in mainland France over a 47-day period following October 27, 2005, the date of the deaths of the two teenagers. Visualization of this data reveals a wavelike, outward, radial spread of rioting behavior originating in Clichy-sous-Bois, the neighborhood of residence for the two boys. This wave moves outward from Paris with the most intense rioting behavior found in departments close to Paris in the days immediately following October 27 and then reaching departments further and further from this epicenter as time passes.

The existence of traveling wave solutions (solutions that travel through space with a constant speed, while maintaining their shape) in numerical simulations has been observed for certain parameter regimes of the model we will present, first proposed by Berestycki, Nadal, and Rodríguez [1]. These solutions show a great deal of qualitative variety in terms of their wave speed and monotonicity. Solutions from certain parameter regimes show good agreement with the spread of rioting behavior observed from the 2005 dataset. Through analysis of these traveling wave solutions, we hope to reach a greater understanding of the model and which parameter regimes produce traveling wave solutions.

The goal of this dissertation is to prove the existence and stability of traveling wave solutions for the system of partial differential equations presented in [1] and described in detail later in this chapter. Existence and stability of traveling waves that is dependent upon certain parameter values can give us insight into what kinds of conditions and interactions give rise to traveling waves of rioting behavior. Since each parameter for our system has a physical representation, we can draw conclusions about what circumstances cause traveling waves of rioting behavior and what circumstances make that behavior more resilient (stable) to the influence of external forces (for example: policing of riots, etc.).

For the remainder of this chapter, we will present the system of partial differential equations that make up the model that is the focus of this dissertation, and we will define the variables and parameters and their physical interpretations. We will briefly describe previous work that has been done in relation to this model. In Chapter 2, we analyze the spatially homogeneous version of our system by finding the parameter regimes that produce multiple steady states and analyzing the stability of those steady states. We present various solutions and results from numerical simulations in Chapter 3 and will point out interesting features of the traveling waves that were observed for different parameter regimes. The stability results of Chapter 2 allow us to utilize some well-established theory to prove the existence of traveling wave solutions for certain parameter values in Chapter 4. Chapter 5 includes calculations for asymptotic decay rates, placing bounds on the traveling wave solutions for specific parameter values. In Chapter 6, we prove the stability of monotone waves and perform a numerical stability analysis for non-monotone waves. We provide a summary and analysis of all results as well as future directions of study in the Discussion and Conclusion.

1.1 An Example: 2005 France Riots

A 2005 French dataset provides the number of "riot-like" events (for example, burning cars, attacks upon police) for a 47-day period after October 27 in each of the country's departments (this dataset is provided by Sebastian Roché, Mirta B. Gordon and Marie-Aude Depuiset). The results of this dataset show a peak of intense rioting behavior that spreads across France. We can see in Figure 1.2 that the rioting behavior reaches its maximum 11 days after October 27 in Department

93 where the neighborhood of the boys, Clichy-sous-Bois, is located. Another example of the rioting data for Department 59 (the northermost department of France) is shown in Figure 1.2. Here we see the qualitative behavior of the graph is very similar to that of Department 93. However, the peak in rioting behavior is reached on the 15th day after October 27, 2005, which implies that it takes some time for this intense rioting behavior to travel across France. The right inset of Figure 1.2 shows the relative distance between Departments 93 and 59 [11].

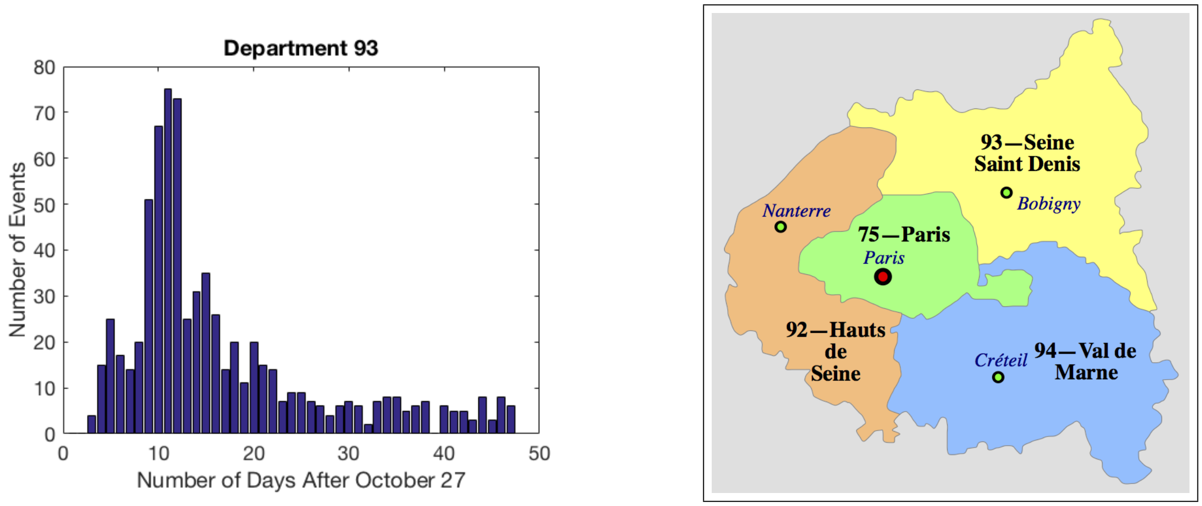

Figure 1.1: Left: the number of riot-like events on each day after October 27, 2005 in Department 93 of France. Right: the location of Department 93 in relation to Paris [11].

From the dataset, we observe this peak of high activity traveling across France, and this behavior is reminiscent of a traveling wave, which we will discuss later in this chapter. This type of spread is also visible in other rioting events [3, 12]. A couple of the key questions surrounding this wave would be what is the speed at which it travels and what is its peak intensity after a certain amount of time has passed or after it has traveled a certain distance? In order to answer these questions, we examine the model presented in the next section. The characteristics of this dataset, and the spread of other riots motivates us to study traveling wave solutions for systems modeling the spread of riots.

1.2 Model

We describe the following system of partial differential equations proposed in [1], which has successfully reproduced the various qualitative characteristics of different rioting patterns described

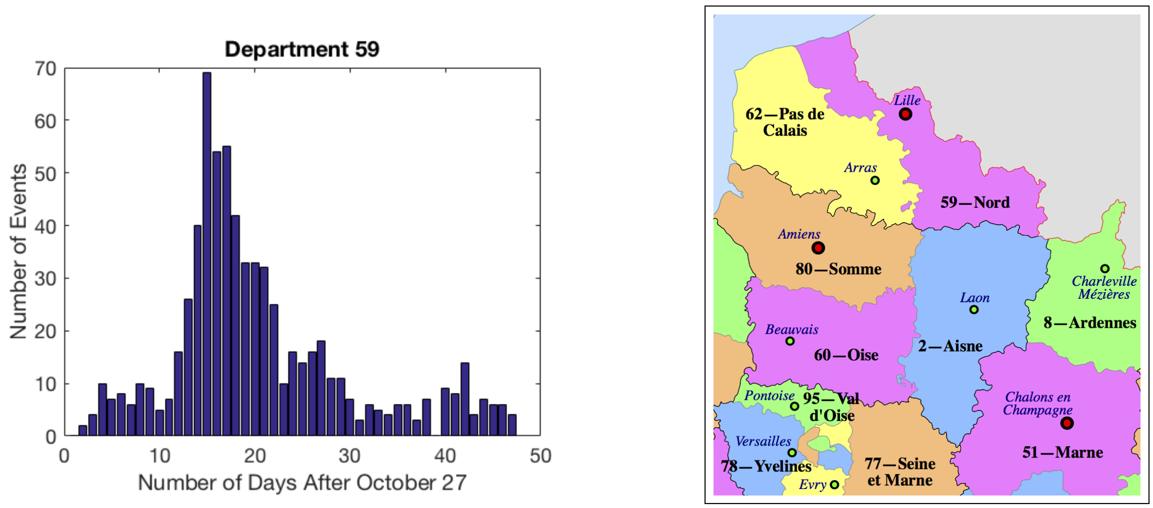

Figure 1.2: Left: the number of riot-like events on each day after October 27, 2005 in Department 59 of France. Right: the location of Department 59 in the northernmost part of France [11]. Department 93 may be seen in the bottom left corner of the map in the small group of four unlabeled departments that make up the right inset of Figure 1.1.

previously and seen in real life events:

$$\begin{cases} u_t = d_1 u_{xx} + r(v)G(u) - u, \quad x \in \mathbb{R},\ t > 0 \\ v_t = d_2 v_{xx} - h(u)v + 1. \end{cases} \tag{1.1}$$

In this model, $u(x,t)$ represents the level of rioting behavior and $v(x,t)$ represents the social tension of a given system at a time t and location x. Social tension is an intangible quantity that can be described as dissatisfaction or anger felt by members of a community due to social injustice, racial discrimination, or financial inequality, etc. It is assumed that the level of rioting behavior and social tension is fundamentally linked. The role of functions $G(u) = \Gamma u(1-u)$, $r(v) = \frac{1}{1+e^{-\beta(v-\alpha)}}$, and $h(u) = \frac{1}{(1+u)^p}$ is to describe the rise and fall of these two quantities in relation to each other. Additionally we assume that rioting behavior decreases proportionally to itself (hence the sink term of u) and that social tension has a base level normalized to one (given by the source term). The parameters $\Gamma, \beta, \alpha > 0$ and $p \in \mathbb{R}$ each have varying affects on the solutions of the system, and they have physical interpretations in terms of rioting intensity and social tension. These will be described shortly, but for a specific definition of these quantities, see [1].

The function $G(u) = \Gamma u(1-u)$ represents the self-reinforcement of rioting behavior once rioting has commenced. This particular instance of a KPP-type term with a carrying capacity for $G(u)$

models the fact that rioting behavior may not grow without bound. There are a finite number of people that can be involved in a riot and a finite number of targets for vandalism, theft, etc. In $G(u)$, Γ is a scaling parameter which controls the rate at which the self-reinforcement increases rioting behavior.

The model assumes that this self-reinforcement only occurs when the social tension of a system is sufficiently high. For example, if a social outburst occurred in a community where the inhabitants were generally satisfied with their daily lives, we would not expect rioting behavior to persist or grow. The sigmoid function $r(v) = \frac{1}{1+e^{-\beta(v-\alpha)}}$ characterizes the transition from a system without self-reinforcement to a system with self-reinforcement. The parameter α indicates the critical level of social tension above which self-reinforcement comes into play. The speed of the transition is determined by β. For $\beta \to \infty$, the sigmoid function approaches a step function with an instantaneous transition between these two states.

We assume social tension will decrease at a rate proportional to itself in a manner influenced by the level of rioting behavior. The function $h(u) = \frac{1}{(1+u)^p}$ models this relationship. The parameter p determines how the level of rioting behavior decreases social tension. For $p > 0$, social tension will decrease more slowly for large values of u, meaning that rioting behavior can be seen to enhance social tension. For $p = 0$, social tension is independent of u. This could model a situation in which rioting behavior is caused by an issue that is not the main cause of social tension within a community. This case also reduces the model to a Fisher-KPP type equation [13]. For $p < 0$, social tension decreases more quickly for large values of u, meaning the rioting behavior provides a release of the built-up social tension and is therefore tension-inhibiting.

For simplicity, the remainder of this document will use the functions $f(u, v) := r(v)G(u) - u$ and $g(u, v) := -h(u)v + 1$ to represent the source and sink terms of the model:

$$\begin{aligned} u_t &= d_1 u_{xx} + f(u, v), \quad \text{for } x \in \mathbb{R},\ t > 0 \\ v_t &= d_2 v_{xx} + g(u, v). \end{aligned} \tag{1.2}$$

1.3 Previous Work

As was mentioned, the model described above was originally proposed in [1]. This paper thoroughly discusses the $p > 0$ case, in which rioting behavior is modeled as a social tension enhancer.

The paper also presents several key results based on varying the value of the parameter α, the level of critical social tension. It describes how altering the value of α can change the system from being bistable to monostable. Using theory from [14], the paper also presents a theorem for the existence of traveling wave solutions based on the value of α. This contrasts with our work, in which we take α constant and look at how the remaining parameters, Γ, β, and p, affect the system and resulting traveling waves.

In 2018, Berestycki, Rossi, and Rodríguez studied the single-site system with a time-periodic source term and demonstrated convergence to positive periodic solutions, or excited cycles, for both $p > 0$ and $p < 0$ [15]. Also in 2018, an epidemiological approach was taken to modeling the spread of riots by using a Susceptible-Infected-Recovered (SIR) type model with a discrete spacial structure. This model was fit to the 2005 France riots dataset and showed excellent agreement for a susceptible population that was based on the proportion of poorly-educated, young males for a given population [10]. The analysis of traveling waves has been applied to other types of social outburst as well such as rioting and censorship and criminal activity [16, 17].

As mentioned in the previous section, for $p = 0$, social tension, $v(x,t)$, is independent of rioting behavior $u(x,t)$. We see that all steady states of the system have $v = 1$, and the equation for u reduces to a Fisher-KPP type equation [13, 18] with

$$u_t = d_1 u_{xx} + \tilde{f}(u),$$

where $\tilde{f}(u) = r(1)G(u) - u$. we see that (1) reduces to a Fisher-KPP type system. Extensive work has been done to show the existence and stability of traveling wave solutions for equations of this type, particularly to prove the existence of traveling waves for certain wave speeds [13, 18, 19, 20, 21, 22, 23, 24, 25, 26, 27].

1.4 Traveling Waves

Traveling waves are solutions that move with a constant speed while maintaining their shape. Therefore, we introduce the moving coordinate system: $z = x - ct$. Traveling wave solutions, $\hat{u}(z)$

and $\hat{v}(z)$, of (1.2) satisfy the following system:

$$\begin{cases} d_1\hat{u}''(z) + c\hat{u}'(z) + f(\hat{u}, \hat{v}) = 0, \\ d_2\hat{v}''(z) + c\hat{v}'(z) + g(\hat{u}, \hat{v}) = 0, \\ \hat{u}(+\infty) = 0,\ \hat{v}(+\infty) = 1,\ \hat{u}(-\infty) = u^*,\ \hat{v}(-\infty) = v^*, \end{cases} \tag{1.3}$$

where $(0, 1)$ represents the trivial stationary point of (1.2) and (u^*, v^*) represents a non-trivial stationary point.

As we will see in Chapter 3, we do find traveling wave solutions from the numerical approximations of solutions to system (1.2) for a large variety of parameter sets. These numerical observations motivate us to establish the existence and stability of traveling wave solutions to our system (1.2). We will also use numerical approximations of the wave speed to reach the conclusion that the wave speed does not vary with parameters p and β, and does have a dependence on the initial conditions for the system of partial differential equations for certain parameter regimes.

CHAPTER 2

Analysis of the Spatially Homogeneous System

We begin by analyzing the stability of the stationary points of the spatially homogeneous system, given by:

$$\begin{cases} u_t = \dfrac{\Gamma u(1-u)}{1+e^{-\beta(v-\alpha)}} - u, \\[2ex] v_t = \dfrac{-v}{(1+u)^p} + 1. \end{cases} \tag{2.1}$$

There are two u-nullclines, $u = 0$ and $v = -\frac{1}{\beta}\log[\Gamma(1-u)-1]+\alpha$, and one v-nullcline, $v = (1+u)^p$. For examples, see Figures 2.2, 2.3, and 2.8.

System (2.1) has a trivial steady state $(u, v) = (0, 1)$, which exists for all parameter regimes. The presence and number of non-trivial steady states $(u, v) = (u^*, v^*)$ varies depending on the parameter values. The non-trivial values u^* and v^* must satisfy the equations:

$$0 = \frac{\Gamma(1-u^*)}{1+e^{-\beta(v^*-\alpha)}} - 1 \quad \text{and} \quad 0 = -\frac{v^*}{(1+u^*)^p} + 1.$$

This steady state is numerically approximated by rootfinding methods except for when $p = 0$, in which case the equations can be solved analytically.

The linearization of (2.1) about the steady states is given by $U' = AU$:

$$\begin{bmatrix} u \\ v \end{bmatrix}' = \begin{bmatrix} f_u(u,v) & f_v(u,v) \\ g_u(u,v) & g_v(u,v) \end{bmatrix} \begin{bmatrix} u \\ v \end{bmatrix},$$

where $U = [u \;\; v]^T$ and A is the 2×2 matrix in the equation above. The matrix A is evaluated separately at the respective steady states to yield linearizations about each state. The eigenvalues, λ, of A are given by:

$$\lambda_{1,2} = \frac{f_u(u,v) + g_v(u,v) \pm \sqrt{[f_u(u,v)+g_v(u,v)]^2 - 4[f_u(u,v)g_v(u,v) - f_v(u,v)g_u(u,v)]}}{2}, \tag{2.2}$$

where the partial derivatives f_u, f_v, g_u, and g_v are given by:

$$\begin{aligned} f_u(u,v) &= \frac{\Gamma(1-2u)}{1+e^{-\beta(v-\alpha)}} - 1, \quad & f_v(u,v) &= \frac{\beta\Gamma e^{-\beta(v-\alpha)} u(1-u)}{(1+e^{-\beta(v-\alpha)})^2}, \\ g_u(u,v) &= \frac{pv}{(1+u)^{p+1}}, & g_v(u,v) &= -\frac{1}{(1+u)^p}. \end{aligned} \tag{2.3}$$

and are evaluated at the one of the steady states $(0,1)$ or (u^*,v^*). We will use this to discuss the stability of each of the steady states.

The existence of one or more non-trivial steady states (u^*,v^*) results from the intersection of the nullclines $v = -\frac{1}{\beta}\log[\Gamma(1-u)-1]+\alpha$ and $v=(1+u)^p$ and depends on the value of p, so the following cases will be discussed: $p=0$, $p<0$, and $p>0$. To simplify this analysis we fix $\alpha = 1$, which is a reasonable choice given that all the different types of traveling wave solutions (monotone, non-monotone, and oscillatory) are observed with this value.

2.1 Phase Plane Analysis: $p = 0$ Case

2.1.1 Trivial Steady State: $(0,1)$

The trivial steady state of $(u,v) = (0,1)$ exists for all parameter values, so any results regarding this steady state will hold for other values of p. Evaluating (2.3), we see that $f_v(0,1) = 0$ and as a result, (2.2) simplifies to the following:

$$\lambda_{1,2} = \frac{f_u(0,1) + g_v(0,1) \pm \sqrt{[f_u(0,1)+g_v(0,1)]^2 - 4f_u(0,1)g_v(0,1)}}{2}.$$

Since we fix $\alpha = 1$, $f_u(0,1) = \frac{\Gamma}{2} - 1$, and the classification of the steady state $(0,1)$ depends on the value of Γ:

Case 1: For $\Gamma > 2$, $f_u(0,1)g_v(0,1) < 0$, so $\lambda_1 > 0$ and $\lambda_2 < 0$, indicating that $(0,1)$ is a **saddle point**.

Case 2: For $1 < \Gamma < 2$, $f_u(0,1)g_v(0,1) > 0$, and $[f_u(0,1)+g_v(0,1)]^2 - 4f_u(0,1)g_v(0,1) > 0$, so $\lambda_1 < 0$ and $\lambda_2 < 0$, indicating that $(0,1)$ is a **stable node**.

Case 3: For $\Gamma = 2$, we have a borderline case in which $\lambda_1 = 0$ and $\lambda_2 < 0$, yielding a **line of non-isolated fixed points**, so we cannot make any definitive statements about the classification of the steady state $(0,1)$ for the nonlinear ODE. However, we can see from the phase diagram in Figure 2.1 that this point behaves as an **unstable fixed point**. **Note:** we are only interested in this case for values of $p > 0$ because for $p \leq 0$, Γ must be greater than 2 in order for the system to have two or more steady states. We do not expect to see a traveling front solution for system (1.2) unless the spatially homogeneous system has at least two steady states.

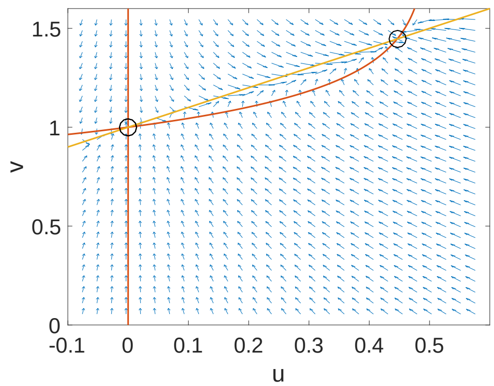

Figure 2.1: Phase planes for the spatially homogeneous system with two steady states indicated by circular markers. This is an example of the borderline case for the trivial steady state. Parameter values are $p = 1$, $\alpha = 1$, $\Gamma = 2$, and $\beta = 5$.

2.1.2 Non-trivial Steady State: (u^*, v^*)

When $p = 0$, the nullcline $v = (1 + u)^p$ becomes a constant function, $v = 1$, and since the logarithmic nullcline mentioned previously is monotone increasing, there is only the possibility of one intersection (u^*, v^*). To ensure this intersection exists, we require $-\frac{1}{\beta}\log[\Gamma - 1] + \alpha < 1$. As $\alpha = 1$ is fixed, this simplifies to $\Gamma > 2$. We are able to solve for this intersection analytically, and it occurs at $(u^*, v^*) = (1 - \frac{1}{\Gamma}(1 + e^{-\beta(1-\alpha)}), 1)$. For $\alpha = 1$, this becomes $(u^*, v^*) = (1 - \frac{2}{\Gamma}, 1)$. For this intersection, the eigenvalues given by (2.2) can be explicitly calculated, and we have the following results:

Case 1: For $p = 0$, $\alpha = 1$, $\Gamma > 2$, $\Gamma \neq 4$, the eigenvalues $\lambda_1, \lambda_2 < 0$, so the non-trivial steady state at $(u^*, v^*) = (1 - \frac{2}{\Gamma}, 1)$ is a **stable node**.

Case 2: For $p = 0$, $\alpha = 1$, $\Gamma = 4$, we have a borderline case in which $\lambda_1 = \lambda_2$ with $\lambda_1, \lambda_2 < 0$, and the non-trivial steady state is a **degenerate stable node**. We are are unable to make any definitive statements about classification of the non-trivial steady state for the nonlinear

ODE; however we can say that the point is **stable**. From the phase plane diagram shown in Figure 2.2, we see that numerically, the steady state appears to behave as a stable node. A second order approximation of the nonlinear system would be necessary to make any concrete statements about the classification of this steady state beyond its stability.

An example of the phase planes for each of these cases is shown in Figure 2.2.

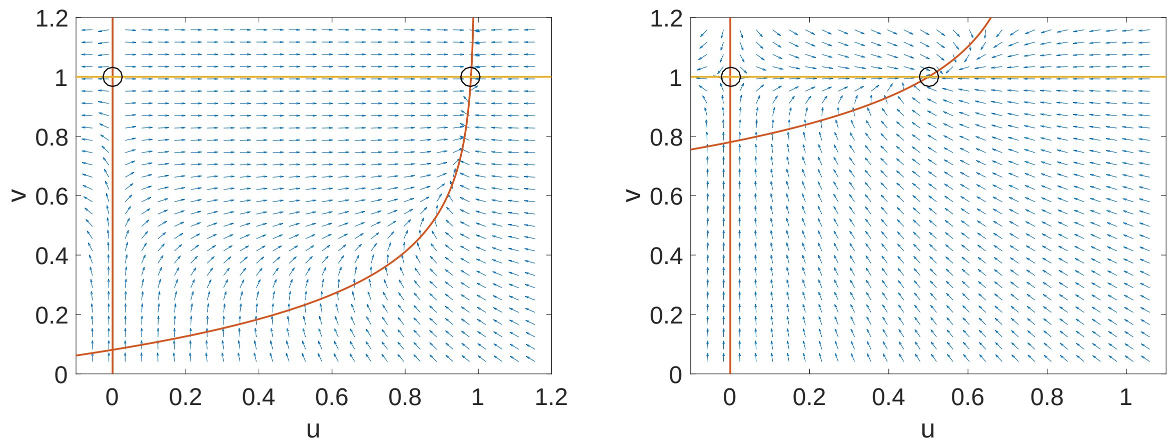

(a) Stable node: $\Gamma = 100$, $\beta = 5$, $\alpha = 1$

(b) Borderline case: $\Gamma = 4$, $\beta = 5$, $\alpha = 1$

Figure 2.2: Phase planes for the spatially homogeneous system with $p = 0$ and two steady states indicated by circular markers.

A summary of the results presented for the phase plane analysis for $p = 0$ is provided in Table 2.1.

$\Gamma > 2$, $\Gamma \neq 4$	There are **two** steady states: $(0, 1)$ is a **saddle point** with eigenvalues $\lambda_1 > 0$, $\lambda_2 < 0$, and $(1 - \frac{2}{\Gamma}, 1)$ is a **stable node** with $\lambda_1, \lambda_2 < 0$ and distinct.
$\Gamma = 4$	There are **two** steady states: $(0, 1)$ is a **saddle point** with eigenvalues $\lambda_1 > 0$, $\lambda_2 < 0$, and $(1 - \frac{2}{\Gamma}, 1)$ is a **stable fixed point** with $\lambda_1, \lambda_2 < 0$ and $\lambda_1 = \lambda_2$.

Table 2.1: Classification and stability of steady states of the spatially homogeneous system for $p = 0$ and $\alpha = 1$.

2.2 Phase Plane Analysis: $p < 0$ Case

As mentioned previously, the results for the classification of the trivial steady state described in Section 2.1.1 still hold for $p < 0$. Focusing our attention on the non-trivial steady state, we note that for $p < 0$ the nullcline $v = (1 + u)^p$ is monotonically decreasing for $u, v > 0$, and

$v = -\frac{1}{\beta}\log[\Gamma(1-u)-1]+\alpha$ is monotonically increasing, so again there is only one possible non-trivial intersection. The requirement mentioned for the case $p = 0$, $\Gamma > 2$, again ensures the existence of this second steady state.

For steady state $(u, v) = (u^*, v^*)$, the partial derivatives of f and g given by (2.3) have the following sign designations:

$$f_u(u^*, v^*) < 0, \quad f_v(u^*, v^*) > 0, \quad g_u(u^*, v^*) < 0, \quad g_v(u^*, v^*) < 0.$$

We see that $f_u(u^*, v^*)g_v(u^*, v^*) - f_v(u^*, v^*)g_u(u^*, v^*) > 0$. Let us denote the discriminant of (2.2) as $\Delta(u^*, v^*) = [f_u(u^*, v^*)+g_v(u^*, v^*)]^2 - 4[f_u(u^*, v^*)g_v(u^*, v^*) - f_v(u^*, v^*)g_u(u^*, v^*)]$. The classification of steady state (u^*, v^*) is dependent on the value of $\Delta(u^*, v^*)$, and we have the results outlined below for $p < 0$ and $\alpha = 1$.

Case 1: For $\Delta(u^*, v^*) > 0$, $\lambda_1 < 0$ and $\lambda_2 < 0$, indicating that (u^*, v^*) is a **stable node**.

Case 2: For $\Delta(u^*, v^*) < 0$, λ_1 and λ_2 have nonzero imaginary components, and $\mathrm{Re}(\lambda_1), \mathrm{Re}(\lambda_2) < 0$, indicating that (u^*, v^*) is a **stable spiral**.

Case 3: For $\Delta(u^*, v^*) = 0$, we have a borderline case in which $\lambda_1 = \lambda_2$ with $\lambda_1, \lambda_2 < 0$, so the nontrivial steady state is a **degenerate stable node**. Again, we cannot make any conclusions about the type of the steady state (u^*, v^*) for the nonlinear system, but we can say that it is **stable**.

Examples of the phase planes for the first two cases are shown in Figure 2.3. A summary of the cases presented for the phase plane analysis for $p < 0$ is provided in Table 2.2.

$\Gamma > 2$, $\Delta(u^*, v^*) > 0$	There are **two** steady states: $(0, 1)$ is a **saddle point** with eigenvalues $\lambda_1 > 0$, $\lambda_2 < 0$, and (u^*, v^*) is a **stable node** with $\lambda_1, \lambda_2 < 0$ and distinct.
$\Gamma > 2$, $\Delta(u^*, v^*) < 0$	There are **two** steady states: $(0, 1)$ is a **saddle point** with eigenvalues $\lambda_1 > 0$, $\lambda_2 < 0$, and (u^*, v^*) is a **stable spiral** with $\mathrm{Re}(\lambda_1), \mathrm{Re}(\lambda_2) < 0$.
$\Gamma > 2$, $\Delta(u^*, v^*) = 0$	There are **two** steady states: $(0, 1)$ is a **saddle point** with eigenvalues $\lambda_1 > 0$, $\lambda_2 < 0$, and (u^*, v^*) is a **stable fixed point** with $\lambda_1, \lambda_2 < 0$ and $\lambda_1 = \lambda_2$.

Table 2.2: Classification and stability of steady states of the spatially homogeneous system for $p < 0$ and $\alpha = 1$, where $\Delta(u^*, v^*) = [f_u(u^*, v^*)+g_v(u^*, v^*)]^2 - 4[f_u(u^*, v^*)g_v(u^*, v^*) - f_v(u^*, v^*)g_u(u^*, v^*)]$.

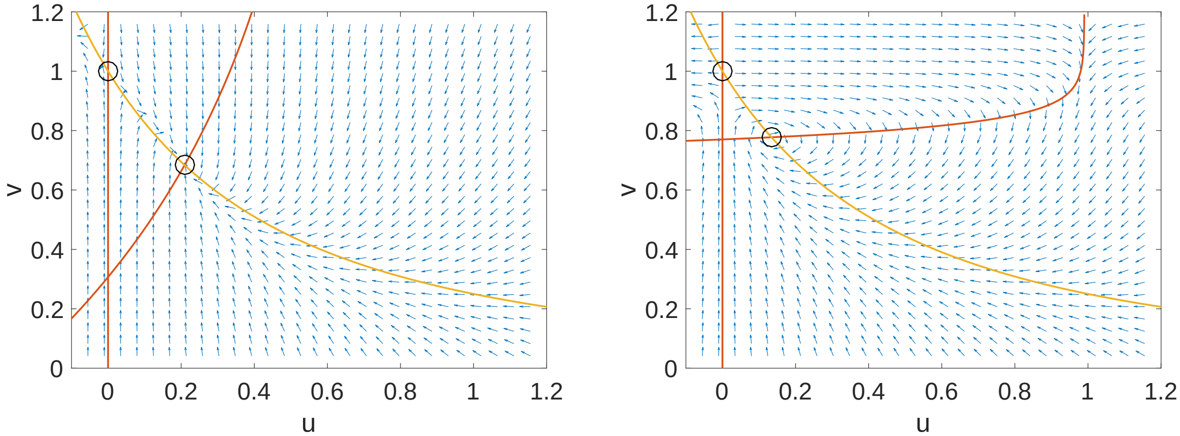

(a) Stable node: $\Gamma = 3$, $\beta = 1$, $\alpha = 1$, $p = -2$ (b) Stable spiral: $\Gamma = 100$, $\beta = 20$, $\alpha = 1$, $p = -2$

Figure 2.3: Two cases for the phase planes of the spatially homogeneous system for $p < 0$. Steady states are indicated by circular markers.

We are interested in knowing which parameter regimes yield a stable node versus a stable spiral in order to be able to distinguish when we are dealing with cases one and two mentioned above. By using a very small negative p value ($\alpha = 1$ still fixed), we see that in Γ, β-space, a region around the value $\Gamma = 4$ appears in which the steady state (u^*, v^*) is a stable spiral. Outside of this region, the non-trivial steady state is instead a stable node. An example of these two regions in Γ, β parameter space are shown in Figure 2.4.

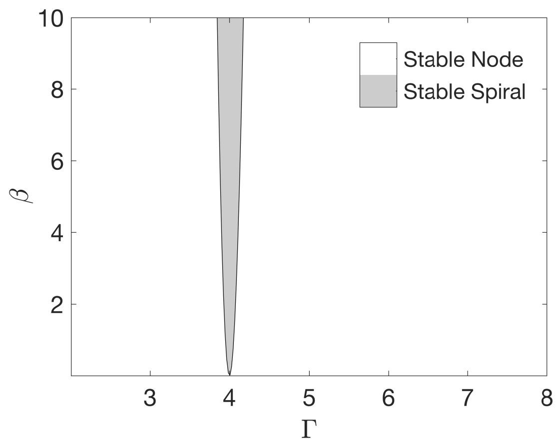

Figure 2.4: Separation of Γ, β-space for $p = -0.001$ and $\alpha = 1$ for the spatially homogeneous system. The different regions indicate different classifications of the non-trivial steady state (u^*, v^*) as either a stable spiral or a stable node.

As p decreases, the area of the stable spiral region expands, followed by the appearance of a tongue in the stable node region as shown in Figure 2.5. This tongue continues to increase in size, but we never see the disappearance of the stable spiral region. For p large and negative, steady state $(u^*, v^*) = (\varepsilon, v^*)$ or $(u^*, v^*) = (u^*, \varepsilon)$ for some $\varepsilon > 0$ and $\varepsilon << 1$. Upon analysis of (2.2), we see that there exists Γ and β sufficiently large to result in $\Delta(u^*, v^*) < 0$, and the stable spiral region never completely disappears.

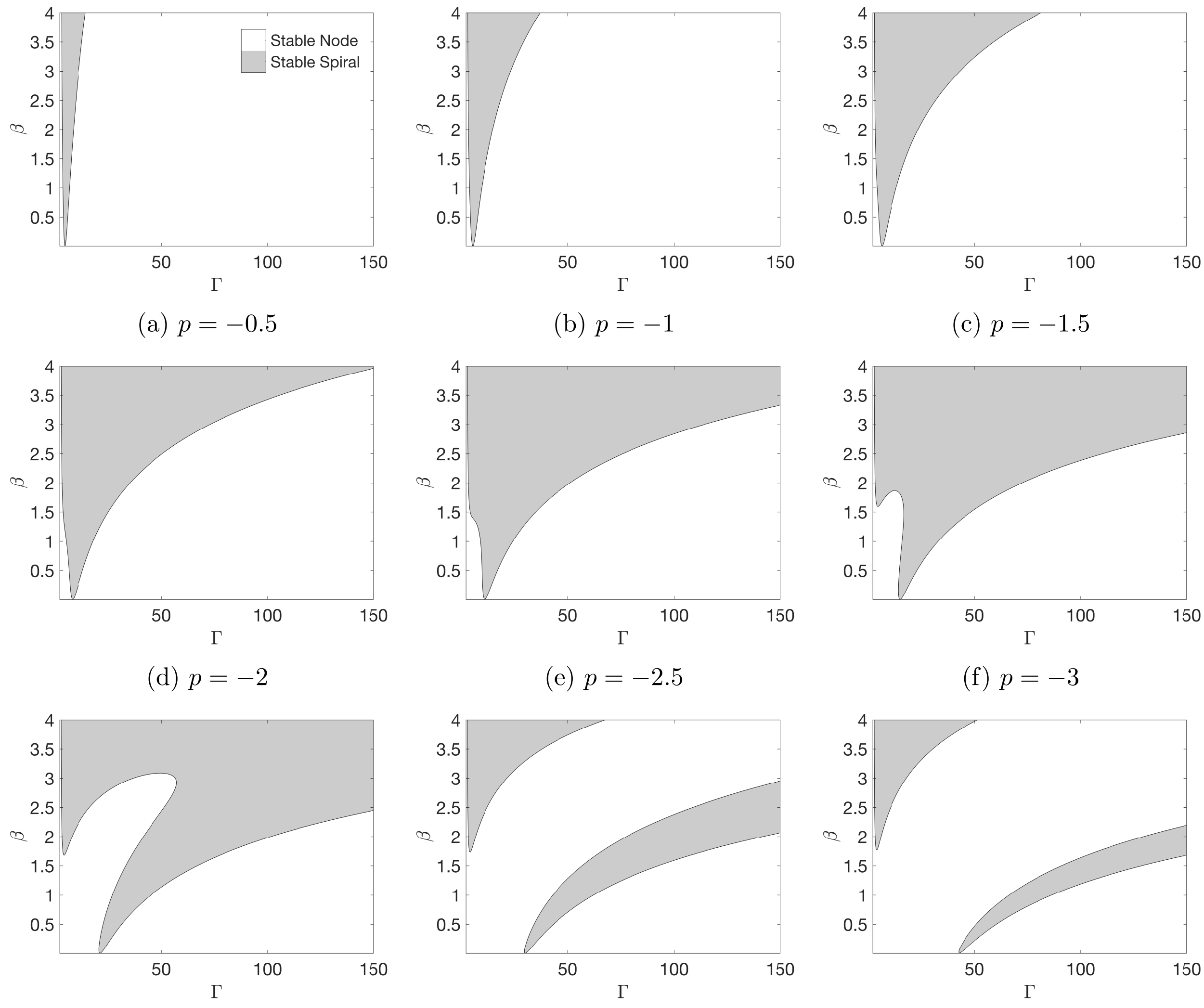

(a) $p = -0.5$ (b) $p = -1$ (c) $p = -1.5$

(d) $p = -2$ (e) $p = -2.5$ (f) $p = -3$

(g) $p = -3.5$ (h) $p = -4$ (i) $p = -4.5$

Figure 2.5: Classification of steady state (u^*, v^*) for increasingly negative values of p in Γ, β-space with $\alpha = 1$. The gray area indicates the values of Γ and β which yield a stable spiral at (u^*, v^*), while the white area indicates values yielding a stable node.

For the non-trivial steady state in the case of $p < 0$, we also wish to know if the non-trivial steady state is globally stable. To this end, we prove the following theorem.

Theorem 2.2.1. *For system 2.1 with $p < 0$, the steady state (u^*, v^*) is globally stable in the open first quadrant.*

Proof. The system given by 2.1, $\dot{\mathbf{u}} = \mathbf{f}(\mathbf{u})$ is a continuously differentiable vector field defined over the simply-connected region $u, v > 0$. We choose $H(u, v) = 1/uv$. Then

$$\begin{aligned}
\nabla \cdot (H\dot{\mathbf{u}}) &= \frac{\partial}{\partial u}(H\dot{u}) + \frac{\partial}{\partial v}(H\dot{v}) \\
&= \frac{\partial}{\partial u}\left(\frac{\Gamma(1-u)}{v(1+e^{-\beta(v-\alpha)})} - \frac{1}{v}\right) + \frac{\partial}{\partial v}\left(-\frac{1}{u(1+u)^p} + \frac{1}{uv}\right) \\
&= -\frac{\Gamma}{v(1+e^{-\beta(v-\alpha)})} - \frac{1}{uv^2} \\
&< 0.
\end{aligned}$$

By Dulac's Criterion, since $\nabla \cdot (H\dot{\mathbf{u}}) < 0$ for $u, v > 0$, there are no closed orbits lying in this region, indicating that (u^*, v^*) is globally stable with respect to system (2.1). □

2.3 Phase Plane Analysis: $p > 0$ Case

For $p > 0$, we again begin with an analysis of the non-trivial steady state. The results presented in Section 2.1.1 concerning the trivial steady state still hold for $p > 0$. With a positive p-value, the nullcline $v = (1 + u)^p$ becomes monotone increasing, which means that multiple non-trivial steady states are possible. We again fix $\alpha = 1$ and use a combination of analysis and the continuation software AUTO [28] to find regions within Γ, β-space in which there exist different numbers of non-trivial steady states (for examples of AUTO codes, see Appendix A.1).

Remark 2.3.1. *Since u and v are considered physical quantities that must by nonnegative, we are only interested in non-trivial steady states (u^*, v^*) with $u^*, v^* > 0$.*

Using AUTO, we find there exists a pair of curves $\Gamma_1(\beta)$ and $\Gamma_2(\beta)$ (for $p > 1$), which split the parameter space into regions with differing numbers of non-trivial steady states. We define $\beta_1 = \Gamma_1^{-1}(2)$ and $\beta_2 = \Gamma_2^{-1}(2)$ and have the following cases for $p > 0$ and $\alpha = 1$:

Case 1: There exists only **one** steady state at the trivial location of $(0, 1)$ if

(a) $1 < \Gamma < \Gamma_1(\beta)$ and $\beta > \beta_1$.

(b) $\Gamma \leq 2$ for $\beta \leq \beta_1$.

Case 2: There exist **two** steady states, the trivial location $(0, 1)$ and a non-trivial location (u^*, v^*), if

(a) $\Gamma = \Gamma_1(\beta)$ or $\Gamma = 2$ and $\beta > \beta_1$.

(b) $\Gamma > 2$ for $p \leq 3$.

(c) $\Gamma > \Gamma_2(\beta)$ for $\beta_1 < \beta < \beta_2$ and $p > 3$.

(d) $\Gamma > 2$ and $\Gamma > \Gamma_2(\beta)$ or $\Gamma \leq \Gamma_1(\beta)$ for $\beta < \beta_1$ and $p > 3$.

Case 3: There exist **three** steady states, one trivial and two non-trivial, if

(a) $\Gamma_1(\beta) < \Gamma < 2$ for $\beta > \beta_1$

(b) $\Gamma = 2$ for $\beta_1 < \beta < \beta_2$ and $p > 3$.

(c) $\Gamma = \Gamma_2(\beta)$ for $\beta < \beta_2$ and $p > 3$.

Case 4: There exist **four** steady states, one trivial and three non-trivial, if

(a) $2 < \Gamma < \Gamma_2(\beta)$ for $\beta_1 < \beta < \beta_2$ and $p > 3$.

(b) $\Gamma_1(\beta) < \Gamma < \Gamma_2(\beta)$ for $\beta < \beta_1$ and $p > 3$.

Figure 2.6 displays these four cases in Γ, β-space for increasing values of positive p. Since the region of the parameter space which allows for four steady states is quite small, Figure 2.7 shows this region in greater detail.

We are able to confirm the existence of the boundary curves in Γ, β-space shown in Figure 2.6 for $p = 1,\ 2,\ 3$, and 4 by using an analytical method, which is discussed in greater detail in Appendix B.1. Using this method and the results from the AUTO runs, we can see that the four steady state region of Γ, β-space does not exist for $p = 3$ and does exist for $p = 4$. Using AUTO, we can find this region for p-values as small as $p = 3.05$. This leads us to conjecture that the four steady state region appears for $p > 3$.

For the non-trivial steady state $(u, v) = (u^*, v^*)$, the partial derivatives of f and g given by (2.3) have the following sign designations for $p > 0$:

$$f_u(u^*, v^*) < 0, \quad f_v(u^*, v^*) > 0, \quad g_u(u^*, v^*) > 0, \quad g_v(u^*, v^*) < 0.$$

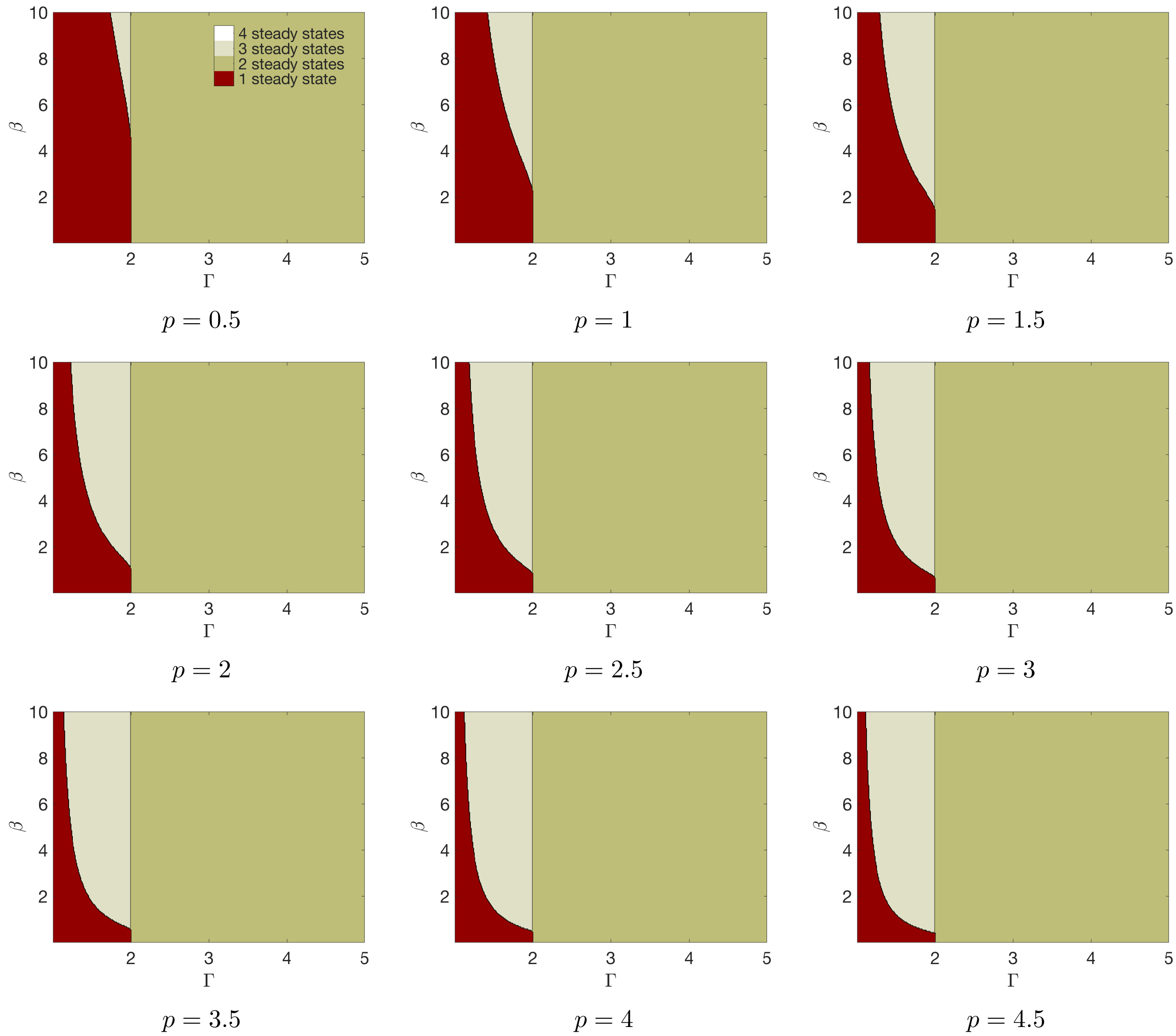

Figure 2.6: The separation of Γ, β-space into regions with different numbers of steady states for $p > 0$ and $\alpha = 1$.

We see that the discriminant of (2.2) $\Delta(u^*, v^*) = [f_u(u^*, v^*) + g_v(u^*, v^*)]^2 - 4[f_u(u^*, v^*)g_v(u^*, v^*) - f_v(u^*, v^*)g_u(u^*, v^*)] > 0$. Therefore the classification of steady state (u^*, v^*) is dependent on the value of $f_u(u^*, v^*)g_v(u^*, v^*) - f_v(u^*, v^*)g_u(u^*, v^*)$, and we have the results outlined below for $p > 0$ and $\alpha = 1$.

Case 1: If $f_u(u^*, v^*)g_v(u^*, v^*) - f_v(u^*, v^*)g_u(u^*, v^*) < 0$, then the eigenvalues given by (2.2) are $\lambda_1 > 0$ and $\lambda_2 < 0$, so (u^*, v^*) is a **saddle point**.

Case 2: If $f_u(u^*, v^*)g_v(u^*, v^*) - f_v(u^*, v^*)g_u(u^*, v^*) > 0$, then $\lambda_1, \lambda_2 < 0$, so (u^*, v^*) is a **stable node**.

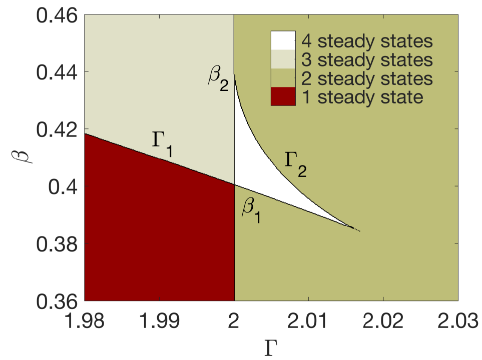

Figure 2.7: The region in Γ, β-space which yields four steady states for $p = 4.5$ and $\alpha = 1$. The curves $\Gamma_1(\beta)$, $\Gamma_2(\beta)$ are labeled as well as their respective intersections with $\Gamma = 2$, β_1 and β_2.

Case 3: If $f_u(u^*, v^*)g_v(u^*, v^*) - f_v(u^*, v^*)g_u(u^*, v^*) = 0$, then we have a borderline case in which $\lambda_1 < 0$ and $\lambda_2 = 0$, so the steady state is part of a **line of isolated fixed points** for the linearized system, and we cannot determine the classification of the steady state for the nonlinear ODE.

Applying these classifications to our four cases for steady states, we have the following designations.

Case 1: If the system has **one** steady state, it is located at $(0, 1)$ and is a **saddle point**.

Case 2: If the system has **two** steady states, $(0, 1)$ may be a **saddle point**, a **stable node**, or may be a **borderline case**. The non-trivial steady state (u^*, v^*) is a **stable node** or a **borderline case** as well.

Case 3: If the system has **three** steady states, $(0, 1)$ is a **stable node**, (u_1^*, v_1^*) is a **saddle point**, and (u_2^*, v_2^*) is a **stable node** with $u_1^* < u_2^*$.

Case 4: If the system has **four** steady states, $(0, 1)$ is a **saddle point**, (u_1^*, v_1^*) is a **stable node**, (u_2^*, v_2^*) is a **saddle point**, and (u_3^*, v_3^*) is a **stable node** with $u_1^* < u_2^* < u_3^*$.

Figure 2.8 shows the phase plane for an instance of each of these cases, excluding the single steady state case as this does not produce traveling fronts for our original system.

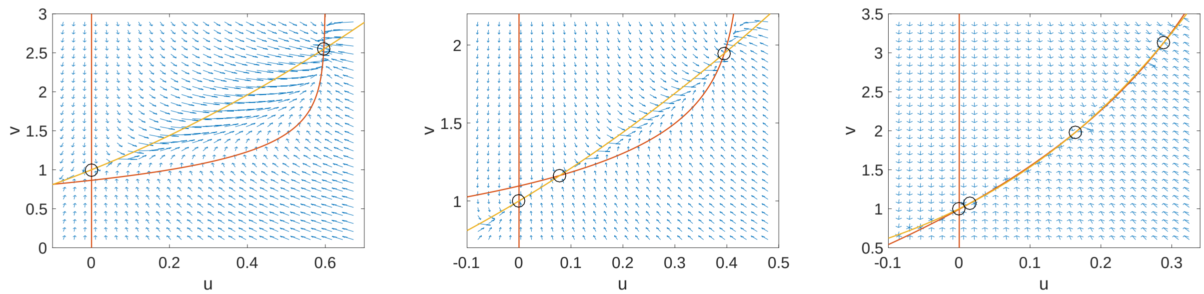

(a) $\Gamma = 2.5$, $\beta = 3$, $\alpha = 1$, $p = 2$

(b) $\Gamma = 1.75$, $\beta = 3$, $\alpha = 1$, $p = 2$

(c) $\Gamma = 2.0026$, $\beta = 0.4021$, $\alpha = 1$, $p = 4.5$

Figure 2.8: Three cases for the phase planes of the spatially homogeneous system for $p > 0$. Steady states are indicated by circular markers.

A summary of the pertinent results for $p > 0$ is provided in Table 2.3. The table omits borderline cases for simplicity of classification and the one steady state case, which will not result in traveling fronts for the system of partial differential equations.

$\Gamma > 2, p \leq 3$ OR $\Gamma > 2$, $p > 3$, $\beta < \Gamma_1^{-1}(\Gamma)$, or $\beta > \Gamma_2^{-1}(\Gamma)$	There are **two** steady states: $(0,1)$ is a **saddle point** with eigenvalues $\lambda_1 > 0$, $\lambda_2 < 0$, and (u^*, v^*) is a **stable node** with $\lambda_1, \lambda_2 < 0$ and distinct.
$\Gamma_1(\beta) < \Gamma < 2$	There are **three** steady states: $(0,1)$ is a **stable node** with eigenvalues $\lambda_1, \lambda_2 < 0$ and distinct; (u_1^*, v_1^*) is a **saddle point** with $\lambda_1 > 0$ and $\lambda_2 < 0$; (u_2^*, v_2^*) is a **stable node** with $\lambda_1, \lambda_2 < 0$ and distinct. For the non-trivial steady states, we have $u_1^* < u_2^*$.
$\Gamma > 2$, $p > 3$, and $\Gamma_1^{-1}(\Gamma) < \beta < \Gamma_2^{-1}(\Gamma)$	There are **four** steady states: $(0,1)$ is a **saddle point** with eigenvalues $\lambda_1 > 0$, $\lambda_2 < 0$; (u_1^*, v_1^*) is a **stable node** with $\lambda_1, \lambda_2 < 0$ and distinct; (u_2^*, v_2^*) is a **saddle point** with $\lambda_1 > 0$ and $\lambda_2 < 0$; (u_3^*, v_3^*) is a **stable node** with $\lambda_1, \lambda_2 < 0$ and distinct. For the non-trivial steady states, we have $u_1^* < u_2^* < u_3^*$.

Table 2.3: Classification and stability of steady states of the spatially homogeneous system for $p > 0$ and $\alpha = 1$.

CHAPTER 3

Numerical Approximations of Traveling Wave Solutions

We wish to understand the effect that the parameters Γ, β, α, and p have on the characteristics of the traveling wave solutions. As discussed at the end of Chapter 1, we also have good reason to expect to see traveling wave solutions from the numerical approximations of our system. Numerical experiments support this theory, yielding traveling wave solutions, $\hat{u}(z)$ and $\hat{v}(z)$, with different behaviors resulting from different parameter sets. The different types of traveling waves we observed and their unique characteristics will be described in this chapter.

3.1 Numerical Approximation Methods

The traveling wave profiles we present in this chapter are approximated and verified through two separate methods. In the first method, we use a first order upwind scheme to approximate the time derivative and a second order central difference to approximate the second derivative with respect to x in (1.2). We solve this discretized system over a finite domain with zero Neumann boundary conditions and various initial conditions. So, for the following problem:

$$\begin{cases} u_t = d_1 u_{xx} + f(u,v), \\ v_t = d_2 v_{xx} + g(u,v), \\ \frac{\partial u}{\partial x}(0,t) = 0, \quad \frac{\partial v}{\partial x}(0,t) = 0, \\ \frac{\partial u}{\partial x}(L,t) = 0, \quad \frac{\partial v}{\partial x}(L,t) = 0, \end{cases}$$

we use the discretized scheme:

$$\mathbf{u}^{k+1} = \frac{d_1 \Delta t}{(\Delta x)^2} A\mathbf{u}^k + \Delta t f(\mathbf{u},\mathbf{v}),$$
$$\mathbf{v}^{k+1} = \frac{d_2 \Delta t}{(\Delta x)^2} B\mathbf{v}^k + \Delta t g(\mathbf{u},\mathbf{v}),$$

where k represents the number of time steps, Δt represents the size of each time step, Δx represents the size of each discretized element of space, $\mathbf{u}^k$ and $\mathbf{v}^k$ represent a vectors of u and v defined at each discretized point of space at time step k,

$$A = \begin{bmatrix} -2+\frac{(\Delta x)^2}{d_1\Delta t} & 2 & 0 & \dots & 0 \\ 1 & -2+\frac{(\Delta x)^2}{d_1\Delta t} & 1 & \dots & 0 \\ & & \ddots & & \\ 0 & \dots & 1 & -2+\frac{(\Delta x)^2}{d_1\Delta t} & 1 \\ 0 & \dots & 0 & 2 & -2+\frac{(\Delta x)^2}{d_1\Delta t} \end{bmatrix},$$

and B is an identical matrix where d_1 is replaced by d_2. For initial conditions, we used a variety of decreasing exponentials for u. For example, we used $u(x,0) = Ce^{-bx}$ with varying values of $C > 0$ and $b > 0$ and also used $u(x,0) = C\delta(x)$ to represent a decreasing exponential with $b \to \infty$. For v, we used a constant function, $v(x,0) = D$, where we require that D is greater than the critical social tension α in order to start the system in an excited (rioting) state.

In the second method, we use a version of the algorithm described in [29] and [30]. We first assume solutions of the form $u(x,t) = \hat{u}(x-ct)$ and $v(x,t) = \hat{v}(x-ct)$, where $z = x - ct$, for (1.2). This results in the system:

$$\begin{cases} d_1\hat{u}''(z) + c\hat{u}'(z) + f(\hat{u},\hat{v}) = 0, \\ d_2\hat{v}''(z) + c\hat{v}'(z) + g(\hat{u},\hat{v}) = 0, \\ \hat{u}(+\infty) = 0,\ \hat{v}(+\infty) = 1,\ \hat{u}(-\infty) = u^*,\ \hat{v}(-\infty) = v^*, \end{cases} \tag{3.1}$$

mentioned at the end of Chapter 1, where $(u,v) = (0,1)$ and $(u,v) = (u^*,v^*)$ are the respective trivial and non-trivial stationary points of the system. We then write (3.1) as a system of first order ODEs:

$$\hat{\mathbf{u}}' = \begin{bmatrix} \hat{u} \\ \hat{v} \\ w \\ y \end{bmatrix}' = \begin{bmatrix} w \\ y \\ -\frac{1}{d_1}(cw + f(\hat{u},\hat{v})) \\ -\frac{1}{d_2}(cy + g(\hat{u},\hat{v})) \end{bmatrix} = \mathbf{f}(\hat{\mathbf{u}}), \tag{3.2}$$

with asymptotic boundary conditions:

$$(\hat{u}, \hat{v}, w, y) \to (0, 1, 0, 0) \quad \text{as} \quad z \to +\infty,$$
$$(\hat{u}, \hat{v}, w, y) \to (u^*, v^*, 0, 0) \quad \text{as} \quad z \to -\infty.$$

For simplicity, we let $\hat{\mathbf{u}} = [\hat{u} \;\; \hat{v} \;\; w \;\; y]^T$, $\hat{\mathbf{u}}_+ = [0 \;\; 1 \;\; 0 \;\; 0]^T$, and $\hat{\mathbf{u}}_- = [u^* \;\; v^* \;\; 0 \;\; 0]^T$. Numerically, we can only solve the problem above for a finite domain, so we need to find an appropriate replacement for the boundary conditions at positive and negative infinity. We employ the following projective boundary conditions for a finite domain of $z \in [-L, L]$:

$$P^s(\hat{\mathbf{u}}_-)(\hat{\mathbf{u}}(-L) - \hat{\mathbf{u}}_-) = 0 \quad \text{and} \quad P^u(\hat{\mathbf{u}}_+)(\hat{\mathbf{u}}(L) - \hat{\mathbf{u}}_+) = 0, \tag{3.3}$$

where $P^s(\hat{\mathbf{u}}_-)$ is a matrix whose rows form a basis for the stable eigenspace of the transpose of the Jacobian of $\mathbf{f}(\hat{\mathbf{u}}_-)$ and $P^u(\hat{\mathbf{u}}_+)$ is a matrix whose rows form a basis for the unstable eigenspace of the transpose of the Jacobian of $\mathbf{f}(\hat{\mathbf{u}}_+)$.

These projective boundary conditions alone are not enough to solve system (3.2). Because of the translational invariance of traveling wave solutions, we must impose an extra condition to guarantee the uniqueness of our solution. Instead of the integral condition suggested in [29], we follow a method similar to that presented in [30] and split the domain $[-L, L]$ in half, using a transformation to reflect the left half of the domain to the right. This results in solving the following eight-dimensional system over the domain $z \in [0, L]$

$$\begin{bmatrix} \hat{\mathbf{u}} \\ \hat{\mathbf{u}}_1 \end{bmatrix} = \begin{bmatrix} \mathbf{f}(\hat{\mathbf{u}}) \\ -\mathbf{f}(\hat{\mathbf{u}}_1) \end{bmatrix}$$

with the projective boundary conditions (3.3) applied to the right side of the domain, the matching condition $\hat{\mathbf{u}}(0) = \hat{\mathbf{u}}_1(0)$, and a prescribed value $\hat{u}(0) = s$. We take $s > 0$, and for monotone traveling waves, we can simply use the average of the two asymptotic rest states for $u(z)$. If the traveling wave is non-monotone, we choose a value closer to zero to ensure that the wave profile does not achieve that value twice over the domain, bringing into question the uniqueness of the numerical solution. It is important to note that based on the dimension of the unstable and stable eigenspaces used for the projective boundary conditions, some adjustments to the system or to the boundary conditions may need to be made (for example, the use of wave speed, c, as a free parameter if the system is over-determined).

Besides the utility of having two methods to double check results, the time evolution method and the boundary value solver have their respective advantages. Using the time evolution method, we can observe the development of the traveling wave, and we can see if the initial conditions have an effect on the solutions (specifically the wave speed). The boundary value solver can simultaneously solve for the wave speed in certain cases, and we are also able to find profiles for unstable waves. This is not possible using the time evolution method. The MATLAB code for each of these respective methods is provided in Appendix A.3. The second method utilizes the MATLAB boundary value problem solver `bvp5c` as well as some of the functions from the STABLAB library. The STABLAB functions have been altered slightly to allow the classification of c as a free parameter. The altered versions of these functions are given in Appendix A.3 as well.

3.2 Results from Numerical Simulations

Numerical results from the two methods show that there is a clear division in the characteristics of the traveling wave solutions depending on the values of the parameters Γ, β, α, and p. One of the characteristics that changes quite clearly depending on these values is the monotonicity of the traveling waves. For $p > 0$, we observe only monotone waves. Two examples of these waves are shown in Figure 3.1.

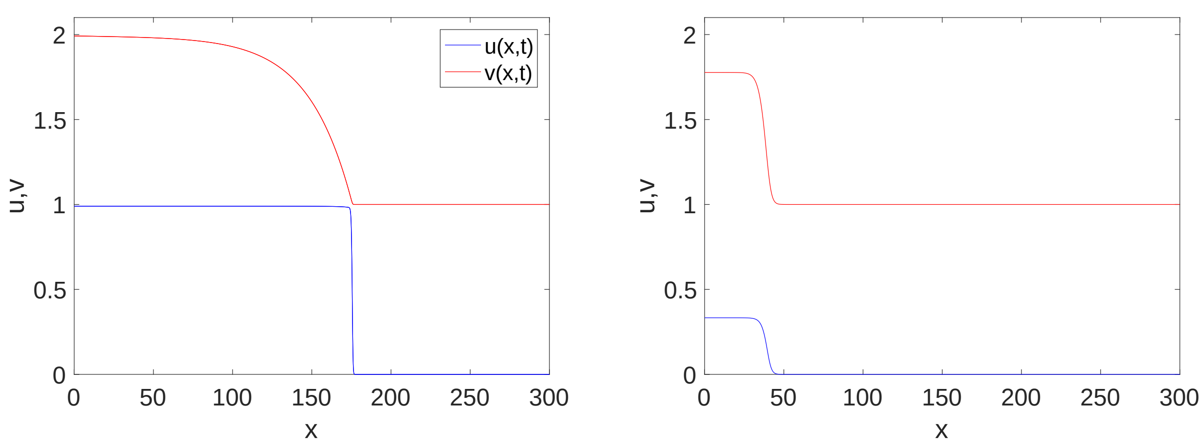

(a) Monostable, two steady state case with $\Gamma = 100$, $\beta = 5$, $\alpha = 1$, and $p = 1$.

(b) Bistable, three steady state case with $\Gamma = 1.5$, $\beta = 10$, $\alpha = 1$, and $p = 2$.

Figure 3.1: Traveling wave profiles for solutions $u(x,t)$ and $v(x,t)$ for $p > 0$.

These two profiles are results of the time evolution method. The profile on the left results from the two steady state (monostable) case discussed in Section 2.3, while the profile on the right is the product of a three steady state (bistable) case.

Remark 3.2.1. *Using the time evolution method, we were unable to find a traveling wave for the four steady state case for $p > 0$. However, using the boundary value solver, we were able to find a front connecting the two stable steady states as shown in Figure 3.2.*

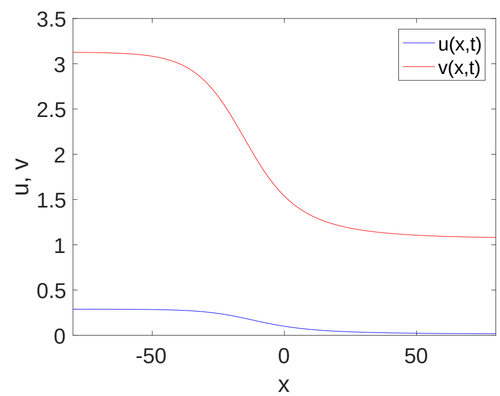

Figure 3.2: Traveling wave profile for solutions $u(x,t)$ and $v(x,t)$ for $p > 0$: bistable case with four steady states and $\Gamma = 2.0026$, $\beta = 0.4021$, $p = 4.5$, and $\alpha = 1$.

For $p = 0$, we observe a monotone wave for $u(x,t)$ and a constant solution of $v(x,t) = 1$ (see Figure 3.3). Since we have not observed non-monotone or oscillatory waves for either $p > 0$ or $p = 0$, we have not seen the traveling peak of high intensity rioting behavior, and if we wish to model a riot in which more than one wave of increased rioting behavior is present, we require more than one triggering event.

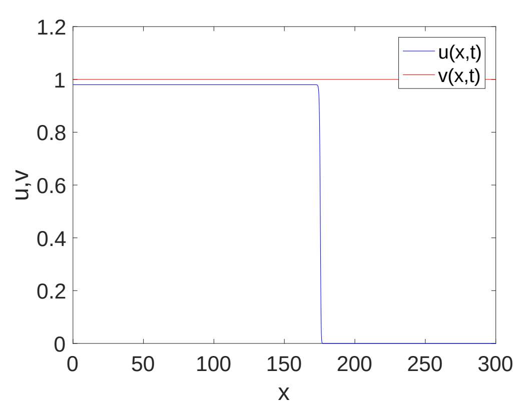

Figure 3.3: Traveling wave profile for solutions $u(x,t)$ and $v(x,t)$ for $p = 0$, $\Gamma = 100$, $\beta = 5$, $\alpha = 1$.

For $p < 0$, we observe both monotone and non-monotone waves depending on the value of the remaining parameters: Γ, β, and α. Within the group of non-monotone waves, there exists a further distinction. We observe solutions in which the traveling wave $u(z)$ is non-monotone and $v(z)$ is monotone as in the case presented in Figure 3.4a, and we observe solutions in which both $u(z)$ and $v(z)$ are oscillatory as shown in Figure 3.4b. Keeping the application of our system in mind, we note that these non-monotone waves indicate fluctuations in rioting behavior and social tension.

Remark 3.2.2. *It is interesting that the oscillatory wave exhibits a kind of "aftershock" behavior: there is an initial peak of maximum rioting behavior, followed by a sharp decrease in activity and then several more peaks of decreasing magnitude follow. This behavior has only been observed for parameter sets in which the value of β is significantly greater, meaning that these fluctuations are only seen when the transition from a peaceful state to a rioting state is very fast.*

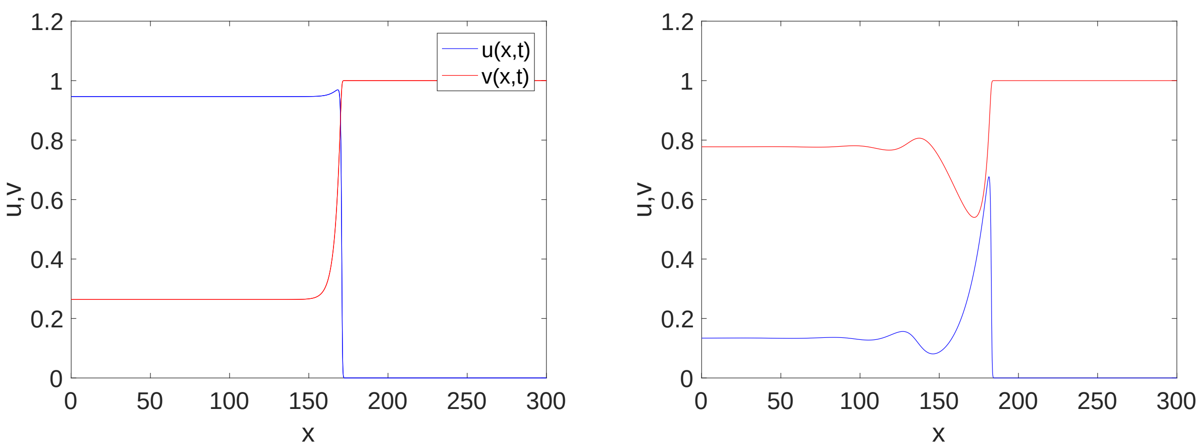

(a) Example of a non-monotone wave with $\Gamma = 100$, $\beta = 2$, $\alpha = 1$, and $p = -2$.

(b) Example of an oscillatory wave with $\Gamma = 100$, $\beta = 20$, $\alpha = 1$, and $p = -2$.

Figure 3.4: Traveling wave profiles for solutions $u(x,t)$ and $v(x,t)$ for $p < 0$.

3.3 Numerical Approximation of Wave Speed

For certain numerical computations, it is necessary to have an numerical approximation of the wave speed of the traveling wave solution after it has reached a consistent profile, and we would like to be able to see how the initial conditions of our system affect the wave speed. For the time evolution method, we also want to ensure that the domain is large enough to allow the traveling wave to reach a steady state in which its profile is consistent and no longer changing.

In order to calculate the wave speed, "buoys" are placed at evenly spaced intervals along the domain in the time evolution method. Each time a buoy is lifted by the wave profile above a threshold height, the wave speed is calculated using the difference in horizontal distance from the previous buoy and the time that passes as the wave travels between the two buoys. A sample profile with buoy markers is shown in Figure 3.5.

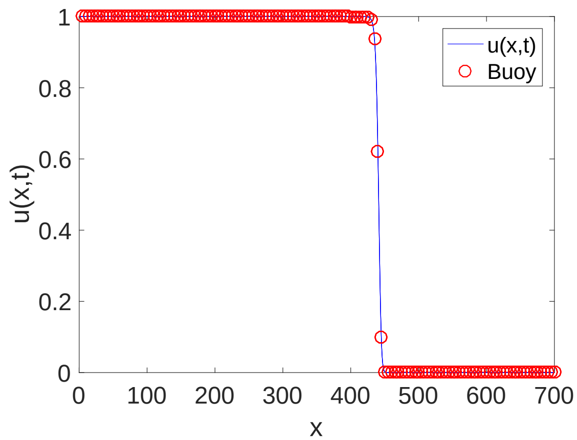

Figure 3.5: A numerically-approximated solution profile for the Fisher-KPP equation with buoys shown.

We assume the wave has reached a consistent steady state once the calculated wave speed remains within ϵ of itself over a fraction of the total domain. For example, for the wave speed experiments presented later in this section, we use $\varepsilon = 0.0005$ and a fraction of 0.15 of a total domain length of 500. For these numbers, an approximate wave speed value would be reported by the program once the calculated wave speed values were consistent to three decimal places over a domain length of 75. The fraction of the domain and epsilon value are arbitrary and depend on the desired accuracy. The fraction of the domain can be increased or the ϵ value can be decreased to achieve greater accuracy for the wave speed approximation.

To test this method, we use two instances of the Fisher-KPP equation [13] and several results known to be true about the wave speed. For the special wave speed $c = 5\sqrt{6}$ and using the change of variables to a moving frame of reference $z = x - ct$, the Fisher-KPP equation has the explicit solution $u(z) = \frac{1}{(1+Ce^{z/\sqrt{6}})^2}$ for $C > 0$ [19]. It is also known that for initial data $u(x,0) = Ce^{-kx}$, the traveling wave solution to the Fisher-KPP equation has wave speed $c = 2$ for $k \geq 1$ and $c = k + \frac{1}{k}$ for $k < 1$ [20, 21, 22, 23, 24].

Using the discretization scheme described in Section 3.1, we use the wave speed approximation method described to find the wave speed of the traveling wave solution for the Fisher-KPP equation with the following initial data:

$$\begin{cases} u_t = u_{xx} + u(1-u) \\ \frac{\partial u}{\partial x}(0,t) = 0, \quad \frac{\partial u}{\partial x}(L,t) = 0, \\ u(x,0) = \frac{1}{(1+e^{x/\sqrt{6}})^2}, \end{cases} \tag{3.4}$$

and

$$\begin{cases} u_t = u_{xx} + u(1-u) \\ \frac{\partial u}{\partial x}(0,t) = 0, \quad \frac{\partial u}{\partial x}(L,t) = 0, \\ u(x,0) = e^{-x}. \end{cases} \tag{3.5}$$

For (3.4), we found a wave speed of $c \approx 2.04081$. Compared to the expected wave speed of $c = \frac{5}{\sqrt{6}}$, this approximation has an absolute error of 4.25×10^{-4}. For (3.5), we found a wave speed of $c \approx 1.99740$ and compared to the expected wave speed of $c = 2$, this approximation has an absolute error of 3.6×10^{-3}.

We can use this method to approximate wave speeds for the monostable and bistable cases. For the bistable case, we may also use boundary value solver with wave speed set as a free parameter as mentioned in the previous section. The MATLAB code for the wave speed approximation method mentioned in this section is provided in Appendix A.3.

3.3.1 Wave Speed Experiments

Since our $p = 0$ case reduces to a Fisher-KPP equation, we can use the theory to check that there are similar conditions for the wave speed of the traveling wave solutions. We expect that there exists some $c_{min} = 2\sqrt{d_1 f_u(0,1)}$ such that for $c < c_{min}$ there exists no traveling wave, and we also expect to see a dependence on initial conditions of the form $u(x,0) = Ce^{-kx}$, where $c = c_{min}$ for $k \geq \sqrt{f_u(0,1)/d_1}$ and $c = d_1 k + f_u(0,1)/k$ for $k < \sqrt{f_u(0,1)/d_1}$ [14, 20, 21, 22, 23, 31, 25]. We wish to make some preliminary observations of the wave speed of the numerically-approximated solutions to the system under different parameter values to see if the behavior for $p = 0$ appears numerically to hold for other values of p.

Since we have chosen to fix $\alpha = 1$ as mentioned in Chapter 2, a change in β should have no effect on the minimum wave speed for the traveling wave solutions for $p = 0$. We test this hypothesis for various values of Γ, specifically values that should yield a whole number wave speed for $c_{min} = 2\sqrt{d_1 f_u(0,1)}$. We let $d_1, d_2 = 1$, and test values of $\Gamma = 10$, 52, and 100, $\beta = 1$, 5, 10, and 50, and $p = 2$, 1, 0, -1, and -2. The results of these runs are shown in Tables 3.1 through 3.5.

		β			
		1	5	10	50
Γ	10	3.9904	3.9904	3.9904	4.3507
	52	9.9354	9.9354	9.9354	9.9354
	100	13.8408	13.8408	13.8318	13.8408

Table 3.1: Approximate minimum wave speed, c_{min}, values for $p = 2$.

		β			
		1	5	10	50
Γ	10	3.9904	3.9904	3.9904	4.1314
	52	9.9354	9.9354	9.9354	9.9354
	100	13.8408	13.8408	13.8408	13.8313

Table 3.2: Approximate minimum wave speed, c_{min}, values for $p = 1$.

		β				
		1	5	10	50	Expected
Γ	10	3.9904	3.9904	3.9904	3.9888	4
	52	9.9354	9.9354	9.9354	9.9354	10
	100	13.8408	13.8408	13.8408	13.8313	14

Table 3.3: Approximate minimum wave speed, c_{min}, values for $p = 0$. The expected wave speed values are calculated using $c_{min} = 2\sqrt{d_1 f_u(0,1)}$.

		β			
		1	5	10	50
Γ	10	3.9904	3.9904	3.9904	3.9853
	52	9.9354	9.9354	9.9354	9.8736
	100	13.8408	13.8408	13.8408	13.6612

Table 3.4: Approximate minimum wave speed, c_{min}, values for $p = -1$.

		β 1	5	10	50
	10	3.9904	3.9904	3.9904	3.9853
Γ	52	9.9354	9.9354	9.9354	9.8736
	100	13.8408	13.8408	13.8313	13.6612

Table 3.5: Approximate minimum wave speed, c_{min}, values for $p = -2$.

We can see that from table to table, there is very little discrepancy in the minimum wave speed values except in the case of $\beta = 50$ and $p > 0$. In these cases, we can see significantly higher approximate wave speed values (see Tables 3.1 and 3.2). It is possible that these differences are due to numerical error, or it could be the case that the minimum wave speed actually does have some dependence on β and p. Based on the $p < 0$ data, we support the former theory since we do not see a corresponding significant change in the wave speed values for $p < 0$, and this difference does not appear for larger values of Γ. Also, we would expect to see deviations in the wave speed for $p < 0$ rather than $p > 0$ because for $p \geq 0$, the system is monotone. For the values $\Gamma = 10$, 52, and 100 and $p = 0$, we would expect to see wave speed values of $c_{min} = 4$, 10, and 14, respectively (see note in Table 3.3). The values in the tables are very close although we do see a decrease in accuracy for larger Γ. We think that this is simply a function of using the same accuracy and domain restrictions for each of these runs and that because of the size of the parameter, it may be necessary to make these restrictions more stringent (run the experiment over a larger domain and require speeds to be within a smaller ε value of each other) for larger values of Γ. This idea is supported by the fact that we also see a loss of accuracy for our expected values of wave speed for large values of β for the runs.

After seeing that we get greater expected accuracy in approximated wave speed for smaller values of Γ and β and seeing that there is little variation between speeds for different values of p, we decide to test the dependence of wave speed on initial conditions, using an initial condition of $u(x, 0) = 5e^{-kx}$ with $k = -.25$, 0.5, 1, 1.5, and 2 for $p = 2$, 1, 0, -1, and -2, $\Gamma = 10$, and $\beta = 1$. We choose smaller values of Γ and β to hopefully get more accurate approximations. The results of these runs are shown in Table 3.6.

The speeds presented in Table 3.6 show excellent agreement between p values and are very close to the expected values. We see some greater deviation in the expected values and the approximated values for $k = 0.25$ and $k = 0.5$, but again, these could be due to less stringent accuracy and domain

		k				
		0.25	0.5	1	1.5	2
	2	16.2338	8.4692	4.9975	4.1641	3.9944
	1	16.2338	8.4692	4.9975	4.1641	3.9944
p	0	16.2338	8.4692	4.9975	4.1641	3.9944
	-1	16.2338	8.4692	4.9975	4.1641	3.9944
	-2	16.2338	8.4692	4.9975	4.1641	3.9944
Expected*		16.25	8.5	5	4.1667	4

Table 3.6: Approximate wave speed, c, values for runs with initial conditions $u(x,0) = 5e^{-kx}$, $\Gamma = 10$, $\beta = 1$. *Expected values are only intended for the case $p = 0$, where we have calculated the values using $c = d_1 k + f_u(0,1)/k$.

restrictions. These various experimental runs support the idea that there is no difference in the wave speed behavior for $p = 0$, $p < 0$, and $p > 0$.

CHAPTER 4

Existence of Traveling Wave Solutions

This chapter is devoted to the existence of traveling wave solutions for $p \geq 0$.

4.1 Background

For the system:

$$\mathbf{u}_t = A\mathbf{u}_{xx} + F(\mathbf{u}), \tag{4.1}$$

where

$$A = \begin{bmatrix} d_1 & 0 \\ 0 & d_2 \end{bmatrix} \text{ and } F(\mathbf{u}) = \begin{bmatrix} f(u,v) \\ g(u,v) \end{bmatrix}, \tag{4.2}$$

there is a traveling wave solution to (4.1) if there is a solution $\mathbf{u}(x,t) = \hat{\mathbf{u}}(x-ct)$, where $z = x - ct$ for some $c \in \mathbb{R}$ that satisfies the system

$$A\hat{\mathbf{u}}'' + C\hat{\mathbf{u}}' + F(\mathbf{u}) = 0 \tag{4.3}$$

and the limits

$$\lim_{z \to \pm\infty} \hat{\mathbf{u}}(z) = \hat{\mathbf{u}}_{\pm}, \tag{4.4}$$

where A is defined as in (4.2) and

$$C = \begin{bmatrix} c & 0 \\ 0 & c \end{bmatrix}.$$

When the parameter $p \geq 0$, system (4.1) is *monotone*, or *order-preserving*, meaning that

$$\frac{\partial F_i}{\partial u_j} \geq 0, \quad \text{for } i,j \in 1,2,\ i \neq j, \tag{4.5}$$

for all $\mathbf{u} \in G$, where G is some domain in $\mathbb{R}^2$ [14].

For the corresponding spatially homogeneous system of (4.1):

$$\frac{d}{dt}(\mathbf{u}) = F(\mathbf{u}),$$

we call the source *bistable* if the stationary points, $\hat{\mathbf{u}}_\pm$ are both stable. We call the source *monostable* if one of the stationary points (either $\hat{\mathbf{u}}_+$ or $\hat{\mathbf{u}}_-$) is unstable.

Much work has been done concerning the existence of traveling waves in monotone systems, and we utilize the several theorems to prove the existence of traveling wave solutions [14, 18, 32, 26, 33]. For the remainder of this document, we will use $DF(\mathbf{u})$ to denote the Jacobian of $F(\mathbf{u})$.

Theorem 4.1.1. *Existence of traveling wave solution for system with bistable source: Assume that system* (4.1) *is monotone and that* $F(\hat{\mathbf{u}}_+) = F(\hat{\mathbf{u}}_-) = 0$*, where* $\hat{\mathbf{u}}_+ < \hat{\mathbf{u}}_-$*. Suppose also that* $F(\mathbf{u})$ *vanishes at a finite number of points* $\mathbf{u}_k$*, with* $\hat{\mathbf{u}}_+ \leq \mathbf{u}_k \leq \hat{\mathbf{u}}_-$ $(k = 1, ..., m)$*. Let us assume that all eigenvalues of the matrices* $DF(\hat{\mathbf{u}}_\pm)$ *lie in the left half-plane and that there exist vectors* $\mathbf{q}_k \geq 0$ *such that* $\mathbf{q}_k DF(\mathbf{u}_k) > 0$, $k = 1, ..., m$*. Then there exists a unique monotone traveling wave: a unique constant* c *(the wave speed) and a unique twice continuously differentiable monotone vector-valued function* $\hat{\mathbf{u}}(z)$ *that is monotonically decreasing and satisfies system* (4.3) *and the limits given in* (4.4)*.*

Theorem 4.1.2. *Existence of traveling wave solution for system with monostable source: Assume that system* (4.1) *is monotone and that* $F(\hat{\mathbf{u}}_+) = F(\hat{\mathbf{u}}_-) = 0$*, where* $\hat{\mathbf{u}}_+ < \hat{\mathbf{u}}_-$*. Suppose also that* $F(\mathbf{u})$ *vanishes at a finite number of points* $\mathbf{u}_k$*, with* $\hat{\mathbf{u}}_+ \leq \mathbf{u}_k \leq \hat{\mathbf{u}}_-$ $(k = 1, ..., m)$*. Let us assume that all eigenvalues of the matrices* $DF(\hat{\mathbf{u}}_-)$ *lie in the left half-plane and that matrices* $DF(\hat{\mathbf{u}}_+)$, $DF(\mathbf{u}_k)$ *with* $k = 1, ..., m$*, have eigenvalues in the right half plane. Then there exists a positive constant* c_{min} *such that for all* $c \geq c_{min}$ *there exist monotone waves satisfying system* (4.3) *and the limits given in* (4.4)*. When* $c < c_{min}$*, such waves do not exist.*

Remark 4.1.1. *We note that for* $p < 0$*, our system is not monotone since* $g_u(u, v) < 0$ *for* $u, v > 0$*, and as a result, we cannot make use of the theory for existence of traveling waves in monotone systems presented above. A future direction of study would be to use a method presented in [34], where we introduce a small parameter and use geometric singular perturbation theory to establish the existence of a traveling front. We would also use the global stability result of Theorem 2.2.1.*

4.2 Case $p \geq 0$

For $p \geq 0$, we can see that our system (1.2) is monotone. As discussed in Sections 2.1 and 2.3, for $p = 0$, the spatially homogeneous system given in (2.1) has a monostable source. In other words, it has two stationary points, one of which is stable and the other unstable. For $p > 0$, we are interested in the cases in which the spatially homogeneous system has two, three, or four stationary points. When there are only two stationary points, the system has a monostable source, but the system is bistable when there are three or four stationary points.

4.2.1 Bistable Case

We consider system (4.1) with $F(\mathbf{u})$ defined as in Section 1.2.

Theorem 4.2.1. *For system* (4.1)*, with the following parameters,* $p > 0$*,* $\Gamma_1(\beta) < \Gamma < 2$ *(i.e., the three stationary point case): there exists a unique monotone, vector-valued traveling wave* $\hat{\mathbf{u}}(z)$ *that is monotonically decreasing, satisfies system* (4.3) *and the limits* (4.4) *and has a unique wave speed, c.*

Proof. As mentioned above, for $p \geq 0$, our system is monotone. Section 2.3 classified the three stationary point case described above as a bistable case. In other words, we have stationary points $\hat{\mathbf{u}}_+ < \mathbf{u}_1 < \hat{\mathbf{u}}_-$ for which the eigenvalues of $DF(\hat{\mathbf{u}}_+)$ and $DF(\hat{\mathbf{u}}_-)$ lie in the left half-plane. In order to apply Theorem 4.1.1 to prove existence of a traveling wave, we only need to prove that there exists a nonnegative vector $\mathbf{q}_1 = [q_1 \;\; q_2]$ such that $\mathbf{q}_1 DF(\mathbf{u}_1) > 0$. Here we use $\mathbf{u}_1 = [u_1 \;\; v_1]$. We see that in order for this to be true, we need

$$\begin{aligned} -q_1|f_u(u_1, v_1)| + q_2|g_u(u_1, v_1)| &> 0 \\ q_1|f_v(u_1, v_1)| - q_2|g_v(u_1, v_1)| &> 0, \end{aligned}$$

where we have used the fact that $f_u(u_1, v_1) < 0$ and $g_v(u_1, v_1) < 0$. Rearranging the inequalities above, we need

$$q_2 > \frac{q_1|f_u(u_1, v_1)|}{|g_u(u_1, v_1)|} \quad \text{and} \quad q_2 < \frac{q_1|f_v(u_1, v_1)|}{|g_v(u_1, v_1)|},$$

and see that there exist $q_1, q_2 \geq 0$ that satisfy these inequalities when

$$\frac{|f_v(u_1, v_1)|}{|g_v(u_1, v_1)|} > \frac{|f_u(u_1, v_1)|}{|g_u(u_1, v_1)|}$$

or equivalently,

$$|f_u(u_1, v_1)||g_v(u_1, v_1)| - |f_v(u_1, v_1)||g_u(u_1, v_1)| < 0.$$

Because the interior stationary point $\mathbf{u}_1$ is a saddle point for both cases, the inequality above is already satisfied. We see that all the conditions for Theorem 4.1.1 are met, and so there exists a unique, monotone traveling wave solution for the three stationary point case for $p > 0$. $\square$

Remark 4.2.1. *In the four stationary point case, we have a bistable case because for the stationary points, ($\mathbf{u}_0 < \hat{\mathbf{u}}_+ < \mathbf{u}_1 < \hat{\mathbf{u}}_-$), $DF(\hat{\mathbf{u}}_+)$ and $DF(\hat{\mathbf{u}}_-)$ both have all negative eigenvalues. However, we are unable to apply the existence theorem for bistable sources (Theorem 4.1.1) because of the trivial, unstable steady state existing outside of the interval created by the two stable steady states. We were, however, able to find traveling front solutions between the two stable stationary points using the bvp5c method discussed in Chapter 3. Running the numerical time evolution with decaying exponential initial conditions did not yield any such waves. We also attempted using the solution profile from the boundary value solver as an initial condition for the time evolution method, and this did not yield a traveling wave solution either. This seems to indicate that while a traveling front may exist between the two stable states, the wave is not asymptotically stable.*

4.2.2 Monostable Case

For the monostable sources, we turn our attention to the case when $p = 0$, and when $p > 0$ with two stationary points. Again, we can take advantage of the monotonicity of our system.

Theorem 4.2.2. *For system* (4.1)*, with the following parameters: 1) $p > 0$, $\Gamma > 2$, or 2) $p = 0$, $\Gamma > 2$, there exist two stationary point cases. For these cases, there exists a positive constant c_{min} such that for $c \geq c_{min}$ there exist monotone waves satisfying system* (4.3) *and the limits* (4.4)*. For $c < c_{min}$, no such waves exist.*

Proof. As mentioned above, we have a monotone system for $p \geq 0$. For the case in which $p = 0$ and $\Gamma > 2$, there are two stationary points, $\hat{\mathbf{u}}_+ < \hat{\mathbf{u}}_-$. As shown in Section 2.1, the eigenvalues of $DF(\hat{\mathbf{u}}_-)$ all lie in the left half plane, and $DF(\hat{\mathbf{u}}_+)$ has one eigenvalue in the right half plane. We can immediately apply Theorem 4.1.2 since every condition is met, so there exists a monotone traveling wave for $p = 0$ and $\Gamma > 2$.

When $p > 0$, we have the exact same results for the eigenvalues of the Jacobians evaluated at the stationary point as outlined in Section 2.3. That is for the parameter sets: 1) $\Gamma > 2$, $p \leq 3$, and 2) $\Gamma > 2$, $p > 3$, and $\Gamma_1^{-1}(\Gamma) < \beta < \Gamma_2^{-1}(\Gamma)$, there are two stationary points, $\hat{\mathbf{u}}_+ < \hat{\mathbf{u}}_-$ for which the eigenvalues of $DF(\hat{\mathbf{u}}_-)$ all lie in the left half plane, and $DF(\hat{\mathbf{u}}_+)$ has one eigenvalue in the right half plane. This satisfies the conditions of Theorem 4.1.2, so there exists a traveling wave solution for these two sets of parameters. $\square$

CHAPTER 5

Asymptotic Behavior of Traveling Wave Solutions

To help prove the stability of the traveling wave solutions later in Chapter 6, we wish to show that for $p \geq 0$, the traveling wave solutions approach their asymptotic rest states exponentially quickly. This also allows us to place bounds on our solutions. To accomplish this, we will utilize a method similar to one presented in [35, 36]. We linearize our system about the traveling wave solution and then look for the asymptotic behavior of the solutions to the linearized system. This will give asymptotic decay rates for the traveling wave solution. For simplicity, we assume $d_1 = d_2 = 1$ in (1.2). This generalization is trivial. Assuming the system has traveling wave solutions $\hat{u}(z)$ and $\hat{v}(z)$, the moving coordinate system $z = x - ct$ may be used with $u_t = v_t = 0$, yielding the following new system:

$$\begin{cases} -cu_z = u_{zz} + f(u, v), \\ -cv_z = v_{zz} + g(u, v), \end{cases}$$

which can be represented as a first order, four dimensional system of equations:

$$\begin{cases} u' = w, \\ v' = y, \\ w' = -cw - f(u, v), \\ y' = -cy - g(u, v). \end{cases} \tag{5.1}$$

As mentioned before, this system has non-trivial steady states $(u^*, v^*, 0, 0)$ with $u^*, v^* > 0$ and trivial state $(0, 1, 0, 0)$, where in most cases u^* and v^* must be numerically calculated and satisfy the equations

$$0 = \frac{\Gamma(1 - u^*)}{1 + e^{-\beta(v^* - \alpha)}} - 1 \quad \text{and} \quad 0 = -\frac{v^*}{(1 + u^*)^p} + 1. \tag{5.2}$$

Depending on the values of the parameters in the system, there may be one, two, or three separate steady states $(u^*, v^*, 0, 0)$ satisfying (5.2).

The linearization of (5.1) about the steady states is given by $U' = AU$:

$$U' = \begin{bmatrix} u \\ v \\ w \\ y \end{bmatrix}' = \begin{bmatrix} 0 & 0 & 1 & 0 \\ 0 & 0 & 0 & 1 \\ -f_u(u,v) & -f_v(u,v) & -c & 0 \\ -g_u(u,v) & -g_v(u,v) & 0 & -c \end{bmatrix} \begin{bmatrix} u \\ v \\ w \\ y \end{bmatrix} = AU, \tag{5.3}$$

where A can be evaluated separately at each of the respective steady states. The eigenvalues, λ, of A are given by

$$[\lambda(c+\lambda)]^2 + [\lambda(c+\lambda)][f_u(u,v) + g_v(u,v)] + f_u(u,v)g_v(u,v) - g_u(u,v)f_v(u,v) = 0.$$

Using the substitution $\mu = \lambda(c+\lambda)$ in the equation above, we have the following values for μ:

$$\begin{aligned} \mu_{1,2} =& \frac{-[f_u(u,v) + g_v(u,v)]}{2} \\ & \frac{\pm\sqrt{[f_u(u,v) + g_v(u,v)]^2 - 4[f_u(u,v)g_v(u,v) - g_u(u,v)f_v(u,v)]}}{2}. \end{aligned} \tag{5.4}$$

The eigenvalues of A are then given by the solutions to $\lambda(c+\lambda) = \mu_1$ and $\lambda(c+\lambda) = \mu_2$:

$$\lambda_{1,2} = \frac{-c \pm \sqrt{c^2 + 4\mu_1}}{2}, \quad \lambda_{3,4} = \frac{-c \pm \sqrt{c^2 + 4\mu_2}}{2}. \tag{5.5}$$

We then use these eigenvalues to determine the asymptotic decay rates of the linearized system (5.3) for $p = 0$ and $p > 0$. For reference, the partial derivatives of $f(u,v)$ and $g(u,v)$ are again given below:

$$\begin{aligned} f_u(u,v) &= \frac{\Gamma(1-2u)}{1+e^{-\beta(v-\alpha)}} - 1, \quad & f_v(u,v) &= \frac{\beta\Gamma e^{-\beta(v-\alpha)}u(1-u)}{(1+e^{-\beta(v-\alpha)})^2}, \\ g_u(u,v) &= \frac{pv}{(1+u)^{p+1}}, & g_v(u,v) &= -\frac{1}{(1+u)^p}. \end{aligned}$$

5.1 Case $p = 0$

For $p = 0$, we assume that $\hat{\mathbf{u}}(z) = [\hat{u}(z)\ \hat{v}(z)]^T$ represents traveling waves satisfying

$$\lim_{z\to+\infty} \hat{\mathbf{u}}(z) = \begin{bmatrix} 0 \\ 1 \end{bmatrix}, \quad \lim_{z\to-\infty} \hat{\mathbf{u}}(z) = \begin{bmatrix} u^* \\ v^* \end{bmatrix}$$

$$\hat{u}(z), \hat{v}(z) > 0, \quad \hat{u}'(z) < 0, \quad \hat{v}'(z) = 0.$$

Proposition 5.1.1. *[35] Asymptotic decay rates for $p = 0$:*

(a) Let $\hat{\mathbf{u}}_+ = [0\ 1]^T$ and $\hat{\mathbf{u}}_- = [u^*\ v^*]^T$. There are nonnegative vectors $\mathbf{k_c}, \mathbf{K_c}, \mathbf{K}_\varepsilon, \mathbf{m}, \mathbf{M}, \mathbf{M}_\delta$ and positive numbers $\lambda_c, \lambda_{c_{min}}, \mu, \mu_f, \varepsilon, \delta$ such that the nonzero elements of $\mathbf{K}_\varepsilon, \mathbf{M}_\delta$ approach ∞ as $\varepsilon, \delta \to 0$ and

$$\begin{cases} \mathbf{k_c} e^{-\lambda_c z} \leq \hat{\mathbf{u}}(z) - \hat{\mathbf{u}}_+ \leq \mathbf{K_c} e^{-\lambda_c z}, & (z \geq 0),\ c > c_{min} \\ \hat{\mathbf{u}}(z) - \hat{\mathbf{u}}_+ \leq \mathbf{K}_\varepsilon e^{-(\lambda_{c_{min}} - \varepsilon)z}, & (z \geq 0),\ c = c_{min} \\ \mathbf{m} e^{\mu z} \leq \hat{\mathbf{u}}_- - \hat{\mathbf{u}}(z) \leq \mathbf{M} e^{\mu z}, & (z \leq 0),\ f_u(u^*, v^*) \neq -1 \\ \hat{\mathbf{u}}_- - \hat{\mathbf{u}}(z) \leq \mathbf{M}_\delta e^{(\mu_f - \delta)z}, & (z \leq 0),\ f_u(u^*, v^*) = -1 \end{cases}$$

(b) There are nonpositive vectors $\mathbf{h_c}, \mathbf{H_c}, \mathbf{H}_\varepsilon, \mathbf{n}, \mathbf{N}, \mathbf{N}_\delta$ and positive numbers $\lambda_c, \lambda_{c_{min}}, \lambda, \mu, \mu_f, \varepsilon, \delta$ such that the nonzero elements of $\mathbf{H}_\varepsilon, \mathbf{N}_\delta$ approach ∞ as $\varepsilon, \delta \to 0$ and

$$\begin{cases} \mathbf{h_c} e^{-\lambda_c z} \geq \hat{\mathbf{u}}'(z) \geq \mathbf{H_c} e^{-\lambda_c z}, & (z \geq 0),\ c > c_{min} \\ \hat{\mathbf{u}}'(z) \geq \mathbf{H}_\varepsilon e^{-(\lambda_{c_{min}} - \varepsilon)z}, & (z \geq 0),\ c = c_{min} \\ \mathbf{n} e^{\mu z} \geq -\hat{\mathbf{u}}'(z) \geq \mathbf{N} e^{\mu z}, & (z \leq 0),\ f_u(u^*, v^*) \neq -1 \\ -\hat{\mathbf{u}}'(z) \geq \mathbf{M}_\delta e^{(\mu_f - \delta)z}, & (z \leq 0),\ f_u(u^*, v^*) = -1 \end{cases}$$

Proof. Using (5.4) and (5.5), we find the eigenvalues of $A|_{(0,1,0,0)}$ and $A|_{(u^*,v^*,0,0)}$ to help determine asymptotic estimates for the traveling wave solution. The eigenvalues for $A|_{(0,1,0,0)}$ and $A|_{(u^*,v^*,0,0)}$ are, respectively,

$$A|_{(0,1,0,0)}: \quad \lambda_{1,2} = \frac{-c \pm \sqrt{c^2 - 4f_u(0,1)}}{2}, \quad \lambda_{3,4} = \frac{-c \pm \sqrt{c^2 + 4}}{2} \quad \text{and} \tag{5.6}$$

$$A|_{(u^*,v^*,0,0)}: \quad \lambda_{5,6} = \frac{-c \pm \sqrt{c^2 - 4f_u(u^*,v^*)}}{2}, \quad \lambda_{7,8} = \frac{-c \pm \sqrt{c^2+4}}{2}. \tag{5.7}$$

The positive (negative) λ with the smallest magnitude is the asymptotic decay rate for the traveling wave as $z \to -\infty$ ($z \to +\infty$). These depend on the values of $f_u(0,1)$ and $f_u(u^*,v^*)$ and consequently, upon the parameters α, β, and Γ as well.

We may omit the case in which $f_u(0,1) \leq 0$ as there is only one steady state for the system, and we are interested in traveling fronts connecting two different steady states. For $p = 0$ and parameters α, β, and Γ which yield $f_u(0,1) > 0$, we have $-f_u(u^*,v^*) = f_u(0,1)$. As a result, λ_1 and λ_2 of (5.6) could have non-zero imaginary parts, and there is the possibility of repeated eigenvalues amongst those listed in (5.7). To deal with this, it is necessary to restrict the value of c for λ_1 and λ_2, requiring $c \geq c_{min} = 2\sqrt{|f_u(0,1)|}$. We must also consider separate cases for different values of $f_u(u^*,v^*)$ for the eigenvalues in (5.7).

For $z \to +\infty$, we first consider the case in which $c > c_{min} = 2\sqrt{|f_u(0,1)|}$. The linear approximation about the steady state $(u,v,w,y) = (0,1,0,0)$ yields

$$\begin{bmatrix} u(z) \\ v(z)-1 \\ w(z) \\ y(z) \end{bmatrix} \approx A_1 \begin{bmatrix} 1 \\ 0 \\ -\lambda \\ 0 \end{bmatrix} e^{-\lambda z} \quad (z \to +\infty),$$

where $\lambda = |\lambda_1| = \dfrac{c - \sqrt{c^2 - 4f_u(0,1)}}{2}$.

If $c = c_{min} = 2\sqrt{|f_u(0,1)|}$, the linear approximation about the same steady state yields

$$\begin{bmatrix} u(z) \\ v(z)-1 \\ w(z) \\ y(z) \end{bmatrix} \approx A_2 z \begin{bmatrix} 1 \\ 0 \\ -\lambda \\ 0 \end{bmatrix} e^{-\lambda z} + O(e^{-\lambda z}) \quad (z \to +\infty),$$

where $\lambda = |\lambda_1| = |\lambda_2| = \dfrac{c}{2}$.

For $z \to -\infty$, we linearize (5.1) about the steady state $(u,v,w,y) = (u^*,v^*,0,0)$. The approximate decay rate of the solution at $z \to -\infty$ differs depending on the value of $f_u(u^*,v^*)$, so we present three separate cases.

For $-1 < f_u(u^*, v^*) < 0$, the decay rate is $\lambda = \lambda_5 = \dfrac{-c + \sqrt{c^2 - 4f_u(u^*, v^*)}}{2}$, with

$$\begin{bmatrix} u^* - u(z) \\ v^* - v(z) \\ -w(z) \\ -y(z) \end{bmatrix} \approx A_3 \begin{bmatrix} 1 \\ 0 \\ -\lambda \\ 0 \end{bmatrix} e^{\lambda z} \quad (z \to -\infty).$$

For $f_u(u^*, v^*) = -1$, we have $\lambda = \lambda_5 = \lambda_7 = \dfrac{-c + \sqrt{c^2 + 4}}{2}$

$$\begin{bmatrix} u^* - u(z) \\ v^* - v(z) \\ -w(z) \\ -y(z) \end{bmatrix} \approx -A_4 z \begin{bmatrix} 1 \\ 0 \\ -\lambda \\ 0 \end{bmatrix} e^{\lambda z} + O(e^{\lambda z}) \quad (z \to -\infty).$$

For $f_u(u^*, v^*) < -1$, the decay rate is $\lambda = \lambda_7 = \dfrac{-c + \sqrt{c^2 + 4}}{2}$, with

$$\begin{bmatrix} u^* - u(z) \\ v^* - v(z) \\ -w(z) \\ -y(z) \end{bmatrix} \approx A_5 \begin{bmatrix} f_v(u^*, v^*) \\ 1 - f_u(u^*, v^*) \\ -\lambda f_v(u^*, v^*) \\ \lambda[f_u(u^*, v^*) - 1] \end{bmatrix} e^{\lambda z} \quad (z \to -\infty).$$

□

5.2 Case $p > 0$

For $p > 0$, we assume that $\hat{\mathbf{u}}(z) = [\hat{u}(z)\ \hat{v}(z)]^T$ represents traveling waves satisfying

$$\lim_{z \to +\infty} \hat{\mathbf{u}}(z) = \begin{bmatrix} 0 \\ 1 \end{bmatrix}, \quad \lim_{z \to -\infty} \hat{\mathbf{u}}(z) = \begin{bmatrix} u^* \\ v^* \end{bmatrix}$$
$$\hat{u}(z), \hat{v}(z) > 0, \quad \hat{u}'(z), \hat{v}'(z) < 0.$$

Proposition 5.2.1. *Asymptotic decay rates for $p > 0$:*

(a) *Let* $\hat{\mathbf{u}}_+ = [0\ 1]^T$ *and* $\hat{\mathbf{u}}_- = [u^*\ v^*]^T$, $\Gamma \neq \Gamma_1(\beta)$, *and* $\Gamma \neq \Gamma_2(\beta)$. *There are nonnegative vectors* $\mathbf{k_c}, \mathbf{K_c}, \mathbf{K}_\varepsilon, \mathbf{m}, \mathbf{M}$ *and positive numbers* $\lambda_c, \lambda_{c_{min}}, \lambda_1, \lambda_2, \mu, \varepsilon$ *such that the nonzero elements of* $\mathbf{K}_\varepsilon$ *approach* ∞ *as* $\varepsilon \to 0$ *and*

$$\begin{cases} \mathbf{k_c} e^{-\lambda_c z} \leq \hat{\mathbf{u}}(z) - \hat{\mathbf{u}}_+ \leq \mathbf{K_c} e^{-\lambda_c z}, & (z \geq 0),\ f_u(0,1) > 0,\ c > c_{min} \\ \hat{\mathbf{u}}(z) - \hat{\mathbf{u}}_+ \leq \mathbf{K}_\varepsilon e^{-(\lambda_{c_{min}} - \varepsilon) z}, & (z \geq 0),\ f_u(0,1) > 0,\ c = c_{min} \\ \mathbf{k_c} e^{-\lambda_1 z} \leq \hat{\mathbf{u}}(z) - \hat{\mathbf{u}}_+ \leq \mathbf{K_c} e^{-\lambda_1 z}, & (z \geq 0),\ f_u(0,1) = 0 \\ \mathbf{k_c} e^{-\lambda_2 z} \leq \hat{\mathbf{u}}(z) - \hat{\mathbf{u}}_+ \leq \mathbf{K_c} e^{-\lambda_2 z}, & (z \geq 0),\ f_u(0,1) < 0 \\ \mathbf{m} e^{\mu z} \leq \hat{\mathbf{u}}_- - \hat{\mathbf{u}}(z) \leq \mathbf{M} e^{\mu z}, & (z \leq 0),\ \Gamma \neq 2, \Gamma_1(\beta), \Gamma_2(\beta) \end{cases}$$

(b) *Let* $\hat{\mathbf{u}}_+ = [0\ 1]^T$ *and* $\hat{\mathbf{u}}_- = [u^*\ v^*]^T$, $\Gamma \neq \Gamma_1(\beta)$, *and* $\Gamma \neq \Gamma_2(\beta)$. *There are nonpositive vectors* $\mathbf{h_c}, \mathbf{H_c}, \mathbf{H}_\varepsilon, \mathbf{n}, \mathbf{N}$ *and positive numbers* $\lambda_c, \lambda_{c_{min}}, \lambda_1, \lambda_2, \mu, \varepsilon$ *such that the nonzero elements of* $\mathbf{H}_\varepsilon$ *approach* ∞ *as* $\varepsilon \to 0$ *and*

$$\begin{cases} \mathbf{h_c} e^{-\lambda_c z} \geq \hat{\mathbf{u}}'(z) \geq \mathbf{H_c} e^{-\lambda_c z}, & (z \geq 0),\ f_u(0,1) > 0,\ c > c_{min} \\ \hat{\mathbf{u}}'(z) \geq \mathbf{H}_\varepsilon e^{-(\lambda_{c_{min}} - \varepsilon) z}, & (z \geq 0),\ f_u(0,1) > 0,\ c = c_{min} \\ \mathbf{h_c} e^{-\lambda_1 z} \geq \hat{\mathbf{u}}'(z) \geq \mathbf{H_c} e^{-\lambda_1 z}, & (z \geq 0),\ f_u(0,1) = 0 \\ \mathbf{h_c} e^{-\lambda_2 z} \geq \hat{\mathbf{u}}'(z) \geq \mathbf{H_c} e^{-\lambda_2 z}, & (z \geq 0),\ f_u(0,1) < 0 \\ \mathbf{n} e^{\mu z} \geq -\hat{\mathbf{u}}'(z) \geq \mathbf{N} e^{\mu z}, & (z \leq 0),\ \Gamma \neq 2, \Gamma_1(\beta), \Gamma_2(\beta) \end{cases}$$

Proof. The eigenvalues of $A|_{(0,1,0,0)}$ are still given by (5.6). The eigenvalues of $A|_{u^*,v^*,0,0}$ are given by (5.4) and (5.5) with f_u, f_v, g_u, and g_v evaluated at $(u,v) = (u^*, v^*)$. For $p > 0$ and $z \to +\infty$, differently from the case when $p = 0$, it is possible that $f_u(0,1)$ takes on all real values. Again for $f_u(0,1) > 0$, we must restrict c to avoid imaginary eigenvalues and require $c \geq c_{min} = 2\sqrt{f_u(0,1)}$.

For $c > c_{min}$, the linear approximation yields the following asymptotic estimate:

$$\begin{bmatrix} u(z) \\ v(z)-1 \\ w(z) \\ y(z) \end{bmatrix} \approx B_1 \begin{bmatrix} f_u(0,1)+1 \\ p \\ -\lambda(f_u(0,1)+1) \\ -\lambda p \end{bmatrix} e^{-\lambda z} \quad (z \to +\infty),$$

where $\lambda = |\lambda_2| = \dfrac{c + \sqrt{c^2 - 4f_u(0,1)}}{2}$. For $c = c_{min}$, we have repeated eigenvalues and the following estimate:

$$\begin{bmatrix} u(z) \\ v(z)-1 \\ w(z) \\ y(z) \end{bmatrix} \approx B_2 z \begin{bmatrix} f_u(0,1)+1 \\ p \\ -\lambda(f_u(0,1)+1) \\ -\lambda p \end{bmatrix} e^{-\lambda z} + O(e^{-\lambda z}) \quad (z \to +\infty),$$

where $\lambda = |\lambda_1| = |\lambda_2| = \dfrac{c}{2}$.

For $f_u(0,1) = 0$, the linearization yields the following estimate:

$$\begin{bmatrix} u(z) \\ v(z)-1 \\ w(z) \\ y(z) \end{bmatrix} \approx B_3 \begin{bmatrix} f_u(0,1)+1 \\ p \\ -\lambda(f_u(0,1)+1) \\ -\lambda p \end{bmatrix} e^{-\lambda z} \quad (z \to +\infty),$$

where $\lambda = |\lambda_2| = c$. Finally, for $f_u(0,1) < 0$, we also have $0 < |f_u(0,1)| < 1$, so the linear approximation about the steady state yields the estimate:

$$\begin{bmatrix} u(z) \\ v(z)-1 \\ w(z) \\ y(z) \end{bmatrix} \approx B_4 \begin{bmatrix} f_u(0,1)+1 \\ p \\ -\lambda(f_u(0,1)+1) \\ -\lambda p \end{bmatrix} e^{\lambda z} \quad (z \to +\infty),$$

where $\lambda = |\lambda_2| = \dfrac{c + \sqrt{c^2 - 4f_u(0,1)}}{2}$.

For $z \to -\infty$, we see that the estimates are dependent upon the values of μ_1 and μ_2. For $\Gamma \neq 2$

and $\Gamma \neq \Gamma_1(\beta), \Gamma_2(\beta)$, we have μ_1 and μ_2 real, positive and distinct, so

$$\begin{bmatrix} u^* - \hat{u}(z) \\ v^* - \hat{v}(z) \\ -w(z) \\ -y(z) \end{bmatrix} \approx A_7 \begin{bmatrix} -f_v(u^*, v^*) \\ \lambda(c+\lambda) + f_u(u^*, v^*) \\ \lambda f_v(u^*, v^*) \\ \lambda(\lambda(c+\lambda) + f_u(u^*, v^*)) \end{bmatrix} e^{\lambda z} \quad (z \to -\infty),$$

with $\lambda = \frac{-c+\sqrt{c^2+4\mu_2}}{2}$. $\square$

Remark 5.2.1. *If $\Gamma = 2$ or $\Gamma = \Gamma_1(\beta), \Gamma_2(\beta)$, one of the eigenvalues will be zero, and we are unable to make an exponential asymptotic estimate.*

CHAPTER 6

Stability of Traveling Wave Solutions

This section is devoted to the analysis of the stability of traveling wave solutions. Simply put, if we use an initial condition that is a perturbation of the traveling wave solution, does the solution eventually return to the traveling wave or some translate of the wave? Since the traveling wave solutions move with speed c, each translate of a traveling wave solution is itself a solution as well. A perturbation will cause the system to converge not to the exact same wave profile, but to a shift of that wave profile. Therefore, we provide a definition for asymptotic stability *with shift.* In the definition below, E is a Banach space, and we consider perturbations from Banach space H, within E. The symbol $\|\cdot\|$ represents the norm of space H.

Definition 6.0.1. *([14]) A wave $\hat{\boldsymbol{u}}(x)$ is asymptotically stable with shift, according to norm $\|\cdot\|$, if there exists $\varepsilon > 0$ such that for $\boldsymbol{u}_0(x) \in E$ with $\boldsymbol{u}_0 - \hat{\boldsymbol{u}} \in H$, $\|\boldsymbol{u}_0 - \hat{\boldsymbol{u}}\| < \varepsilon$, the solution $\boldsymbol{u}(x,t)$ with initial condition $\boldsymbol{u}(x,0) = \boldsymbol{u}_0(x)$ exists for all $t > 0$, is unique, $\boldsymbol{u}(x,t) - \hat{\boldsymbol{u}}(x) \in H$, and satisfies the estimate*

$$\|\boldsymbol{u}(x,t) - \hat{\boldsymbol{u}}(x+h)\| \leq Ke^{-bt} \tag{6.1}$$

for some $h \in \mathbb{R}$ which depends on $\boldsymbol{u}_0(x)$, and $K > 0$ and $b > 0$ are independent of t, h, and $\boldsymbol{u}_0(x)$.

6.1 Background

We discuss two approaches for proving the stability of traveling wave solutions. The first approach utilizes existing theory regarding stability for monotone systems. The second approach involves linearizing our system about the traveling wave solution and then performing an analysis of the spectrum of resulting linear operator to make sure that the spectrum is not located in the closed, deleted, right half plane.

6.1.1 Monotone Systems

Once again we consider the system (4.1), which we have already shown is monotone for $p \geq 0$. Because of this, we can make use of the theory developed in [14, 37] to prove the stability of traveling wave solutions for $p \geq 0$. We begin by introducing a moving coordinate frame in (4.1), using the change of variables $z = x - ct$ and $\tau = t$, which yields the monotone system

$$\mathbf{u}_\tau = A\mathbf{u}_{zz} + C\mathbf{u}_z + F(\mathbf{u}), \tag{6.2}$$

where A and C have been defined in (4.1).

For the Banach spaces mentioned above, we choose the space C of continuous, bounded, vector-valued functions for E, and for the space of perturbations, H, we choose the space C_ω of vector-valued functions $\mathbf{u}$ such that

$$\lim_{z \to |\infty|} \mathbf{u}(z)(1 + e^{\omega z}) = 0,$$

where $\omega \geq 0$. The norm of C_ω is given by

$$\|\mathbf{u}\|_\omega = \sup |\mathbf{u}(z)(1 + e^{\omega z})| \quad \text{for } z \in \mathbb{R},$$

where $|\cdot|$ denotes the Euclidean norm in $\mathbb{R}^n$.

We now present the following theorem from [14]. In the theorem below, we define $DF(\hat{\mathbf{u}})$ to be *functionally irreducible* if we replace any identically zero elements with zero and all other elements with one and have a resulting numerical matrix which is irreducible.

Theorem 6.1.1. *Stability of monotone traveling waves: Assume that a monotone wave solution $\hat{\mathbf{u}}(z)$ of system (6.2) with speed c exists. Suppose $DF(\hat{\mathbf{u}})$ is a functionally irreducible matrix with nonnegative off diagonal elements, and matrices $DF(\hat{\mathbf{u}}_-)$ and $\omega^2 A - \omega C + DF(\hat{\mathbf{u}}_+)$ have all their eigenvalues in the left half plane for some nonnegative $\omega \in \mathbb{R}$. Then if $\hat{\mathbf{u}}'(z)e^{\omega z} \to 0$ as $z \to \infty$, the wave $\hat{\mathbf{u}}(z)$ is asymptotically stable with shift in the norm $\|\cdot\|_\omega$.*

Remark 6.1.1. *Although the case $p = 0$ results in a monotone system, we will not be able to use Theorem 6.1.1 because for $g_u(\hat{u}, \hat{v}) \equiv 0$ and so $DF(\hat{\mathbf{u}})$ is functionally reducible. As a result, we will have to treat the case $p = 0$ along with the $p < 0$ case.*

6.1.2 Spectrum of the Linear Operator

We start by linearizing the system about the traveling wave solution and studying the spectrum of the linear operator stemming from this process. The spectrum of this linear operator gives us information about the stability of the wave with respect to the linearized system, which we call *spectral stability.*

Let $\hat{\mathbf{u}}(z) = [\hat{u}(z) \quad \hat{v}(z)]^T$ be a traveling wave solution that satisfies (4.3) and (4.4) and take $u(z,\tau) = \hat{u}(z) + w(z,\tau)$ and $v(z,\tau) = \hat{v}(z) + y(z,\tau)$, where $\mathbf{w} = [w(z,\tau) \quad y(z,\tau)]^T$ are small perturbations. We linearize (6.2) about the traveling wave solutions, $\hat{u}(z)$ and $\hat{v}(z)$, by substituting $u(z,\tau)$ and $v(z,\tau)$ into (6.2). After simplifying and keeping only first order terms, we have the following linearized system

$$\mathbf{w}_\tau = A\mathbf{w}_{zz} + C\mathbf{w}_z + DF(\hat{\mathbf{u}})\mathbf{w}. \tag{6.3}$$

Assume that the perturbations are of the form: $\mathbf{w} = [w(z,\tau) \ y(z,\tau)]^T = e^{\lambda\tau}[w(z) \ y(z)]^T$ and substitute into (6.3) to obtain the eigenvalue problem:

$$\lambda\mathbf{w} = \mathcal{L}\mathbf{w}, \tag{6.4}$$

where

$$\mathbf{w} = \begin{bmatrix} w \\ y \end{bmatrix}, \quad F(\mathbf{u}) = \begin{bmatrix} f(u,v) \\ g(u,v) \end{bmatrix},$$

and $\mathcal{L}$ is the linear operator

$$\mathcal{L} := A\partial_{zz} + C\partial_z + DF(\hat{\mathbf{u}}). \tag{6.5}$$

We now provide several definitions relating to the stability analysis of the traveling wave solutions.

Definition 6.1.1. *[38] The spectrum of $\mathcal{L}$, denoted $\sigma(\mathcal{L})$, is composed of all $\lambda \in \mathbb{C}$ for which $\mathcal{L} - \lambda\mathbb{I}$ is not invertible.*

(i) The point spectrum, $\sigma_{pt}(\mathcal{L})$, consists of all isolated eigenvalues of $\mathcal{L}$ with finite multiplicity. More specifically, it consists of those $\lambda \in \mathbb{C}$ for which $\mathcal{L} - \lambda\mathbb{I}$ is a Fredholm operator of index zero, has a non-trivial null space, and $\mathcal{L} - \tilde{\lambda}\mathbb{I}$ is invertible for all $\tilde{\lambda} \neq \lambda$ in a small neighborhood of λ.

(ii) The essential spectrum, $\sigma_e(\mathcal{L})$, is the complement $\sigma(\mathcal{L})\backslash\sigma_{pt}(\mathcal{L})$.

To facilitate the search for the spectrum of $\mathcal{L}$, it is typical to rewrite (6.4) as a first order system:

$$\begin{cases} \dfrac{dw}{dz} = r, \\ \dfrac{dy}{dz} = s, \\ \dfrac{dr}{dz} = -cr + (\lambda - f_u(\hat{u}, \hat{v}))w - f_v(\hat{u}, \hat{v})y, \\ \dfrac{ds}{dz} = -cs - g_u(\hat{u}, \hat{v})w + (\lambda - g_v(\hat{u}, \hat{v}))y. \end{cases} \tag{6.6}$$

From this point onward $f_u(\hat{u}, \hat{v})$ will be written as f_u unless otherwise stated (the same is true for f_v, g_u, and g_v, respectively). We further restructure (6.6) and define a new operator $\mathcal{T}(\lambda)$ with spectrum equivalent to that of $\mathcal{L} - \lambda\mathbb{I}$ [39, 40]:

$$\mathcal{T}(\lambda) \begin{bmatrix} w \\ y \\ r \\ s \end{bmatrix} := \left(\frac{d}{dz} - A(z; \lambda) \right) \begin{bmatrix} w \\ y \\ r \\ s \end{bmatrix} := \begin{bmatrix} w \\ y \\ r \\ s \end{bmatrix}' - \begin{bmatrix} 0 & 0 & 1 & 0 \\ 0 & 0 & 0 & 1 \\ \lambda - f_u & -f_v & -c & 0 \\ -g_u & \lambda - g_v & 0 & -c \end{bmatrix} \begin{bmatrix} w \\ y \\ r \\ s \end{bmatrix}. \tag{6.7}$$

Essential Spectrum In order to place bounds on and identify the essential spectrum of $\mathcal{T}(\lambda)$ (and consequently $\mathcal{L}$), we first define $A_\pm$ as

$$A_\pm(\lambda) := \lim_{z \to \pm\infty} A(z; \lambda). \tag{6.8}$$

In conjunction with (6.8), the following Definition 6.1.2 and Theorem 6.1.2 will allow us to find the region of the complex plane comprising the essential spectrum.

Definition 6.1.2. *[38, 41] The Morse indices of $A_\pm(\lambda)$ are the dimensions of the respective unstable eigenspaces.*

Theorem 6.1.2. *[38, 42, 43] $\lambda \in \mathbb{C}$ is in the essential spectrum of $\mathcal{T}(\lambda)$ if one of the following is true:*

(i) at least one of $A_\pm(\lambda)$ is not hyperbolic (i.e., has an eigenvalue with real part equal to zero)

(ii) $A_\pm(\lambda)$ are both hyperbolic, but their Morse indices differ.

To determine the dimensions of the unstable eigenspaces of $A_\pm(\lambda)$, we find the eigenvalues of the matrices, known as the *spatial eigenvalues*, μ. The characteristic equation for $A_\pm$ is

$$[\mu(c+\mu)]^2 + \mu(c+\mu)[-(\lambda - g_v) - (\lambda - f_u)] + (\lambda - f_u)(\lambda - g_v) - f_v g_u = 0, \tag{6.9}$$

where the first partial derivatives of functions f and g are evaluated at the asymptotic rest states at $z \to -\infty$ and $z \to +\infty$ for A_- and A_+, respectively.

From Theorem 6.1.2, we see that any boundaries for the essential spectrum will occur when $\mu = ik$ for $k \in \mathbb{R}$. Substituting $\mu = ik$ into (6.9) yields at most four parametric curves for λ which represent the boundaries of the essential spectrum:

$$\lambda = \frac{-2k^2 + (f_u + g_v) + 2ikc \pm \sqrt{(f_u + g_v)^2 - 4f_u g_v + 4f_v g_u}}{2} \tag{6.10}$$

Shifting the Essential Spectrum As we shall see later, the essential spectrum for our cases of $p = 0$ and $p < 0$ extend into the right half plane, indicating spectral instability. This instability is only relative to a particular norm, and by introducing a weighted norm, we are able to find a class of perturbations which eventually decay for our traveling wave solutions [38, 37]. If the instabilities of our system are convective, then the perturbations will decay for fixed values of z as $t \to \infty$, while growing as $z \to \infty$. We can use an exponentially-weighted norm defined as

$$\|u\|_\omega^2 = \int_{-\infty}^{\infty} |e^{-\omega z} u(z)|^2 dz$$

and let $L^2_\omega(\mathbb{R})$ be the space of perturbations consisting of functions $u(z)$ that satisfy $\|u(z)\|_\omega < \infty$. For $\omega > 0$, the exponential weight will cause a reduction in growth or the decay of perturbations traveling towards $z \to \infty$. Then we can find the spectrum of $\mathcal{L}$ relative to the new norm $\|\cdot\|_\omega$, and the weight will have the effect of shifting the essential spectrum to the left, possibly out of the right half of the complex plane entirely.

To find the spectrum of $\mathcal{L}$ (equivalently $T(\lambda)$), we substitute the scaled perturbation $\mathbf{w}(z) =$

$e^{-\omega z}\tilde{\mathbf{w}}(z)$ into (6.6), which yields a new operator

$$T^{\omega}(\lambda)\begin{bmatrix}\tilde{w}\\ \tilde{y}\\ \tilde{r}\\ \tilde{s}\end{bmatrix} := \left(\frac{d}{dz} - [A(z;\lambda)+\omega\mathbb{I}]\right)\begin{bmatrix}\tilde{w}\\ \tilde{y}\\ \tilde{r}\\ \tilde{s}\end{bmatrix}.$$

Employing the same method from Section 6.1.2, the boundaries of the essential spectrum for $\mathcal{L}$ with respect to the norm $\|\cdot\|_{\omega}$ are given by

$$\lambda = \frac{f_u+g_v}{2} - k^2 + \omega^2 - c\omega + ik(c-2\omega) \pm \frac{\sqrt{(f_u+g_v)^2 - 4f_ug_v + 4f_vg_u}}{2}. \tag{6.11}$$

Point Spectrum After identifying the location of the essential spectrum, spectral stability remains dependent on the location of the point spectrum, which could still exist in the right half of the complex plane. For $p = 0$, we will show that a bound may be placed on the point spectrum, proving stability by using the following theorem from [44]:

Theorem 6.1.3. *Suppose a positive solution exists for the equation $\mathcal{L}_{\omega}w = 0$. Then the equation $\mathcal{L}_{\omega}u = \lambda u$ with $u(\pm\infty) = 0$ has no solutions different from zero for* $\operatorname{Re}\lambda \geq 0$.

For $p < 0$, we use a combination of analytical and numerical methods to show that there are no point spectra located in the right half plane. To find the point spectrum of the linear operator, we use the Evans function, an analytic function of λ that is specifically constructed so that its roots will coincide with the point spectra the linear operator $\mathcal{T}^{\omega}(\lambda)$ [38, 45, 46, 47, 48].

The construction of the Evans function relies on the properties of the point spectrum outlined in Definition 6.1.1. Essentially, we would like to find those λ for which $\mathcal{T}^{\omega}(\lambda)$ has a non-trivial null space. For such a λ, there should be a solution to the first order system

$$\tilde{\mathbf{w}}' = [A(z;\lambda)+\omega\mathbb{I}]\tilde{\mathbf{w}}, \tag{6.12}$$

which decays to zero as $|z| \to \infty$. As $z \to \infty$, system (6.12) behaves as

$$\tilde{\mathbf{w}}' = [A(\lambda)_{+}+\omega\mathbb{I}]\tilde{\mathbf{w}}.$$

For λ in the right half of the complex plane, as $z \to \infty$, if a solution decays to zero, then it must do so along one of the two directions of the stable subspace of $A_+(\lambda)$, which we denote $E_+(\lambda)$. Similarly, for $z \to -\infty$, solutions decaying to zero must do so along the unstable subspace of $A_-(\lambda)$, $E_-(\lambda)$. We choose an analytic basis of decaying solutions $\tilde{\mathbf{w}}_1^-, ..., \tilde{\mathbf{w}}_k^-$ and $\tilde{\mathbf{w}}_{k+1}^+, ..., \tilde{\mathbf{w}}_n^+$, which span the unstable and stable manifolds $E_\pm(\lambda)$. In our case, k, the dimension of the unstable subspace E_-, and n, the dimension of the stable subspace E_+ are equivalent and both equal to two.

The linear independence or dependence of these vectors should be consistent for all values of z, so we choose to evaluate them at $z = 0$. This basis of solutions is then used to construct the Evans function.

Definition 6.1.3. *The Evans function is defined as*

$$D(\lambda) = \det(\tilde{\boldsymbol{w}}(\lambda)_1^-, ..., \tilde{\boldsymbol{w}}(\lambda)_k^-, \tilde{\boldsymbol{w}}(\lambda)_{k+1}^+, ..., \tilde{\boldsymbol{w}}(\lambda)_n^+)|_{z=0}.$$

From the definition, we see that for $D(\lambda) = 0$, there is an intersection of the unstable and stable manifolds, signifying the existence of a solution which decays as $|z| \to \infty$ and consequently, a value of λ for which $\mathcal{T}^\omega(\lambda)$ has a non-trivial null space.

Explicit calculation of the Evans function is difficult even for simple systems, so instead we turn to numerical computation of the roots. In our case, we are not specifically interested in the values of λ for which $D(\lambda) = 0$. Rather, we are interested in whether these values exist in the right half of the complex plane. To determine this, we make use of the *argument principle*, which states that for a meromorphic function, $f(z)$, defined inside and along a simple, closed contour $\gamma(t)$ with no zeros or poles on γ, the following must hold:

$$N - P = \frac{1}{2\pi i} \oint_\gamma \frac{f'(z)}{f(z)} dz,$$

where N and P represent the number of zeros and poles, respectively, of $f(z)$ inside γ [49].

Using the argument principle and the Evans function, $D(\lambda)$, we apply the change of variables $w = D(\lambda)$ with $\lambda = \gamma(t)$ to get:

$$\frac{1}{2\pi i} \oint_\gamma \frac{D'(\lambda)}{D(\lambda)} d\lambda = \frac{1}{2\pi i} \oint_{D\circ\gamma} \frac{dw}{w} = \mathrm{Ind}(D \circ \gamma, 0),$$

where $\mathrm{Ind}(D \circ \gamma, 0)$ represents the winding number about $\lambda = 0$ of $D(\lambda)$ evaluated along the contour

$\gamma(t)$. Since the Evans function is analytic in the right half of the complex plane, we can choose γ to be a closed, counterclockwise, semi-circular contour in the right half plane. Because of the analyticity of $D(\lambda)$, we have

$$N = \frac{1}{2\pi i}\oint_{\gamma}\frac{D'(\lambda)}{D(\lambda)}d\lambda = \mathrm{Ind}(D\circ\gamma, 0).$$

In other words, we can find the number of zeros, N, of the Evans function, $D(\lambda)$, within γ by evaluating the Evans function along γ and then finding the winding number of the resulting contour $D\circ\gamma$ about $\lambda = 0$. A winding number of zero will indicate a lack of zeros within γ as well as a lack of point spectra and will provide support for the spectral stability of the traveling wave solution with respect to $\|\cdot\|_{\omega}$. We will further limit the area of search by using the adjoint operator of $\mathcal{L}$ to come up with a bound on the search area. This is discussed below.

Placing a Bound on the Point Spectrum To numerically prove that there are no eigenvalues in the right half of the complex plane, we would of course want to make the radius of the semi-circular contour as large as possible. However, this becomes very computationally expensive and is impossible, considering we will always be searching within a limited contour and not throughout the entire right half plane. Work has been done to find more computationally efficient ways of calculating the winding number for contours with radii of significant magnitude in [50, 51].

We will take a different approach from the brute force method and show that the region in the right half of the complex plane capable of supporting eigenvalues is bounded. As a result, we can place a more reasonable bound on the radius of the semi-circular contour and are assured that eigenvalues do not exist outside of this region in the right half of the complex plane. We follow a method presented in [52] and again look at the linear operator:

$$\mathcal{L} := A\partial_z^2 + C\partial_z + DF(\hat{\mathbf{u}}).$$

Incorporating the fact that we are dealing with scaled perturbations in order to shift the essential spectrum, the linear operator becomes

$$\mathcal{L}_{\omega} := A\partial_z^2 + C_{\omega}\partial_z + (\omega^2 - c\omega + DF(\hat{\mathbf{u}}))$$

with adjoint

$$\mathcal{L}_\omega^* := A\partial_z^2 - C_\omega\partial_z + (\omega^2 - c\omega + DF(\hat{\mathbf{u}})^T),$$

where

$$C_\omega = \begin{bmatrix} c-2\omega & 0 \\ 0 & c-2\omega \end{bmatrix}. \tag{6.13}$$

For an eigenvalue of $\mathcal{L}_\omega$, λ, and some perturbation, $\tilde{\mathbf{w}} \in H^2$, we have

$$\mathcal{L}_\omega^*\mathcal{L}_\omega\tilde{\mathbf{w}} = |\lambda|^2\tilde{\mathbf{w}}. \tag{6.14}$$

From (6.14), we have the identity

$$\langle(\mathcal{L}_\omega^*\mathcal{L}_\omega - |\lambda|^2)\tilde{\mathbf{w}}, \tilde{\mathbf{w}}\rangle = 0,$$

where $\langle\cdot,\cdot\rangle$ is the L^2 inner product. To place a bound on the contour, we will show that for sufficiently large λ, the inner product will be negative, making the above relationship impossible. Using this process does, however, require us to put further restrictions on the type of perturbations which are allowed.

We prove the following lemma.

Lemma 6.1.1. *Given a perturbation, $\tilde{\mathbf{w}}$, with component functions in H^2, there exists a λ such that for $|\lambda|^2 > \lambda_0$, where*

$$\begin{aligned} \lambda_0 &= \frac{M}{m}, \\ M &= \|\partial_z^2\tilde{\mathbf{w}}\|_2^2 + \frac{c^2}{2}\|\partial_z\tilde{\mathbf{w}}\|_2^2 + (\|DF(\hat{\boldsymbol{u}})\|_\infty + \|DF(\hat{\boldsymbol{u}})^T\|_\infty)\int_{-\infty}^{\infty}|\tilde{\mathbf{w}}\cdot\partial_z^2\tilde{\mathbf{w}}|\,dz \\ &\quad + \left(\frac{c^4}{16} + \frac{c^2}{4}\|DF(\hat{\boldsymbol{u}})^T + DF(\hat{\boldsymbol{u}})\|_\infty + \|DF(\hat{\boldsymbol{u}})^T DF(\hat{\boldsymbol{u}})\|_\infty\right)\|\tilde{\mathbf{w}}\|_2^2, \quad \textit{and} \\ m &= \|\tilde{\mathbf{w}}\|_2^2, \end{aligned} \tag{6.15}$$

no solution exists for (6.14).

Proof. We choose the maximal weight of $\omega = \frac{c}{2}$, which shifts the essential spectrum of the linear operator into the left half plane for all wave speed values $c > 2\sqrt{f_u(0,1)}$. Substituting this value yields

$$\int_{-\infty}^{\infty}(\partial_z^4\tilde{\mathbf{w}})\cdot\tilde{\mathbf{w}}+\Big(-\frac{c^2}{2}+DF(\hat{\mathbf{u}})+DF(\hat{\mathbf{u}})^T\Big)\partial_z^2\tilde{\mathbf{w}}\cdot\tilde{\mathbf{w}}+\partial_z^2(DF(\hat{\mathbf{u}}))\tilde{\mathbf{w}}\cdot\tilde{\mathbf{w}}$$
$$+2\partial_z(DF(\hat{\mathbf{u}}))\partial_z\tilde{\mathbf{w}}\cdot\tilde{\mathbf{w}}+\left[\frac{c^4}{16}-\frac{c^2}{4}(DF(\hat{\mathbf{u}})^T+DF(\hat{\mathbf{u}}))+DF(\hat{\mathbf{u}})^TDF(\hat{\mathbf{u}})-|\lambda|^2\right]\tilde{\mathbf{w}}\cdot\tilde{\mathbf{w}}\,dz=0.$$

Through some simplification, we have

$$\int_{-\infty}^{\infty}(\partial_z^4\tilde{\mathbf{w}})\cdot\tilde{\mathbf{w}}+\Big(-\frac{c^2}{2}+DF(\hat{\mathbf{u}})^T\Big)\partial_z^2\tilde{\mathbf{w}}\cdot\tilde{\mathbf{w}}+\partial_z^2(DF(\hat{\mathbf{u}})\tilde{\mathbf{w}})\cdot\tilde{\mathbf{w}}$$
$$+\left[\frac{c^4}{16}-\frac{c^2}{4}(DF(\hat{\mathbf{u}})^T+DF(\hat{\mathbf{u}}))+DF(\hat{\mathbf{u}})^TDF(\hat{\mathbf{u}})-|\lambda|^2\right]\tilde{\mathbf{w}}\cdot\tilde{\mathbf{w}}\,dz=0.$$

In order to use integration by parts to simplify the expression above, we require that the perturbation, $\tilde{\mathbf{w}}$ and its derivative, $\partial_z\tilde{\mathbf{w}}$ both decay to $\mathbf{0}$ as $z\to\pm\infty$. This yields

$$\int_{-\infty}^{\infty}\partial_z^2\tilde{\mathbf{w}}\cdot\partial_z^2\tilde{\mathbf{w}}+\frac{c^2}{2}\partial_z\tilde{\mathbf{w}}\cdot\partial_z\tilde{\mathbf{w}}+DF(\hat{\mathbf{u}})^T\partial_z^2\tilde{\mathbf{w}}\cdot\tilde{\mathbf{w}}-\partial_z(DF(\hat{\mathbf{u}})\tilde{\mathbf{w}})\cdot\partial_z\tilde{\mathbf{w}}$$
$$+\left[\frac{c^4}{16}-\frac{c^2}{4}(DF(\hat{\mathbf{u}})^T+DF(\hat{\mathbf{u}}))+DF(\hat{\mathbf{u}})^TDF(\hat{\mathbf{u}})-|\lambda|^2\right]\tilde{\mathbf{w}}\cdot\tilde{\mathbf{w}}\,dz=0.$$

We use integration by parts again and rewrite several terms with L^2-norms:

$$\|\partial_z^2\tilde{\mathbf{w}}\|_2^2+\frac{c^2}{2}\|\partial_z\tilde{\mathbf{w}}\|_2^2+\int_{-\infty}^{\infty}DF(\hat{\mathbf{u}})^T\partial_z^2\tilde{\mathbf{w}}\cdot\tilde{\mathbf{w}}+DF(\hat{\mathbf{u}})\tilde{\mathbf{w}}\cdot\partial_z^2\tilde{\mathbf{w}}$$
$$+\left[\frac{c^4}{16}-\frac{c^2}{4}(DF(\hat{\mathbf{u}})^T+DF(\hat{\mathbf{u}}))+DF(\hat{\mathbf{u}})^TDF(\hat{\mathbf{u}})-|\lambda|^2\right]\tilde{\mathbf{w}}\cdot\tilde{\mathbf{w}}\,dz=0.$$

We can now place a bound on the left side of the equation and see that it is

$$\le\|\partial_z^2\tilde{\mathbf{w}}\|_2^2+\frac{c^2}{2}\|\partial_z\tilde{\mathbf{w}}\|_2^2+\left(\frac{c^4}{16}+\frac{c^2}{4}\|DF(\hat{\mathbf{u}})^T+DF(\hat{\mathbf{u}})\|_\infty+\|DF(\hat{\mathbf{u}})^TDF(\hat{\mathbf{u}})\|_\infty-|\lambda|^2\right)\|\tilde{\mathbf{w}}\|_2^2$$
$$+(\|DF(\hat{\mathbf{u}})\|_\infty+\|DF(\hat{\mathbf{u}})^T\|_\infty)\int_{-\infty}^{\infty}|\tilde{\mathbf{w}}\cdot\partial_z^2\tilde{\mathbf{w}}|\,dz. \tag{6.16}$$

We see that for the values indicated in (6.15), the quantity in (6.16) is negative, and so there is no solution to the equation (6.14). □

Spectral Stability to Asymptotic Stability After locating the spectrum of the operator for the linearized system, the following theorem can be used to establish spectral stability.

Definition 6.1.4. *[38] The operator $\mathcal{L}$ in* (6.5) *is spectrally stable if the spectrum is absent from the closed, deleted right half of the complex plane, so for all $\lambda \in \sigma(\mathcal{L})$, $\{\lambda \in \mathbb{C}\backslash\{0\} | \mathrm{Re}(\lambda) < 0\}$.*

Once we have established the spectral stability of the system, the question remains: does this imply nonlinear stability as well? We refer to the following result from [53].

Theorem 6.1.4. *Spectral Stability implies Nonlinear Stability with Asymptotic Phase: Let $\hat{\mathbf{u}}(z)$ and its translates be $\hat{\mathbf{u}}(z+h)$ be traveling wave solutions of the partial differential equation* (6.2)*. Provided that the diffusion matrix is strictly positive, if the spectrum of the linear operator, $\mathcal{L} := A\partial_{zz} + C\partial_z + DF(\hat{\mathbf{u}})$, posed on an appropriate Banach space satisfies $\Sigma\backslash\{0\} \subset \{\lambda : \mathrm{Re}(\lambda) < -\delta\}$ for some $\delta > 0$ and if $\lambda = 0$ is a simple eigenvalue, then the traveling wave $\hat{\mathbf{u}}(z)$ is nonlinearly stable with asymptotic phase.*

6.2 Case $p > 0$

In this section, we prove the stability of traveling wave solutions for two of the cases of traveling waves whose existence was proved in Chapter 4: $p > 0$ with bistable source (three stationary points) and $p > 0$ with monostable source (two stationary points).

6.2.1 Bistable Source with $p > 0$

We consider system (4.1) with $F(\mathbf{u})$ defined as in Section 1.2.

Theorem 6.2.1. *For system* (4.1)*, with the following parameters, $p > 0$, $\Gamma_1(\beta) < \Gamma < 2$ (i.e., the three stationary point case): the traveling wave connecting the two asymptotic rest states, $\hat{\mathbf{u}}_+$ and $\hat{\mathbf{u}}_-$, is asymptotically stable with shift in the norm $\|\cdot\|_\omega$ as defined in Section 6.1.1.*

Proof. Since system (4.1) is monotone for $p \geq 0$, we know that $DF(\hat{\mathbf{u}})$ has nonnegative off diagonal elements, and since none of the elements are identically zero, we see that it is functionally irreducible as well. As discussed in Section 2.3, in the bistable case, the eigenvalues of both $DF(\hat{\mathbf{u}}_+)$ and $DF(\hat{\mathbf{u}}_-)$ are all located in the left half plane, so we see that eigenvalue condition of Theorem 6.1.1 is satisfied for $\omega = 0$. It now remains to show that $\hat{\mathbf{u}}'(z) \to 0$ as $z \to \infty$. Since $\hat{\mathbf{u}}'(z)$ is a monotone wave and $\hat{\mathbf{u}}_+ < \hat{\mathbf{u}}_-$, we know that $\hat{\mathbf{u}}'(z) < 0$. Because $\hat{\mathbf{u}}(z)$ satisfies $\lim_{z\to\infty} \hat{\mathbf{u}}(z) = \hat{\mathbf{u}}_+$, we have that $\lim_{z\to\infty} \hat{\mathbf{u}}'(z) = 0$. Since all the conditions of theorem 6.1.1 are met, we know that the traveling wave solutions existing for the bistable source case with $p > 0$ are asymptotically stable with shift in the norm $\|\cdot\|_\omega$. $\square$

6.2.2 Monostable Source with $p > 0$

For the monostable sources, we turn our attention to the case when $p > 0$ with two stationary points.

Theorem 6.2.2. *For system* (4.1)*, with the following parameters: $p > 0$ and $\Gamma > 2$, there exist two stationary points. The traveling wave connecting these two asymptotic rest states, $\hat{\mathbf{u}}_+$ and $\hat{\mathbf{u}}_-$, is asymptotically stable with shift in the norm $\|\cdot\|_\omega$ as defined in Section 6.1.1.*

Proof. Again, the monotonicity of (4.1) implies that $DF(\hat{\mathbf{u}})$ has nonnegative off diagonal elements, and it is functionally irreducible. From Section 2.3, we know that all the eigenvalues of $DF(\hat{\mathbf{u}}_-)$ lie in the left half plane. Since $DF(\hat{\mathbf{u}}_+)$ has one eigenvalue in the right half plane, we need to prove the existence of a nonnegative ω for which the eigenvalues of $\omega^2 A - \omega C + DF(\hat{\mathbf{u}}_+)$ are all located in the left half plane. In addition to that, we need to prove that the limit mentioned in Theorem 6.1.1 holds. We will separate our discussion into two cases: the case in which $\Gamma = 2$ ($f_u(0,1) = 0$) and the case in which $\Gamma > 2$ ($f_u(0,1) > 0$. These different values of Γ yield different principal eigenvalues (eigenvalues with maximal real part) for $DF(\hat{\mathbf{u}}_+)$.

Case $\Gamma = 2$ When $\Gamma = 2$, we have $f_u(0,1) = 0$, and the maximal eigenvalue of $DF(\hat{\mathbf{u}}_+) = 0$, so we can take $\omega > 0$ sufficiently small to shift that eigenvalue into the left half plane. In order to apply Theorem 6.1.1, we only need to show that $\lim\limits_{z\to\infty} \hat{\mathbf{u}}'(z)e^{\omega z} = 0$. Using the asymptotic decay rates found in Section 5.2, we see that for $z \geq 0$

$$\mathbf{h_c} e^{-\lambda_1 z} \geq \hat{\mathbf{u}}'(z) \geq \mathbf{H_c} e^{-\lambda_1 z},$$

where $\mathbf{h_c}$ and $\mathbf{H_c}$ are nonpositive vectors and $\lambda_1 = c$. So, we can see that as long as we choose $0 < \omega < c$, the limit will be satisfied, and all conditions of Theorem 6.1.1 are met, proving the stability of the monotone wave.

Case $\Gamma > 2$ For $\Gamma > 2$, the principal eigenvalue of $DF(\hat{\mathbf{u}}_+)$ is $\lambda_+ = f_u(0,1) > 0$. It is possible to find a nonnegative ω that will shift all the eigenvalues of $\omega^2 a - c\omega + DF(\hat{\mathbf{u}}_+)$ into the left half plane by simply calculating the eigenvalues. We see that the following range of values for ω will shift eigenvalues into the left half plane:

$$\frac{c-\sqrt{c^2-4f_u(0,1)}}{2}<\omega<\frac{c+\sqrt{c^2-4f_u(0,1)}}{2}.$$

We see that an appropriate value ω will only exist as long as $c>2\sqrt{f_u(0,1)}$. This in turn gives us a lower bound for the speed of our traveling wave solution, and the minimum wave speed, c_{min}. It is important to note, however, that waves can attain this minimum wave speed as seen in Theorem 4.1.2 in Chapter 4.

To complete the conditions of Theorem 6.1.1, we now show that $\lim_{z\to\infty}\hat{\mathbf{u}}'(z)e^{\omega z}=0$. We again turn to the asymptotic decay estimates of Section 5.2. We see that for $\Gamma=2$, $f_u(0,1)>0$, and as mentioned above, we have $c>c_{min}$ in order to insure the existence of the proper weight, ω. With these constraints, we have the following asymptotic estimate for $z\geq 0$

$$\mathbf{h_c}e^{-\lambda_c z}\geq\hat{\mathbf{u}}'(z)\geq\mathbf{H_c}e^{-\lambda_c z},$$

where $\mathbf{h_c}$ and $\mathbf{H_c}$ are nonpositive vectors and $\lambda_c=\dfrac{c+\sqrt{c^2-4f_u(0,1)}}{2}$. With the range of appropriate values of ω specified above, we see that $\omega<\lambda_c$, and so the limit is satisfied, and the traveling wave solution is stable. □

6.3 Monostable Source with $p=0$

In this section, we will prove the stability of the monostable source case with $p=0$. We will prove the stability with respect to the exponentially-weighted norm defined as

$$\|u\|_\omega^2=\int_{-\infty}^{\infty}|e^{-\omega z}u(z)|^2dz$$

and let $L^2_\omega(\mathbb{R})$ be the space of perturbations consisting of functions $u(z)$ that satisfy $\|u(z)\|_\omega<\infty$.

Theorem 6.3.1. *For system* (4.1)*, with the following parameters: $p=0$ and $\Gamma>2$, there exist two stationary points. The traveling wave connecting these two asymptotic rest states, $\hat{\mathbf{u}}_+$ and $\hat{\mathbf{u}}_-$, is asymptotically stable with shift in the norm $\|\cdot\|_\omega$ as defined above.*

Proof. As we have seen previously, for $p=0$, $g_u(u^*,v^*)=0$, so using (6.10) for $z\to-\infty$, we have the two corresponding essential spectrum boundaries:

$$\lambda_1^- = -k^2 + f_u(u^*, v^*) + ikc \quad \text{and} \quad \lambda_2^- = -k^2 + g_v(u^*, v^*) + ikc.$$

For $z \to \infty$ and $p = 0$, (6.10) yields the curves:

$$\lambda_1^+ = -k^2 + f_u(0, 1) + ikc \quad \text{and} \quad \lambda_2^+ = -k^2 + g_v(0, 1) + ikc.$$

Additionally, for $p = 0$, $g_v(u, v) = -1$ for all $u, v \geq 0$, so we see that λ_2^- and λ_2^+ are coincident. An example of the essential spectrum in this case is shown in Figure 6.1. (For a description of the calculation of the regions of the essential spectrum, please see the next section.)

Remark 6.3.1. *It is important to note that because $f_u(0, 1) > 0$, the curve λ_1^+ extends into the right half of the complex plane as shown in Figure 6.1. This implies spectral instability, and as a result, we will have to shift the essential spectrum into the left half plane by using the previously mentioned exponentially-weighted norm.*

Using (6.11), we see that the boundaries of the essential spectrum under the exponentially-weighted norm are

$$\begin{aligned}
\lambda_1^+ &= f_u(0, 1) - k^2 + \omega^2 - c\omega + ik(c - 2\omega), \\
\lambda_2^+ &= g_v(0, 1) - k^2 + \omega^2 - c\omega + ik(c - 2\omega), \\
\lambda_1^- &= f_u(u^*, v^*) - k^2 + \omega^2 - c\omega + ik(c - 2\omega).
\end{aligned}$$

We want to find a value of ω which will shift all curves completely into the left half of the complex plane. Previously, the rightmost point of the curves occurred when $k = 0$, so to shift the essential spectrum into the left half of the complex plane, we first require

$$\text{Re}(\lambda_1^+) = f_u(0, 1) + \omega^2 - c\omega < 0.$$

This inequality is satisfied for $c > 2\sqrt{f_u(0, 1)}$ and

$$\frac{c - \sqrt{c^2 - 4f_u(0, 1)}}{2} < \omega < \frac{c + \sqrt{c^2 - 4f_u(0, 1)}}{2}.$$

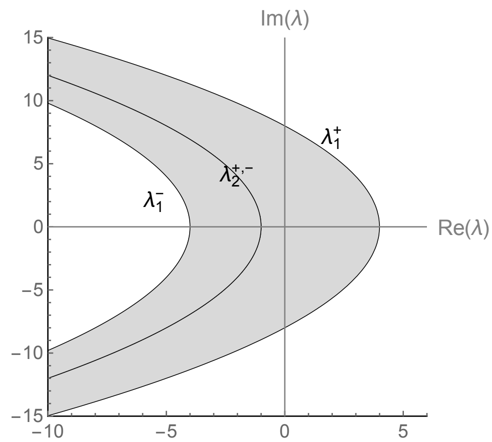

Figure 6.1: Essential spectrum for parameters $\Gamma = 10$, $p = 0$, $\beta = 5$, and $\alpha = 1$. The essential spectrum lies in the shaded region.

For the remaining two curves, $\mathrm{Re}(\lambda_1^-) < 0$ and $\mathrm{Re}(\lambda_2^+) < 0$ for $p = 0$, so they will remain in the left half plane. As a result, if $c > 2\sqrt{f_u(0,1)}$ and inequality (6.17) holds, then the essential spectrum is shifted out of closed, deleted, right half of the complex plane.

We now deal with the point spectrum. We can see $v = 1$ for both of the steady states of this case and is a solution to the v equation within our system when $p = 0$. We can then focus our attention on the remaining equation:

$$u_t = u_{xx} + \frac{\Gamma u(1-u)}{1 + e^{-\beta(1-\alpha)}} - u.$$

After performing the same change of coordinates $z = x - ct$ and utilizing the exponential weight for perturbations, we have the following linear operator for our remaining equation:

$$\mathcal{L}_\omega := \partial_{zz} + (c - 2\omega)\partial_z + (\omega^2 - c\omega + f_u(\hat{u})).$$

First, we will show that $w(z) = \hat{u}'(z)e^{\omega z}$ is an eigenfunction of $\mathcal{L}_\omega$ with eigenvalue zero and $\omega = \frac{c}{2}$:

$$\begin{aligned}
\mathcal{L}_\omega w &= \partial_{zz}(w) + (c - 2\omega)\partial_z(w) + (\omega^2 - c\omega + f_u(\hat{u}))w \\
&= e^{\frac{c}{2}z}\left(\hat{u}''' + c\hat{u}'' + \frac{c^2}{4}\hat{u}'\right) + e^{\frac{c}{2}z}\left(-\frac{c^2}{4} + f_u(\hat{u})\right)\hat{u}' \\
&= e^{\frac{c}{2}z}\frac{d}{dz}\left(\hat{u}'' + c\hat{u}' + f(\hat{u})\right) \\
&= 0.
\end{aligned}$$

Since $\hat{u}(z)$ is a monotonically decreasing traveling wave, $\hat{u}'(z) < 0$, so $w(z) < 0$. We can use a simple change of coordinates to show that $w(z) > 0$, so we have a positive solution for the equation $\mathcal{L}_\omega w = 0$. Theorem 6.1.3 then shows that there are no other eigenvalues with positive real part, and the point spectrum of $\mathcal{L}_\omega$ is located in the left half plane. Since the entire spectrum of the operator is in the left half plane, the traveling wave solution is spectrally stable.

Referring back to Theorem 6.1.4, we see that the diffusion matrix for our system (4.1) is strictly positive and the eigenvalues of the linear operator mentioned in the theorem lie in the left half plane (except for the eigenvalue of zero) for perturbations from the space $L^2_{c/2}(\mathbb{R})$, so spectral stability implies asymptotic stability with shift. □

6.4 Monostable Source with $p < 0$

In this section, we will prove the stability of the monostable source case with $p < 0$. As with the monostable $p = 0$ case, we will prove the stability with respect to the exponentially-weighted norm defined as

$$\|u\|_\omega^2 = \int_{-\infty}^{\infty} |e^{-\omega z} u(z)|^2 dz$$

and let $L^2_\omega(\mathbb{R})$ be the space of perturbations consisting of functions $u(z)$ that satisfy $\|u(z)\|_\omega < \infty$. For $p < 0$, even proving spectral stability is far more difficult without the monotonicity of the system, and we resort to a combination of analytical and numerical methods to place a bound on the spectrum. As we will see, for our system, once we have proven this weaker form of spectral stability, asymptotic stability with shift also applies.

Theorem 6.4.1. *For system* (4.1)*, with the following parameters: $p < 0$ and $\Gamma > 2$, there exist two stationary points. The traveling wave connecting these two asymptotic rest states, $\hat{\mathbf{u}}_+$ and $\hat{\mathbf{u}}_-$, is asymptotically stable with shift in the norm $\|\cdot\|_\omega$ as defined above.*

Proof. **6.4.1 Essential Spectrum**

Again, using (6.10), four λ-curves result when evaluating the partial derivatives at the two asymptotic rest states. For $z \to \infty$ and $p \geq 0$, (6.10) yields two distinct curves:

$$\lambda_1^+ = -k^2 + f_u(0,1) + ikc \quad \text{and} \quad \lambda_2^+ = -k^2 + g_v(0,1) + ikc,$$

since $f_u(0,1) > 0$ and $g_v(0,1) < 0$.

Depending on the values of the parameters Γ, β, α, and p in the original system, it is possible that the remaining two boundaries coincide. We see that there are three separate cases for the structure of the essential spectrum boundaries found by sending $z \to -\infty$. In fact, there are three general cases, depending on the value of the discriminant in (6.10) evaluated at $z \to -\infty$, which we denote $\Delta = (f_u + g_v)^2 - 4f_u g_v + 4f_v g_u$.

For $\Delta < 0$, there are two distinct boundary curves

$$\lambda_1^- = -k^2 + \frac{f_u(u^*, v^*) + g_v(u^*, v^*)}{2} + i\left(kc + \frac{\sqrt{|\Delta|}}{2}\right)$$
$$\lambda_2^- = -k^2 + \frac{f_u(u^*, v^*) + g_v(u^*, v^*)}{2} + i\left(kc - \frac{\sqrt{|\Delta|}}{2}\right)$$

as shown in Figure 6.2.

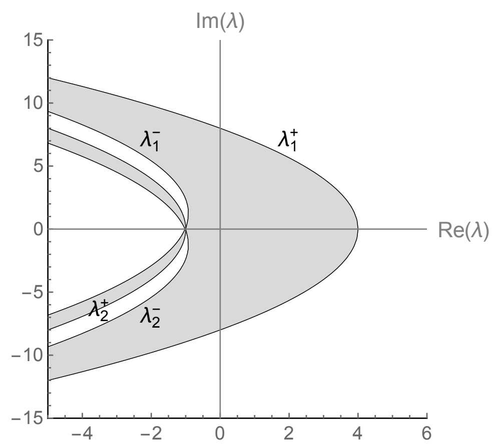

Figure 6.2: Essential spectrum for $\Delta < 0$ with parameters $\Gamma = 10$, $p = -4$, $\beta = 5$, and $\alpha = 1$. The essential spectrum lies in the shaded region.

When $\Delta = 0$, these two curves become coincident:

$$\lambda_{1,2}^- = -k^2 + \frac{f_u(u^*, v^*) + g_v(u^*, v^*)}{2} + ikc. \tag{6.17}$$

An example of this is illustrated in Figure 6.3. Finally for $\Delta > 0$, there are again two distinct curves:

$$\begin{aligned} \lambda_1^- &= -k^2 + \frac{f_u(u^*, v^*) + g_v(u^*, v^*) + \sqrt{\Delta}}{2} + ikc, \\ \lambda_2^- &= -k^2 + \frac{f_u(u^*, v^*) + g_v(u^*, v^*) - \sqrt{\Delta}}{2} + ikc, \end{aligned} \tag{6.18}$$

which is also shown in Figure 6.3.

As $p < 0$, then $f_u(u^*, v^*) < 0$, $f_v(u^*, v^*) > 0$, $g_u(u^*, v^*) < 0$, and $g_v(u^*, v^*) < 0$, so λ_1^- and λ_2^- never extend into the right half of the complex plane.

With these possible boundaries for the essential spectrum, we determine the Morse indices of A_+ and A_- for each region of the complex plane created by the λ-curves. The essential spectrum lies in the regions where the Morse indices differ. Based on Definition 6.1.2, the Morse indices are equivalent to the number of spatial eigenvalues with negative real part. Solving (6.9) for μ, we see that the spatial eigenvalues are

$$\begin{aligned} \mu_1 &= \frac{-c + \sqrt{c^2 + 4\nu_1}}{2}, \quad \mu_2 = \frac{-c - \sqrt{c^2 + 4\nu_1}}{2}, \\ \mu_3 &= \frac{-c + \sqrt{c^2 + 4\nu_2}}{2}, \quad \text{and} \quad \mu_4 = \frac{-c - \sqrt{c^2 + 4\nu_2}}{2}, \end{aligned} \tag{6.19}$$

where

$$\begin{aligned} \nu_1 &= \frac{2\lambda - g_v - f_u + \sqrt{(g_v + f_u)^2 - 4f_u g_v + 4f_v g_u}}{2} \quad \text{and} \\ \nu_2 &= \frac{2\lambda - g_v - f_u - \sqrt{(g_v + f_u)^2 - 4f_u g_v + 4f_v g_u}}{2}. \end{aligned} \tag{6.20}$$

We start by looking at the very rightmost region of the complex plane created by the essential spectrum boundaries where $\text{Re}(\lambda) \to +\infty$. Using (6.20) and (6.19), we see that for $\text{Re}(\lambda) \to +\infty$, $\nu_1, \nu_2 > 0$ for both A_+ and A_-, so the dimension of the unstable eigenspaces for both $A_\pm$ is two. Similarly, we look at the very leftmost region of the complex plane and see that for $\text{Re}(\lambda) \to -\infty$, $\nu_1, \nu_2 < 0$ for both $A_\pm$, so the dimension of the unstable eigenspaces for both $A_\pm$ is four. This indicates that as the real part of a given λ decreases and it traverses the essential spectrum boundaries, the dimension of the unstable eigenspaces of $A_\pm$ must each increase by two. By definition, the essential spectrum boundary curves consist of those λ for which either A_+ or A_- has spatial eigenvalues with zero real part. Therefore, crossing any of $\lambda_{1,2}^+$ or $\lambda_{1,2}^-$ from left to right will decrease the dimension of the unstable eigenspace of A_+ or A_-, respectively, by one. For coincident curves, the dimension decreases by two. Regions of the essential spectrum where the dimension of the unstable eigenspaces for A_+ and A_- differ are shown in Figures 6.2 through 6.3. More detailed examples of calculations of these dimensions may be found in Appendix C.1.

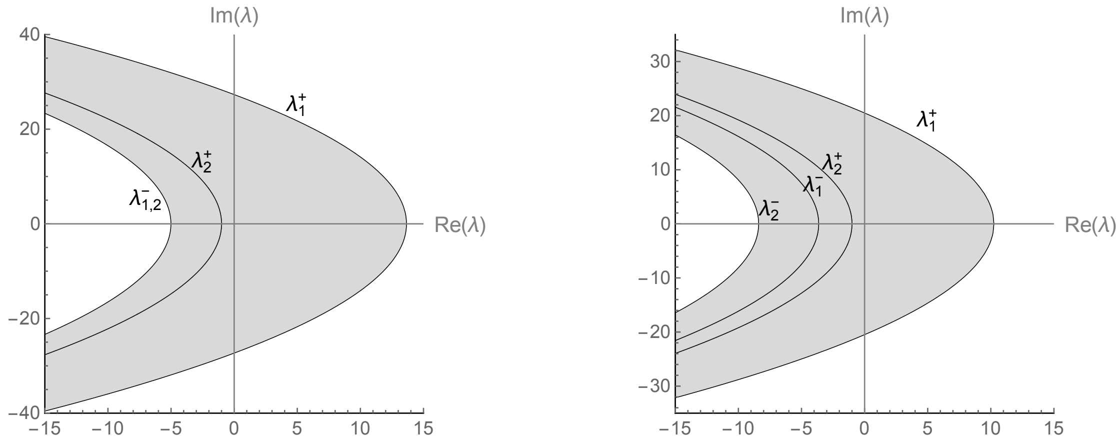

(a) $\Delta = 0$ with parameters $\Gamma \approx 15.069$, $p = -2$, $\beta = 5$, and $\alpha = (2 - \frac{2}{\Gamma})^p \approx 0.287$.

(b) $\Delta > 0$ with parameters $\Gamma = 20$, $p = -2$, $\beta = 0.5$, and $\alpha = 0.5$.

Figure 6.3: Essential spectrum for the case $\Delta = 0$ and $\Delta > 0$. The essential spectrum lies in the shaded region.

Remark 6.4.1. *It is important to note that because of the sign of $f_u(0,1)$, the curve λ_1^+ extends into the right half of the complex plane as shown in Figures 6.2 through 6.3. Because of this, the traveling wave solutions for $p < 0$ are spectrally unstable. However, given that we were able to find traveling wave solutions by solving the time evolution numerically with various initial conditions and parameter values, we would expect to find that the traveling wave solutions are stable with respect to certain perturbations. In what follows, we will discuss a restricted class of perturbations for which the traveling wave solutions are stable.*

6.4.2 Shifting the Essential Spectrum

We take advantage of the restricted class of perturbations described in 6.1.2 and see that (6.11) will yield at most four λ-curves since the partial derivatives are evaluated at both $z \to \pm\infty$, and we want to find a value of ω which will shift all curves completely into the left half of the complex plane. Previously, the rightmost point of the curves occurred when $k = 0$, so to shift the essential spectrum into the left half of the complex plane, we first require

$$\mathrm{Re}(\lambda_1^+) = f_u(0,1) + \omega^2 - c\omega < 0 \quad \text{and} \quad \mathrm{Re}(\lambda_2^+) = g_v(0,1) + \omega^2 - c\omega < 0.$$

Because of the sign of $f_u(0,1)$ and $g_v(0,1)$, both inequalities are satisfied for $c > 2\sqrt{f_u(0,1)}$ and

$$\frac{c-\sqrt{c^2-4f_u(0,1)}}{2} < \omega < \frac{c+\sqrt{c^2-4f_u(0,1)}}{2}.$$

For the remaining two curves, $\mathrm{Re}(\lambda_1^-) < 0$ and $\mathrm{Re}(\lambda_2^-) < 0$ for $p = 0$ and for all values of Δ for $p < 0$ as discussed in Section 6.1.2. As a result, if $c > 2\sqrt{f_u(0,1)}$ and

$$\frac{c-\sqrt{c^2-4f_u(0,1)}}{2} < \omega < \frac{c+\sqrt{c^2-4f_u(0,1)}}{2}, \tag{6.21}$$

then the essential spectrum is shifted out of closed, deleted, right half of the complex plane. This tells us that the essential spectrum shows no evidence of instabilities for the traveling wave solutions with respect to $\|\cdot\|_\omega$ for $p < 0$. An example of a shifted essential spectrum is shown in Figure 6.4 for the case $p < 0$ and $\Delta < 0$.

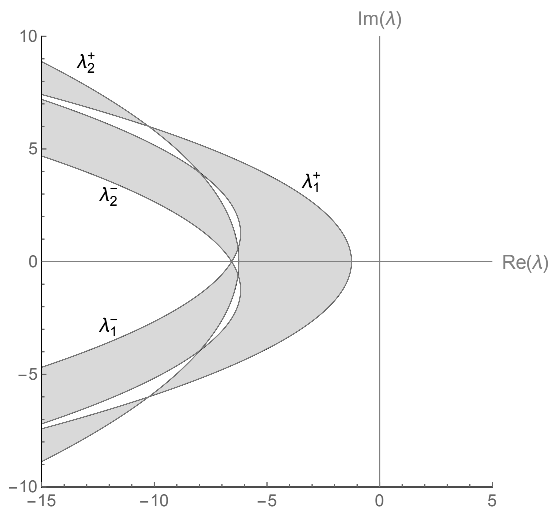

Figure 6.4: Shifted essential spectrum for $\Delta < 0$ with parameters $\Gamma = 10$, $p = -4$, $\beta = 5$, and $\alpha = 1$. The wave speed $c = 5$ with $\omega = 3.5$, which is within the range specified in (6.21). Since $c > 2\sqrt{f_u(0,1)}$, the essential spectrum is shifted completely into the left half of the complex plane.

6.4.3 Point Spectrum

We now turn our attention to the point spectrum. We utilize the MATLAB-based toolbox STABLAB to perform the numerical computation of the Evans function [54]. We evaluate the Evans function on a semi-circular contour, γ, with finite radius. An example of such a contour is shown in Figure 6.5. The contour does not contain or pass through the point $\lambda = 0$ as that is an eigenvalue of the linear operator associated with the translational invariance of traveling wave solutions.

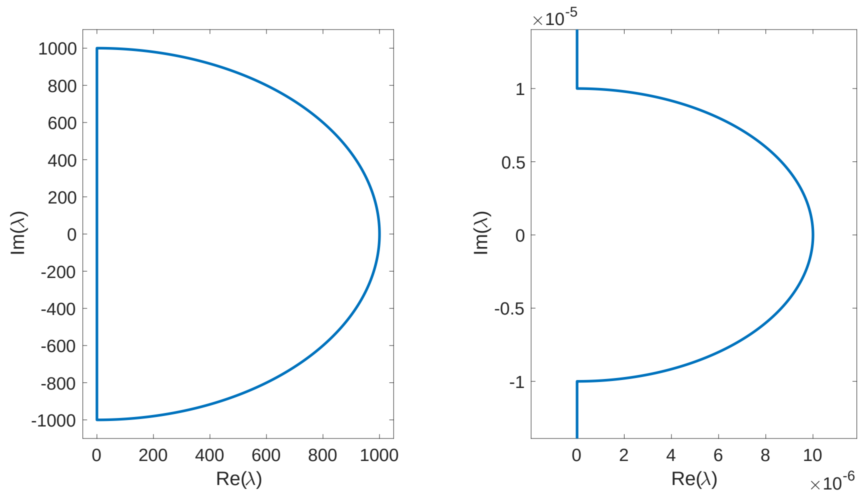

Figure 6.5: Left: Semi-circular contour, γ. Right: A magnification of γ about $\lambda = 0$.

6.4.4 Placing a Bound on the Point Spectrum

We can utilize Lemma 6.1.1 to decide an appropriate radius for our semi-circular contour in order to assure our search for the point spectrum is occurring within an appropriate region, and that outside this region, no point spectra exist. We can accomplish this given a perturbation and a parameter set.

As an example, let $\tilde{\mathbf{w}} = e^{-z^2}[1 \ \ 1]^T$ and let the parameter set be $\Gamma = 10$, $p = -4$, $\beta = 5$, and $\alpha = 1$ (equivalent to the parameters for the $\Delta < 0$ case). For these parameters, the wave speed is $c = 4$ as determined by the range of ω values for our shifted spectrum. For our example perturbation, we have

$$\begin{aligned}
\|\tilde{\mathbf{w}}\|_2^2 &= \int_{-\infty}^{\infty} 2(e^{-z^2})^2 dz = \sqrt{2\pi}, \\
\|\partial_z \tilde{\mathbf{w}}\|_2^2 &= \int_{-\infty}^{\infty} 8z^2(e^{-z^2})^2 dz = \sqrt{2\pi}, \\
\|\partial_z^2 \tilde{\mathbf{w}}\|_2^2 &= \int_{-\infty}^{\infty} 2(4z^2-2)^2(e^{-z^2})^2 dz = 3\sqrt{2\pi}, \quad \text{and}
\end{aligned}$$

$$\int_{-\infty}^{\infty} |\tilde{\mathbf{w}} \cdot \partial_z^2 \tilde{\mathbf{w}}| dz \approx 3.79909.$$

Using computational methods to calculate the L^∞-norms for (6.15), we have

$$\begin{aligned} \|DF(\hat{\mathbf{u}})\|_\infty &\approx 6.6415, \\ \|DF(\hat{\mathbf{u}})^T\|_\infty &\approx 8, \\ \|DF(\hat{\mathbf{u}}) + DF(\hat{\mathbf{u}})^T\|_\infty &\approx 12, \quad \text{and} \\ \|DF(\hat{\mathbf{u}})^T DF(\hat{\mathbf{u}})\|_\infty &\approx 36. \end{aligned} \tag{6.22}$$

For this particular perturbation and set of parameters, we see that $\lambda_0 \approx 133.1909$, so the radius of our previously mentioned semi-circular contour, γ, does not need to be greater than $|\lambda| = \sqrt{\lambda_0} \approx 11.5408$. So, given a specific perturbation and parameter set, we can find an appropriate contour radius in our search for the point spectrum.

Since we observe changes in the essential spectrum for various values of Δ in (6.10), we investigate the Evans function output for each of the previous parameters sets yielding different values of Δ. The Evans function outputs are shown in Figures 6.6 and 6.7. For each output, we evaluated the Evans function along a semi-circular contour with radius 1000, significantly larger than the required bound found in the example above. Similarly, we calculated a bound for the parameter set corresponding to $\Delta = 0$ and $\Delta > 0$ using the same perturbation and found that the radius of γ did not need to be greater than 29.2199 and 22.4449, respectively. For each contour, the winding number about $\lambda = 0$ was zero, indicating a lack of point spectra within the semi-circular contour γ, and providing evidence for the spectral stability of the linearized system.

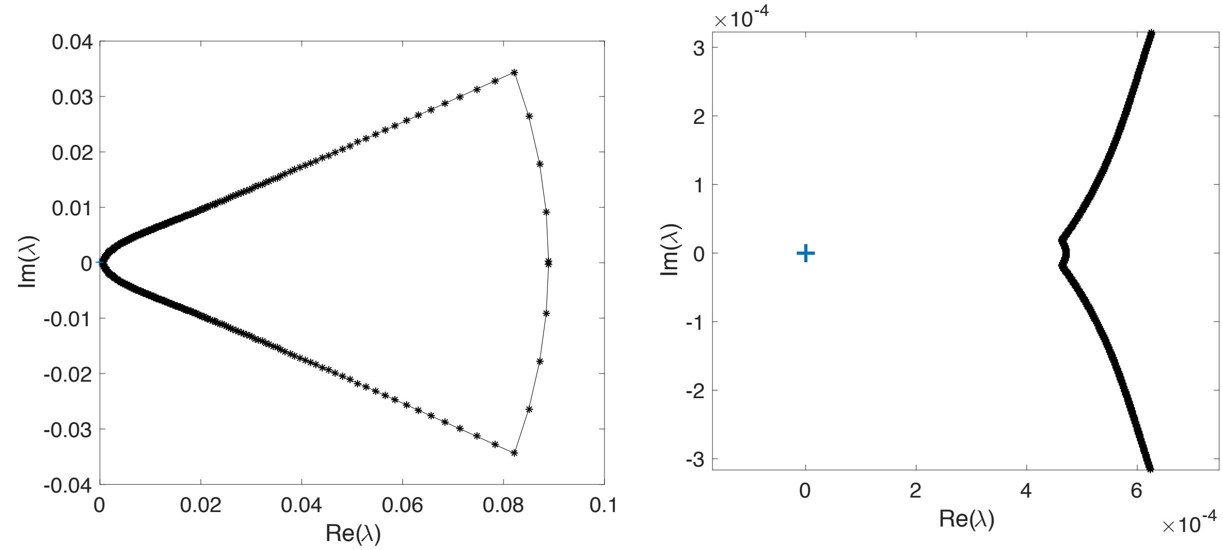

Figure 6.6: Evans function output for $\Delta < 0$ with parameters $\Gamma = 10$, $p = -4$, $\beta = 5$, and $\alpha = 1$. A blue "+" symbol indicates the origin on the far left of the plot. A magnification of the region around the origin is shown on the right.

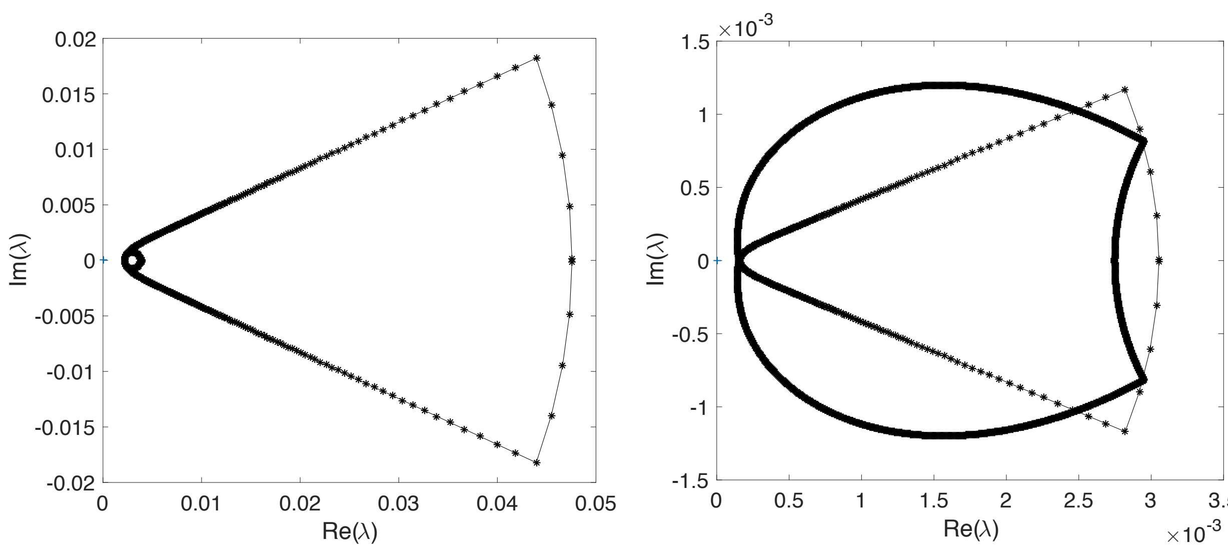

(a) $\Delta = 0$ with parameters $\Gamma \approx 15.069$, $p = -2$, $\beta = 5$, and $\alpha = (2 - \frac{2}{\Gamma})^p \approx 0.287$.

(b) $\Delta > 0$ with parameters $\Gamma = 20$, $p = -2$, $\beta = 0.5$, and $\alpha = 0.5$.

Figure 6.7: Evans function output for $\Delta = 0$ and $\Delta > 0$. A blue "+" symbol indicates the origin on the far left of each plot.

Again we refer to Theorem 6.1.4. For our system, the diffusion matrix is positive, the operator $\mathcal{L}$ satisfies the spectrum and eigenvalue requirements for the space $\mathcal{L}^2_\omega$ and for perturbations with the properties mentioned in the point spectrum analysis, so the spectral stability of the traveling wave solutions does imply nonlinear stability with a shift. $\square$

CHAPTER 7

Discussion and Conclusion

Our goal in starting this work was to gain more information about the system (1.2) presented in [1], particularly with respect to changes in the characteristics of traveling wave solutions due to the values of parameters p, Γ, and β (α held constant), and to use our observations to generate more insight into the system as a model for the spreading of social outbursts.

Through this process, we have identified parameter regimes that yield different numbers of steady states for the spatially homogeneous system and were able to classify those steady states using the help of AUTO. This led to the discovery of a small parameter set yielding four steady states. We can see that the existence of traveling wave solutions for system (1.2) depends only on the values of Γ and p and not β. In other words, for any β value, we can find parameters Γ and p that will yield traveling wave solutions. This can be interpreted in the following way: we have made the simplification of $\alpha = 1$, which is also the base level of social tension, so when the critical social tension level is equivalent to the base social tension level, we will see the spread of rioting behavior in the form of a traveling wave as long as the rate at which social tension reinforces rioting behavior, Γ, is sufficiently high, and it does not matter how fast a transition from an at rest state to an excited or rioting state occurs (this value is encapsulated by β). This is true for any value of p, meaning it does not matter whether rioting behavior is tension-enhancing ($p > 0$), tension-inhibiting ($p < 0$), or independent of social tension ($p = 0$).

There is still work to be done in this area, as we would like to be able to say something about the existence and stability of waves for the system with parameters that yield four steady states. We also would like to establish the exact parameter independence for the four steady state case. Based on numerics and the AUTO results, we suspect that the four steady state case starts appearing for p-values greater than three, but this is difficult to prove analytically. We also would like to either confirm or disprove the existence of *more* than four steady states. With five steady states, it is possible that we would begin to see systems of traveling waves, so this would be an interesting area of future study if there did exist a parameter regime yielding five steady states.

Through the numerical approximations of solutions, we have seen clear evidence of traveling wave solutions and have found differences in the monotonicity of these solutions based on the parameters. We know that we will only see non-monotone waves for $p < 0$. Because of this and because of the fact that we have seen clear evidence of a traveling peak in the 2005 France riot dataset, the data seems to support the theory that rioting behavior is tension-inhibiting (i.e., rioting provides a release of social tension) as opposed to tension-enhancing in the case of $p > 0$ (i.e., rioting leads to a slower decay of social tension). In the $p < 0$ regime, we see the full range of traveling wave behaviors: monotone waves, non-monotone waves, and oscillatory waves, but we have yet to understand the exact dependence on the parameters for these behaviors. It is likely that the classification of the non-trivial steady state, along with the relation between the eigenvectors of the linearized spatially homogeneous system and the nullclines could have some role in the distinction between monotone and purely non-monotone waves. We suspect that the oscillatory waves occur when the non-trivial steady state is classified as a stable spiral as opposed to a stable node. As mentioned in Chapter 3, these oscillations are more intense and visible by simple observation for β large. In terms of the physical interpretation of the system, this means that the faster the transition from a relaxed state to a rioting state occurs, the more intense the aftershocks for a riot will be. Future confirmation of these conjectures would provide even greater insight into the relationships of these parameters and their effect on the characteristics of riots.

Numerical approximation methods have also allowed us to estimate wave speed for our traveling wave solutions, and we have found support for the conjecture that our system follows the established findings for wave speed of the Fisher-KPP equation for $p = 0$. In addition, numerical experiments with wave speed support the idea that these same wave speed characteristics for the $p = 0$ case should apply for the monostable cases for $p > 0$ and $p < 0$. It should be possible to prove these results in the future. These results are important as they give a relationship between the speed of the spread of rioting behavior and the initial conditions of the system, or the characteristics of the triggering event. We see that for an initial triggering event that is less localized, the spread of the rioting behavior is faster.

For the monostable and bistable (two and three steady state) instances of our system for $p \geq 0$, we were able to prove the existence and stability of monotone traveling wave solutions using accepted theory. We also made use of the asymptotic decay rates for $p \geq 0$ presented in Chapter 5. In the monostable cases, we had to make use of a restricted class of perturbations to establish the stability results. We were also able to prove the stability of traveling wave solutions for $p < 0$, although proving the existence of such waves is still an open problem. As with wave speed, the $p < 0$ case was similar to the monostable $p \geq 0$ case in that the essential spectrum of the linearized operator needed to be shifted before continuing to prove stability. To deal with the location of the point spectrum for $p < 0$, we had to utilize a combination of numerical computation of the Evans function and the adjoint of the linearized operator in order to establish a bound on our search region for the point spectrum in the right half plane.

Proving existence and stability of traveling waves for specific parameter regimes allows us to make some assertions about the types of conditions that give rise to traveling waves and under what conditions those traveling waves will be more resilient (stable) to external forces. For example, for the two and three steady state cases (monostable and bistable cases) for $p \geq 0$, if Γ is sufficiently large and $p \leq 3$ (i.e., if the rate of self-excitation for the riots is large enough and the tension-enhancing quality of rioting behavior is not too high), we should see traveling waves of rioting behavior that are stable. We can make the same statement for $p > 3$; however, we have to place some restrictions on Γ and β to avoid the four steady state case. While we can say that traveling waves for $p < 0$ are stable, we are not yet able to prove that the waves we observed under numerical simulations exist. Given the similarities between the non-monotone waves observed in numerical simulations and the non-monotone waves observed in the 2005 France riots dataset, this would be an important next step in the continuing this work.

This system was developed with the intent to reproduce the dynamics of a complex human behavior and social interaction. Answering any of the open problems above will lead to a greater understanding of the dynamics that accompany the spread of riots.

APPENDIX A

Source Code for Numerics

A.1 AUTO Codes

A.1.1 riotbif.f90

```
!-----------------------------------------------------------------------
!-----------------------------------------------------------------------
!  riotbif.f90 - cusp normal form
!-----------------------------------------------------------------------
!-----------------------------------------------------------------------

SUBROUTINE FUNC(NDIM,U,ICP,PAR,IJAC,F,DFDU,DFDP)
!--------- ----

! Evaluates the algebraic equations or ODE right hand side

! Input arguments :
!      NDIM   :   Dimension of the algebraic or ODE system
!      U      :   State variables
!      ICP    :   Array indicating the free parameter(s)
!      PAR    :   Equation parameters

! Values to be returned :
!      F      :   Equation or ODE right hand side values

! Normally unused Jacobian arguments : IJAC, DFDU, DFDP (see manual)

  IMPLICIT NONE
  INTEGER, INTENT(IN) :: NDIM, IJAC, ICP(*)
  DOUBLE PRECISION, INTENT(IN) :: U(NDIM), PAR(*)
  DOUBLE PRECISION, INTENT(OUT) :: F(NDIM)
  DOUBLE PRECISION, INTENT(INOUT) :: DFDU(NDIM,NDIM),DFDP(NDIM,*)

  DOUBLE PRECISION x, gamma, beta, alpha, p

  x = U(1)
  gamma = PAR(1)
  beta = PAR(2)
  alpha = PAR(3)
  p = PAR(4)
  F(1)= gamma*(1-x)/(1+EXP(-beta*((1+x)**p-alpha)))-1

END SUBROUTINE FUNC
```

```
!----------------------------------------------------------------------
!----------------------------------------------------------------------

SUBROUTINE STPNT(NDIM,U,PAR,T)
!--------- -----

! Input arguments :
!      NDIM   :   Dimension of the algebraic or ODE system

! Values to be returned :
!      U      :   A starting solution vector
!      PAR    :   The corresponding equation-parameter values

! Note : For time- or space-dependent solutions this subroutine has
!        the scalar input parameter T contains the varying time or space
!        variable value.

  IMPLICIT NONE
  INTEGER, INTENT(IN) :: NDIM
  DOUBLE PRECISION, INTENT(INOUT) :: U(NDIM),PAR(*)
  DOUBLE PRECISION, INTENT(IN) :: T

! Initialize the equation parameters
! gamma, beta, alpha, p
! Run_01
! PAR(1:4) = (/ 2.0d0, 5.0d0, 1.0d0, 2.0d0/)

! Run_02
 PAR(1:4) = (/ 2.0d0, 5.0d0, 1.0d0, 1.0d0/)

! Run_03
! PAR(1:4) = (/ 2.0d0, 5.0d0, 1.0d0, 0.5d0/)

! Run_04
! PAR(1:4) = (/ 2.0d0, 5.0d0, 1.0d0, 1.5d0/)

 ! Run_05
 ! PAR(1:4) = (/ 2.0d0, 5.0d0, 1.0d0, 1.05d0/)

 ! Run_06
 ! PAR(1:4) = (/ 2.0d0, 5.0d0, 1.0d0, 2.5d0/)

 ! Run_07
 ! PAR(1:4) = (/ 2.0d0, 5.0d0, 1.0d0, 3.0d0/)

 ! Run_08
 ! PAR(1:4) = (/ 2.0d0, 5.0d0, 1.0d0, 3.5d0/)
```

```
 ! Run_09
 ! PAR(1:4) = (/ 2.0d0, 5.0d0, 1.0d0, 4.0d0/)

 ! Run_10
 ! PAR(1:4) = (/ 2.0d0, 5.0d0, 1.0d0, 4.5d0/)

 ! Run_11
 ! PAR(1:4) = (/ 2.0d0, 5.0d0, 1.0d0, 20.0d0/)

! Initialize the solution
  U(1) = 0.0d0

END SUBROUTINE STPNT

!----------------------------------------------------------------------
!----------------------------------------------------------------------

SUBROUTINE BCND(NDIM,PAR,ICP,NBC,U0,U1,FB,IJAC,DBC)
!--------- ----

! Boundary Conditions

! Input arguments :
!      NDIM   :   Dimension of the ODE system
!      PAR    :   Equation parameters
!      ICP    :   Array indicating the free parameter(s)
!      NBC    :   Number of boundary conditions
!      U0     :   State variable values at the left boundary
!      U1     :   State variable values at the right boundary

! Values to be returned :
!      FB     :   The values of the boundary condition functions

! Normally unused Jacobian arguments : IJAC, DBC (see manual)

  IMPLICIT NONE
  INTEGER, INTENT(IN) :: NDIM, ICP(*), NBC, IJAC
  DOUBLE PRECISION, INTENT(IN) :: PAR(*), U0(NDIM), U1(NDIM)
  DOUBLE PRECISION, INTENT(OUT) :: FB(NBC)
  DOUBLE PRECISION, INTENT(INOUT) :: DBC(NBC,*)

!X FB(1)=
!X FB(2)=

END SUBROUTINE BCND

!----------------------------------------------------------------------
!----------------------------------------------------------------------
```

```
SUBROUTINE ICND(NDIM,PAR,ICP,NINT,U,UOLD,UDOT,UPOLD,FI,IJAC,DINT)
!--------- ----

! Integral Conditions

! Input arguments :
!      NDIM   :   Dimension of the ODE system
!      PAR    :   Equation parameters
!      ICP    :   Array indicating the free parameter(s)
!      NINT   :   Number of integral conditions
!      U      :   Value of the vector function U at ‘time’ t

! The following input arguments, which are normally not needed,
! correspond to the preceding point on the solution branch
!      UOLD   :   The state vector at ’time’ t
!      UDOT   :   Derivative of UOLD with respect to arclength
!      UPOLD  :   Derivative of UOLD with respect to ‘time’

! Normally unused Jacobian arguments : IJAC, DINT

! Values to be returned :
!      FI     :   The value of the vector integrand

  IMPLICIT NONE
  INTEGER, INTENT(IN) :: NDIM, ICP(*), NINT, IJAC
  DOUBLE PRECISION, INTENT(IN) :: PAR(*)
  DOUBLE PRECISION, INTENT(IN) :: U(NDIM), UOLD(NDIM), UDOT(NDIM), UPOLD(NDIM)
  DOUBLE PRECISION, INTENT(OUT) :: FI(NINT)
  DOUBLE PRECISION, INTENT(INOUT) :: DINT(NINT,*)

!X FI(1)=

END SUBROUTINE ICND

!----------------------------------------------------------------------
!----------------------------------------------------------------------

SUBROUTINE FOPT(NDIM,U,ICP,PAR,IJAC,FS,DFDU,DFDP)
!--------- ----
!
! Defines the objective function for algebraic optimization problems
!
! Supplied variables :
!      NDIM   :   Dimension of the state equation
!      U      :   The state vector
!      ICP    :   Indices of the control parameters
!      PAR    :   The vector of control parameters
```

```
!
! Values to be returned :
!      FS      :   The value of the objective function
!
! Normally unused Jacobian argument : IJAC, DFDP

  IMPLICIT NONE
  INTEGER, INTENT(IN) :: NDIM, ICP(*), IJAC
  DOUBLE PRECISION, INTENT(IN) :: U(NDIM), PAR(*)
  DOUBLE PRECISION, INTENT(OUT) :: FS
  DOUBLE PRECISION, INTENT(INOUT) :: DFDU(NDIM),DFDP(*)

!X FS=

END SUBROUTINE FOPT

!----------------------------------------------------------------------
!----------------------------------------------------------------------

SUBROUTINE PVLS(NDIM,U,PAR)
!--------- ----

  IMPLICIT NONE
  INTEGER, INTENT(IN) :: NDIM
  DOUBLE PRECISION, INTENT(IN) :: U(NDIM)
  DOUBLE PRECISION, INTENT(INOUT) :: PAR(*)

!----------------------------------------------------------------------
! NOTE :
! Parameters set in this subroutine should be considered as ``solution
! measures'' and be used for output purposes only.
!
! They should never be used as `true'' continuation parameters.
!
! They may, however, be added as ``over-specified parameters'' in the
! parameter list associated with the AUTO-Constant NICP, in order to
! print their values on the screen and in the ``p.xxx file.
!
! They may also appear in the list associated with AUTO-Constant NUZR.
!
!----------------------------------------------------------------------
! For algebraic problems the argument U is, as usual, the state vector.
! For differential equations the argument U represents the approximate
! solution on the entire interval [0,1]. In this case its values must
! be accessed indirectly by calls to GETP, as illustrated below.
!----------------------------------------------------------------------
!
! Set PAR(2) equal to the L2-norm of U(1)
```

```
!X PAR(2)=GETP('NRM',1,U)
!
! Set PAR(3) equal to the minimum of U(2)
!X PAR(3)=GETP('MIN',2,U)
!
! Set PAR(4) equal to the value of U(2) at the left boundary.
!X PAR(4)=GETP('BV0',2,U)
!
! Set PAR(5) equal to the pseudo-arclength step size used.
!X PAR(5)=GETP('STP',1,U)
!
!----------------------------------------------------------------------
! The first argument of GETP may be one of the following:
!        'NRM' (L2-norm),     'MAX' (maximum),
!        'INT' (integral),    'BV0 (left boundary value),
!        'MIN' (minimum),     'BV1' (right boundary value).
!
! Also available are
!   'STP' (Pseudo-arclength step size used).
!   'FLD' (`Fold function', which vanishes at folds).
!   'BIF' (`Bifurcation function', which vanishes at singular points).
!   'HBF' (`Hopf function'; which vanishes at Hopf points).
!   'SPB' ( Function which vanishes at secondary periodic bifurcations).
!----------------------------------------------------------------------


END SUBROUTINE PVLS

!----------------------------------------------------------------------
!----------------------------------------------------------------------
```

A.1.2 c.riotbif

```
# ================================
# Run_01 Gamma start at 2.0, p = 2
# ================================
# parnames = {1:'gamma', 2:'beta', 3:'alpha', 4:'p'}
# unames = {1:'x'}
# NDIM=   1, IPS =   1, IRS =   0, ILP =   1
# ICP =  ['gamma', 'beta', 'alpha', 'p']
# NTST=   20, NCOL=   4, IAD =   3, ISP =   2, ISW = 1, IPLT= 0, NBC= 0, NINT= 0
# NMX=  2000, NPR=   20, MXBF=   0, IID =   3, ITMX= 8, ITNW= 7, NWTN= 3, JAC= 0
# EPSL= 1e-06, EPSU = 1e-06, EPSS =0.0001
# DS  =  0.001, DSMIN= 0.0005, DSMAX=   0.01, IADS=   1
# NPAR = 4, THL =  {}, THU =  {}
# UZSTOP = {'gamma': [1.1, 25.0]}

# =================================
# Run_02 Gamma start at 2.0, p = 1
# =================================
 parnames = {1:'gamma', 2:'beta', 3:'alpha', 4:'p'}
 unames = {1:'x'}
 NDIM=   1, IPS =   1, IRS =   0, ILP =   1
 ICP =  ['gamma', 'beta', 'alpha', 'p']
 NTST=   20, NCOL=   4, IAD =   3, ISP =   2, ISW = 1, IPLT= 0, NBC= 0, NINT= 0
 NMX=  2000, NPR=   20, MXBF=   0, IID =   3, ITMX= 8, ITNW= 7, NWTN= 3, JAC= 0
 EPSL= 1e-06, EPSU = 1e-06, EPSS =0.0001
 DS  =  0.001, DSMIN= 0.0005, DSMAX=   0.01, IADS=   1
 NPAR = 4, THL =  {}, THU =  {}
 UZSTOP = {'gamma': [1.001, 25.0]}

# ==================================
# Run_03 Gamma start at 2.0, p = 0.5
# ==================================
# parnames = {1:'gamma', 2:'beta', 3:'alpha', 4:'p'}
# unames = {1:'x'}
# NDIM=   1, IPS =   1, IRS =   0, ILP =   1
# ICP =  ['gamma', 'beta', 'alpha', 'p']
# NTST=   20, NCOL=   4, IAD =   3, ISP =   2, ISW = 1, IPLT= 0, NBC= 0, NINT= 0
# NMX=  2000, NPR=   20, MXBF=   0, IID =   3, ITMX= 8, ITNW= 7, NWTN= 3, JAC= 0
# EPSL= 1e-06, EPSU = 1e-06, EPSS =0.0001
# DS  =  0.001, DSMIN= 0.0005, DSMAX=   0.01, IADS=   1
# NPAR = 4, THL =  {}, THU =  {}
# UZSTOP = {'gamma': [1.1, 25.0]}

# ==================================
# Run_04 Gamma start at 2.0, p = 1.5
# ==================================
```

```
# parnames = {1:'gamma', 2:'beta', 3:'alpha', 4:'p'}
# unames = {1:'x'}
# NDIM=   1, IPS =   1, IRS =   0, ILP =   1
# ICP =  ['gamma', 'beta', 'alpha', 'p']
# NTST=   20, NCOL=   4, IAD =   3, ISP =   2, ISW = 1, IPLT= 0, NBC= 0, NINT= 0
# NMX=  2000, NPR=   20, MXBF=   0, IID =   3, ITMX= 8, ITNW= 7, NWTN= 3, JAC= 0
# EPSL= 1e-06, EPSU = 1e-06, EPSS =0.0001
# DS  =  0.001, DSMIN= 0.0005, DSMAX=   0.01, IADS=   1
# NPAR = 4, THL =  {}, THU =  {}
# UZSTOP = {'gamma': [1.1, 25.0]}

# ===================================
# Run_05 Gamma start at 2.0, p = 1.05
# ===================================
# parnames = {1:'gamma', 2:'beta', 3:'alpha', 4:'p'}
# unames = {1:'x'}
# NDIM=   1, IPS =   1, IRS =   0, ILP =   1
# ICP =  ['gamma', 'beta', 'alpha', 'p']
# NTST=   20, NCOL=   4, IAD =   3, ISP =   2, ISW = 1, IPLT= 0, NBC= 0, NINT= 0
# NMX=  520, NPR=   20, MXBF=   0, IID =   3, ITMX= 8, ITNW= 7, NWTN= 3, JAC= 0
# EPSL= 1e-06, EPSU = 1e-06, EPSS =0.0001
# DS  =  0.001, DSMIN= 0.0005, DSMAX=   0.01, IADS=   1
# NPAR = 4, THL =  {}, THU =  {}
# UZSTOP = {'gamma': [1.1, 25.0]}

# ===================================
# Run_06 Gamma start at 2.0, p = 2.5
# ===================================
# parnames = {1:'gamma', 2:'beta', 3:'alpha', 4:'p'}
# unames = {1:'x'}
# NDIM=   1, IPS =   1, IRS =   0, ILP =   1
# ICP =  ['gamma', 'beta', 'alpha', 'p']
# NTST=   20, NCOL=   4, IAD =   3, ISP =   2, ISW = 1, IPLT= 0, NBC= 0, NINT= 0
# NMX=  2000, NPR=   20, MXBF=   0, IID =   3, ITMX= 8, ITNW= 7, NWTN= 3, JAC= 0
# EPSL= 1e-06, EPSU = 1e-06, EPSS =0.0001
# DS  =  0.001, DSMIN= 0.0005, DSMAX=   0.01, IADS=   1
# NPAR = 4, THL =  {}, THU =  {}
# UZSTOP = {'gamma': [1.1, 25.0]}

# ===================================
# Run_07 Gamma start at 2.0, p = 3.0
# ===================================
# parnames = {1:'gamma', 2:'beta', 3:'alpha', 4:'p'}
# unames = {1:'x'}
# NDIM=   1, IPS =   1, IRS =   0, ILP =   1
# ICP =  ['gamma', 'beta', 'alpha', 'p']
# NTST=   20, NCOL=   4, IAD =   3, ISP =   2, ISW = 1, IPLT= 0, NBC= 0, NINT= 0
# NMX=  2000, NPR=   20, MXBF=   0, IID =   3, ITMX= 8, ITNW= 7, NWTN= 3, JAC= 0
```

```
# EPSL= 1e-06, EPSU = 1e-06, EPSS =0.0001
# DS  =  0.001, DSMIN= 0.0005, DSMAX=   0.01, IADS=   1
# NPAR = 4, THL =  {}, THU =  {}
# UZSTOP = {'gamma': [1.1, 25.0]}

# ===================================
# Run_08 Gamma start at 2.0, p = 3.5
# ===================================
# parnames = {1:'gamma', 2:'beta', 3:'alpha', 4:'p'}
# unames = {1:'x'}
# NDIM=   1, IPS =   1, IRS =   0, ILP =   1
# ICP =  ['gamma', 'beta', 'alpha', 'p']
# NTST=   20, NCOL=   4, IAD =   3, ISP =   2, ISW = 1, IPLT= 0, NBC= 0, NINT= 0
# NMX=  2000, NPR=   20, MXBF=   0, IID =   3, ITMX= 8, ITNW= 7, NWTN= 3, JAC= 0
# EPSL= 1e-06, EPSU = 1e-06, EPSS =0.0001
# DS  =  0.001, DSMIN= 0.0005, DSMAX=   0.01, IADS=   1
# NPAR = 4, THL =  {}, THU =  {}
# UZSTOP = {'gamma': [1.1, 25.0]}

# ===================================
# Run_09 Gamma start at 2.0, p = 4
# ===================================
# parnames = {1:'gamma', 2:'beta', 3:'alpha', 4:'p'}
# unames = {1:'x'}
# NDIM=   1, IPS =   1, IRS =   0, ILP =   1
# ICP =  ['gamma', 'beta', 'alpha', 'p']
# NTST=   20, NCOL=   4, IAD =   3, ISP =   2, ISW = 1, IPLT= 0, NBC= 0, NINT= 0
# NMX=  2000, NPR=   20, MXBF=   0, IID =   3, ITMX= 8, ITNW= 7, NWTN= 3, JAC= 0
# EPSL= 1e-06, EPSU = 1e-06, EPSS =0.0001
# DS  =  0.001, DSMIN= 0.0005, DSMAX=   0.01, IADS=   1
# NPAR = 4, THL =  {}, THU =  {}
# UZSTOP = {'gamma': [1.1, 25.0]}

# ===================================
# Run_10 Gamma start at 2.0, p = 4.5
# ===================================
# parnames = {1:'gamma', 2:'beta', 3:'alpha', 4:'p'}
# unames = {1:'x'}
# NDIM=   1, IPS =   1, IRS =   0, ILP =   1
# ICP =  ['gamma', 'beta', 'alpha', 'p']
# NTST=   20, NCOL=   4, IAD =   3, ISP =   2, ISW = 1, IPLT= 0, NBC= 0, NINT= 0
# NMX=  2000, NPR=   20, MXBF=   0, IID =   3, ITMX= 8, ITNW= 7, NWTN= 3, JAC= 0
# EPSL= 1e-06, EPSU = 1e-06, EPSS =0.0001
# DS  =  0.001, DSMIN= 0.0005, DSMAX=   0.01, IADS=   1
# NPAR = 4, THL =  {}, THU =  {}
# UZSTOP = {'gamma': [1.1, 25.0]}

# ===================================
```

```
# Run_11 Gamma start at 2.0, p = 20
# ==================================
# parnames = {1:'gamma', 2:'beta', 3:'alpha', 4:'p'}
# unames = {1:'x'}
# NDIM=   1, IPS =   1, IRS =   0, ILP =   1
# ICP =  ['gamma', 'beta', 'alpha', 'p']
# NTST=   20, NCOL=   4, IAD =   3, ISP =   2, ISW = 1, IPLT= 0, NBC= 0, NINT= 0
# NMX=  2000, NPR=   20, MXBF=   0, IID =   3, ITMX= 8, ITNW= 7, NWTN= 3, JAC= 0
# EPSL= 1e-06, EPSU = 1e-06, EPSS =0.0001
# DS  =  0.001, DSMIN= 0.0005, DSMAX=   0.01, IADS=   1
# NPAR = 4, THL =  {}, THU =  {}
# UZSTOP = {'gamma': [1.1, 25.0]}
```

A.1.3 riotbif.auto

```
#===================
# AUTO Demo riotbif
#===================

# Load the files riotbif.f90 and c.riotbif into the AUTO
# command interpreter.
riotbif = load('riotbif')
# Run and store the result in the Python variable mu
gamma = run(riotbif)
# Run backwards, and append to mu
gamma = gamma + run(riotbif,DS='-')
# Load continuation from first fold point LP
lp1 = load(gamma('LP1'), ISW=2)
# Run and save in file riotbif
riotbif = run(lp1)
# Run backwards and append to riotbif
riotbif = riotbif + run(lp1,DS='-')


# save and plot
save(gamma,'gamma_run11')
save(riotbif,'riotbif_run11')
# export in MATLAB readable file
gamma.writeRawFilename('gamma_run11.dat')
riotbif.writeRawFilename('riotbif_run11.dat')

# Found extra fold point for gamma in Run 03 for p = 0.5
```

A.2 Mathematica Code

A.2.1 steadyStates.nb

```
Clear["Global‘*"];
\[Alpha] = 1;

p = 1;
v1[u_] := (-1/\[Beta]) Log[\[CapitalGamma] (1 - u) - 1] + \[Alpha];
v2[u_] := (1 + u)^p;
derivv[u_] := v2[u] - v1[u]; u1 =
Solve[-p (1 + u)^(p -
        1) \[Beta] (-1 + (1 - u) \[CapitalGamma]) + \[CapitalGamma] ==
    0, u];
bd1 = derivv[u] /. {u1};
c1 = ContourPlot[
   bd1 == 0, {\[CapitalGamma], 1.4, 1.6}, {\[Beta], 8, 10}];
Show[c1]

p = 2;
v1[u_] := (-1/\[Beta]) Log[\[CapitalGamma] (1 - u) - 1] + \[Alpha];
v2[u_] := (1 + u)^p;
derivv[u_] := v2[u] - v1[u]; {u1, u2} =
 Solve[-p (1 + u)^(p -
        1) \[Beta] (-1 + (1 - u) \[CapitalGamma]) + \[CapitalGamma] ==
    0, u];
bd1 = derivv[u] /. {u1};
bd2 = derivv[u] /. {u2};
c1 = ContourPlot[bd1 == 0, {\[CapitalGamma], 1, 10}, {\[Beta], 0, 10}];
c2 = ContourPlot[bd2 == 0, {\[CapitalGamma], 1, 10}, {\[Beta], 0, 10}];
Show[c1, c2]

p = 3;
v1[u_] := (-1/\[Beta]) Log[\[CapitalGamma] (1 - u) - 1] + \[Alpha];
v2[u_] := (1 + u)^p;
derivv[u_] := v2[u] - v1[u]; {u1, u2, u3} =
 Solve[-p (1 + u)^(p -
        1) \[Beta] (-1 + (1 - u) \[CapitalGamma]) + \[CapitalGamma] ==
    0, u];
bd1 = derivv[u] /. {u1};
bd2 = derivv[u] /. {u2};
bd3 = derivv[u] /. {u3};
c1 = ContourPlot[bd1 == 0, {\[CapitalGamma], 1, 10}, {\[Beta], 0, 10}];
c1 = ContourPlot[
   bd1 == 0, {\[CapitalGamma], 1.999, 2.001}, {\[Beta], 0.65, .68}];
c2 = ContourPlot[bd2 == 0, {\[CapitalGamma], 1, 10}, {\[Beta], 0, 10}];
c3 = ContourPlot[bd3 == 0, {\[CapitalGamma], 1, 10}, {\[Beta], 0, 10}];
```

```
Show[c1, c3]

p = 4;
v1[u_] := (-1/\[Beta]) Log[\[CapitalGamma] (1 - u) - 1] + \[Alpha];
v2[u_] := (1 + u)^p;
derivv[u_] := v2[u] - v1[u]; {u1, u2, u3, u4} =
 Solve[-p (1 + u)^(p -
        1) \[Beta] (-1 + (1 - u) \[CapitalGamma]) + \[CapitalGamma] ==
    0, u];
bd1 = derivv[u] /. {u1};
bd2 = derivv[u] /. {u2};
bd3 = derivv[u] /. {u3};
bd4 = derivv[u] /. {u4};
c1 = ContourPlot[bd1 == 0, {\[CapitalGamma], 1, 10}, {\[Beta], 0, 10}];
c2 = ContourPlot[bd2 == 0, {\[CapitalGamma], 1, 10}, {\[Beta], 0, 10}];
c3 = ContourPlot[bd3 == 0, {\[CapitalGamma], 1, 10}, {\[Beta], 0, 10}];
c4 = ContourPlot[bd4 == 0, {\[CapitalGamma], 1, 10}, {\[Beta], 0, 10}];
(*c1 = ContourPlot[bd1 == 0,{\[CapitalGamma],1.99,2.008},{\[Beta],\
0.46,0.5}];
c2 = ContourPlot[bd2 == 0,{\[CapitalGamma],1.99,2.005},{\[Beta],0.\
3,0.5}];
c3 = ContourPlot[bd3 == 0,{\[CapitalGamma],1.99,2.005},{\[Beta],0.\
3,0.5}];
c4 = ContourPlot[bd4 == 0,{\[CapitalGamma],1.99,2.005},{\[Beta],0.\
3,0.5}];*)
Show[c1, c2, c3, c4]
```

A.3 MATLAB Codes

A.3.1 phasePlane.m

```
%% Phase Plane Portrait
% creates phase plane portrait of for spatially homogeneous riot model
close all; clc;
clear all;


filename = 'phase_plane_ode_ppos_4int.pdf';
p.gamma = 2.0026;
p.beta = 0.4021;
p.ppar = 4.5;
p.alpha = 1;
umin = [-0.1 0.5];
umax = [0.34 3.5];

% filename = 'phase_plane_ode_ppos_3int.pdf';
% p.gamma = 1.75;
% p.beta = 3;
% p.ppar = 2;
% p.alpha = 1;
% umin = [-0.1 0.7];
% umax = [0.5 2.2];

% filename = 'phase_plane_ode_ppos_2int.pdf'
% p.gamma = 2.5;
% p.beta = 3;
% p.ppar = 2;
% p.alpha = 1;
% umin = [-0.1 0];
% umax = [0.7 3];

%
% filename = 'phase_plane_ode_p0_borderline.pdf';
% p.gamma = 4;
% p.beta = 5;
% p.ppar = 0;
% p.alpha = 1;
% umin = [-0.1 0];
% umax = [1.1 1.2];

% filename = 'phase_plane_ode_g2_borderline.pdf';
% p.gamma = 2;
% p.beta = 5;
% p.ppar = 1;
```

```
% p.alpha = 1;
% umin = [-0.1 0];
% umax = [0.6 1.6];

% filename = 'phase_plane_ode_p0.pdf';
% p.gamma = 100;
% p.beta = 5;
% p.ppar = 0;
% p.alpha = 1;
% umin = [-0.1 0];
% umax = [1.2 1.2];

% filename = 'phase_plane_ode_pneg_node.pdf';
% p.gamma = 3;
% p.beta = 1;
% p.ppar = -2;
% p.alpha = 1;
% umin = [-0.1 0];
% umax = [1.2 1.2];

% filename = 'phase_plane_ode_pneg_spiral.pdf';
% p.gamma = 100;
% p.beta = 20;
% p.ppar = -2;
% p.alpha = 1;
% umin = [-0.1 0];
% umax = [1.2 1.2];

f = @(t,U) [p.gamma*U(1)*(1-U(1))/(1+exp(-p.beta*(U(2)-p.alpha)))-U(1);...
            -U(2)/(1+U(1))^p.ppar+1];
null1 = @(v) 0;
null2 = @(u) -(1/p.beta)*log(p.gamma*(1-u)-1)+p.alpha;
null3 = @(u) (1+u).^p.ppar;

u1 = linspace(umin(1),umax(1),30);
u2 = linspace(umin(2),umax(2),30);

% for Parameter Sets 1 and 2
% unull = linspace(umin(1),1-1/p.gamma,100);
% for Parameter Set 3
unull = linspace(umin(1),1-1/p.gamma,5000);
unull2 = linspace(umin(1),umax(1),100);

% creates two matrices one for all the u-values on the grid, and one for
% all the v-values on the grid. Note that u and v are matrices of the same
% size and shape, in this case 20 rows and 20 columns

[u,v] = meshgrid(u1,u2);
```

```
x = zeros(size(u));
y = zeros(size(u));

% we can use a single loop over each element to compute the derivatives at
% each point (u1, u2) and normalize to create velocity vectors of same
% length
t=0; % we want the derivatives at each point at t=0, i.e. the starting time
for i = 1:numel(u)
    Uprime = f(t,[u(i); v(i)]);
    x(i) = Uprime(1)/sqrt(Uprime(1)^2+Uprime(2)^2);
    y(i) =  Uprime(2)/sqrt(Uprime(1)^2+Uprime(2)^2);
%     x(i) = Uprime(1);
%     y(i) = Uprime(2);
end

%%
U = null_intersect(p);

% use scale of 0.5 to make arrows for figure more visible
titlestring = ['Phase Plane: ','\Gamma = ',...
    num2str(p.gamma),', \beta = ',num2str(p.beta),', \alpha = ',...
    num2str(p.alpha),', p = ',num2str(p.ppar)];
h=figure(1)
quiver(u(2:end-1,2:end-1),v(2:end-1,2:end-1),...
    x(2:end-1,2:end-1),y(2:end-1,2:end-1),0.5);
axis([umin(1) umax(1) umin(2) umax(2)])
set(gca,'FontSize',20)
% title(titlestring, 'FontSize', 18)
xlabel('u')
ylabel('v')

if (isempty(U))
% plot the nullclines
    hold on
    plot([0 0],[umin(2) umax(2)],'Color',[0.8500 0.3250 0.0980],...
        'LineWidth',1.5)
    plot(unull(1:(end-1)),null2(unull(1:(end-1))),'Color',...
        [0.8500 0.3250 0.0980],'LineWidth',1.5)
    plot(unull2,null3(unull2),'Color',[0.9290 0.6940 0.1250],...
        'LineWidth',1.5)
    plot(0, 1,'o','Color','black', 'MarkerSize', 16)
else
    hold on
    plot([0 0],[umin(2) umax(2)],'Color',[0.8500 0.3250 0.0980],...
        'LineWidth',1.5)
    plot(unull(1:(end-1)),null2(unull(1:(end-1))),'Color',...
        [0.8500 0.3250 0.0980],'LineWidth',1.5)
```

```
    plot(unull2,null3(unull2),'Color',[0.9290 0.6940 0.1250],...
        'LineWidth',1.5)
    plot(0, 1,'o','Color','black', 'MarkerSize', 16)
    plot(U(1,:),U(2,:),'o','Color','black', 'MarkerSize', 16)
end

set(h,'Units','Inches');
pos = get(h,'Position');
set(h,'PaperPositionMode','Auto','PaperUnits','Inches',...
    'PaperSize',[pos(3), pos(4)])
print(h,filename,'-dpdf','-r0')
```

A.3.2 bifurcation.ppos.m

```
clear all; clc; close all;

fu = @(u,v,p) p.gamma*(1-2*u)./(1+exp(-p.beta*(v-p.alpha))) - 1;
fv = @(u,v,p) p.gamma*p.beta*exp(-p.beta*(v-p.alpha)).*u.*(1-u)./...
    (1+exp(-p.beta*(v-p.alpha))).^2;
gu = @(u,v,p) p.ppar*v./(1+u).^(p.ppar+1);
gv = @(u,v,p) -1/(1+u).^p.ppar;

filename = 'steady_states_common_ppos305_zoom.pdf';
p.ppar = 3.05;
p.alpha = 1;
gamma = linspace(1.999999,2.000001,801);
beta = linspace(0.6556,0.6557,801);
% gamma = linspace(1.0001,5,400);
% beta = linspace(0.0001,10,200);

% filename = 'steady_states_common_ppos10_zoom.pdf';
% p.ppar = 4.5;
% p.alpha = 1;
% gamma = linspace(1.98,2.03,501);
% beta = linspace(0.36,0.46,401);

% filename = 'steady_states_common_ppos01.pdf';
% p.ppar = 2;
% p.alpha = 1;
% gamma = linspace(1.0001,5,400);
% beta = linspace(0.0001,10,200);

% filename = 'steady_states_common_ppos02.pdf';
% p.ppar = 1;
% p.alpha = 1;
% gamma = linspace(1.0001,5,400);
% beta = linspace(0.0001,10,200);

% filename = 'steady_states_common_ppos03.pdf';
% p.ppar = 0.5;
% p.alpha = 1;
% gamma = linspace(1.0001,5,400);
% beta = linspace(0.0001,10,200);

% filename = 'steady_states_common_ppos04.pdf';
% p.ppar = 1.5;
% p.alpha = 1;
% gamma = linspace(1.0001,5,400);
% beta = linspace(0.0001,10,200);
```

```
% filename = 'steady_states_common_ppos06.pdf';
% p.ppar = 2.5;
% p.alpha = 1;
% gamma = linspace(1.0001,5,400);
% beta = linspace(0.0001,10,200);

% filename = 'steady_states_common_ppos07.pdf';
% p.ppar = 3;
% p.alpha = 1;
% gamma = linspace(1.0001,5,400);
% beta = linspace(0.0001,10,200);

% filename = 'steady_states_common_ppos08.pdf';
% p.ppar = 3.5;
% p.alpha = 1;
% gamma = linspace(1.0001,5,400);
% beta = linspace(0.0001,10,200);

% filename = 'steady_states_common_ppos09.pdf';
% p.ppar = 4;
% p.alpha = 1;
% gamma = linspace(1.0001,5,400);
% beta = linspace(0.0001,10,200);

% filename = 'steady_states_common_ppos10.pdf';
% p.ppar = 4.5;
% p.alpha = 1;
% gamma = linspace(1.0001,5,400);
% beta = linspace(0.0001,10,200);

[G,B] = meshgrid(gamma,beta);
numInts = zeros(size(G));

% for p>0
% for beta vs. Gamma, plots number of non-trivial intersections
for i = 1:numel(G)
    p.gamma = G(i);
    p.beta = B(i);
    U = null_intersect(p);
    [m,n]=size(U);
    numInts(i) = n+1;
end

%%
filename = 'steady_states_common_ppos305_zoom.pdf';
h = figure(3);
contourf(gamma, beta, numInts, 'LevelList', [1 2 3 4])
```

```
set(gca,'FontSize',22)
xlabel('\Gamma')
ylabel('\beta')
caxis([1 4])
map = pink(4);
colormap(map)
% colorbar('Position', [0.53 0.68 0.05 0.20],'Ticks',...
%[1.375,2.125,2.875, 3.625],'TickLabels',{'1 steady state',...
%'2 steady states','3 steady states','4 steady states'})

set(h,'Units','Inches');
pos = get(h,'Position');
set(h,'PaperPositionMode','Auto','PaperUnits','Inches',...
    'PaperSize',[pos(3), pos(4)])
print(h,filename,'-dpdf','-r400')

%%
h = figure(3)
contourf(gamma, beta, numInts, 'LevelList', [1 2 3 4])
set(gca,'FontSize',22)
text(2.001,0.392,'\beta_1','FontSize',22)
text(1.9965,0.438,'\beta_2','FontSize',22)
text(1.989,0.415,'\Gamma_1','FontSize',22)
text(2.0068,0.408,'\Gamma_2','FontSize',22)
xlabel('\Gamma')
ylabel('\beta')
caxis([1 4])
map = pink(4);
colormap(map)
colorbar('Position', [0.53 0.68 0.05 0.20],'Ticks',...
    [1.375,2.125,2.875, 3.625],'TickLabels',{'1 steady state',...
    '2 steady states','3 steady states','4 steady states'})

set(h,'Units','Inches');
pos = get(h,'Position');
set(h,'PaperPositionMode','Auto','PaperUnits','Inches',...
    'PaperSize',[pos(3), pos(4)])
print(h,filename,'-dpdf','-r400')
```

A.3.3 `PDESolver.m`

This program solves the time evolution problem for our system. Note that the program utilizes the function following, `null_intersect.m`.

```
%% pde system solver
clear all; close all; clc;

%set x steps
xmin = 0;
% xmax = 500;
xmax = 100;

% n = 20000;
n = 4000;
X = linspace(xmin, xmax, n+1)';

T = 0;

delx = (xmax - xmin)/n;
delt = 1/10000;
% delt=1/8000;

%set parameters
A = 10;
gam = 80;
p = -4;
d1 = 1;
d2 = 1;

a = 1;
vb = 1;
u0 = 1;
bet = 4;

vstart = 3.5;

r.gamma = gam;
r.ppar = p;
r.beta = bet;
r.alpha = a;

SP = null_intersect(r);


%set initial conditions
```

```
%     uinit = A*exp(-0.5*X)+SP(1,1);
    uinit = A*(X == xmin);%((xmax-xmin)/2));

    %uinit = A*ones(n+1,1);
    vinit = vstart*ones(n+1,1);

%set functions f and g
f = @(u, v) gam*u.*(u0-u)./(1+exp(-bet*(v-a))) - u;
g = @(u, v) -v./((1 + u).^p) + vb;

%set coefficient matrices for u and v
c1 = delt*d1/(delx)^2;
c2 = delt*d2/(delx)^2;

%used no flux boundary conditions; creates tridiagonal matrix with nonzero
%entries in top right and bottom left corners (for BC)
ec = ones(n+1,1);
ed = ones(n-1,1);
B1 = spdiags([c1*[ed; 2; 2] (1-2*c1)*ec c1*[2; 2; ed]], [-1 0 1], n+1, n+1);
B2 = spdiags([c2*[ed; 2; 2] (1-2*c2)*ec c2*[2; 2; ed]], [-1 0 1], n+1, n+1);

uprev = uinit;
vprev = vinit;

%timesteps
U = zeros(n+1,1);
V = zeros(n+1,1);

figure(1)
%calculate time steps:
while(T<=500000)
    if mod(T,50000)==0
        disp(num2str(T))
        plot(X,U,X,V)
        hold on
    end
    U = B1*uprev + delt*f(uprev,vprev);
    V = B2*vprev + delt*g(uprev,vprev);
    uprev = U;
    vprev = V;
    T = T + 1;
end
```

A.3.4 null_intersect.m

```
function [ out ] = null_intersect( p )
%
% Returns: the stable steady states of the system given specific parameter
% values
%
% result is a 2 by n matrix (n being the number of roots returned.

%clc;
null = @(u) p.gamma*(1-u)./(1+exp(-p.beta*((1+u).^p.ppar-p.alpha))) - 1;
vfun = @(u) (1+u).^p.ppar;
U = linspace(0,1,200);

out = null(U);
changenull = diff(out>0);

% p
% find(changenull == 1)
% find(changenull == -1)

% this version throws error for 3 non trivial intersections
% sideL = [find(changenull == 1); find(changenull == -1)];
% use this for counting number of intersections
sides = [find(changenull == 1) find(changenull == -1)];
sideL = sort(sides);
out = zeros(2,length(sideL));

% if (length(sideL)>1)
%     fprintf('More than one root for nullcline found.')
% end

for i=1:length(sideL)
    x0 = [U(sideL(i)) U(sideL(i)+1)];
    uroot = fzero(null,x0);
    out(1,i) = uroot;
    out(2,i) = vfun(uroot);
end

end
```

A.3.5 `riotmodel_cparam.m`

The following program solves the first order system of ODEs mentioned in Chapter 3 for a traveling wave profile. It makes use of the built-in MATLAB solver *bvp5c* and also calls the separate, altered, STABLAB functions `@double_Fc`, `@Fc`, which follow directly. The STABLAB function `@projection1` is also utilized by this program, but this function will not be included in this work as it is part of the standard STABLAB library and has not been altered for its use in this program.

```
function [out,proj] = riotmodel_cparam()

%%Uses projective boundary conditions and a phase condition to solve for
%%traveling wave profile of riot model with specified wave speed and tries to
%find specified wave speed p.c over
%%split finite domain.  Graphs result along with initial guess
%%use param = 4, s.I = 80, 800 points for four intersection case

global s p b

%d, gamma are parameters;
% filename = 'ppos_monotone_wave_4int.pdf';
p.beta = 0.4021;
p.gamma = 2.0026;
p.ppar =4.5;

% p.beta = 9;
% p.gamma = 1.5;
% p.ppar =1;

p.alpha = 1;
param= 4;  %starting guess for wave speed
p.d = [1;1];

U = null_intersect(p);
if(numel(U)==2)
    p.ul=[U; 0;0];
    p.ur=[0;1;0;0];
    p.pin = 0.1;
elseif(numel(U)==4)
    p.ul=[U(:,2);0;0];
    p.ur=[0;1;0;0];
    p.pin = 0.1;
else
    p.ul=[U(:,3);0;0]
    p.ur=[U(:,1);0;0]
```

```
%     p.ur = [0;1;0;0]
    p.pin = 0.1;
end


%structure variables
s.I=80;
s.larray=[5;6;7;8];
s.rarray=[1;2;3;4];
s.side=1;

%dependent structure variables
s.R=s.I;
s.L=-s.I;

s.sol = getprofile2(param);
out = [min([real(s.sol.y(5,:)) real(s.sol.y(1,:))]) ...
     min([s.sol.y(5,:) s.sol.y(1,:)]) sum(sum(abs(imag(s.sol.y))))>0];
proj = s.sol;


%%
s.I = 80;
filename = 'ppos_monotone_wave_4int.pdf';
h=figure(1)
plot(-proj.x, proj.y(5,:),'Color','blue')
hold on
plot(-proj.x, proj.y(6,:),'Color','red')
plot(proj.x,proj.y(1,:),'Color','blue')
plot(proj.x,proj.y(2,:),'Color','red')
set(gca,'FontSize',20)
% axis([-s.I s.I 0 3.5])
xlabel('x')
ylabel('u, v')
legend('u(x,t)','v(x,t)')
% titlestring = ['Solution Profiles \Gamma = ',num2str(p.gamma),...
%     ', \beta = ',num2str(p.beta),', \alpha = ',num2str(p.alpha), ', p = ',...
%     num2str(p.ppar)];
% title(titlestring,'FontSize',18)
hold off

set(h,'Units','Inches');
pos = get(h,'Position');
set(h,'PaperPositionMode','Auto','PaperUnits','Inches','PaperSize',[pos(3), pos(4)])
print(h,filename,'-dpdf','-r0')

%%%%%%%%%%%%%%%%%%%%%%%%%%%%%%%%%%%%%%%%%%%%%%%%%%%%%%%%%%%%
function sol = getprofile2(param)
```

```
global s p
% BVP solver

options = bvpset('RelTol', 1e-6, 'AbsTol', 1e-8,'Nmax', 20000);
solinit = bvpinit(linspace(0,s.I,800),@guess2, param);
sol = bvp5c(@double_Fc,@bc2,solinit,options);
%%%%%%%%%%%%%%%%%%%%%%%%%%%%%%%%%%%%%%%%%%%%%%%%%%%%%%%%%%%
function out = guess2(x)
global s p
initval = @(x) (1+exp((x)./sqrt(6))).^-2;
initvalprime = @(x) (-2/sqrt(6))*(1+exp((x)./sqrt(6))).^(-3).*exp((x)./sqrt(6));

out = [initval((s.R/s.I)*x);
    initval(-(s.R/s.I)*x);
    initvalprime((s.R/s.I)*x);
    initvalprime(-(s.R/s.I)*x)
    initval((s.L/s.I)*x);
    initval(-(s.L/s.I)*x);
    initvalprime((s.L/s.I)*x);
    initvalprime(-(s.L/s.I)*x)
    ];
%%%%%%%%%%%%%%%%%%%%%%%%%%%%%%%%%%%%%%%%%%%%%%%%%%%%%%%%%%%
function out = bc2(ya,yb,param)
global s b p

AM = Flinear(p.ul,param);
PM = projection1(AM,-1);
b.LM = orth(PM.').';

AP = Flinear(p.ur,param);
PP = projection1(AP,1);
b.LP = orth(PP.').';

out = [ya(s.rarray,:)-ya(s.larray,:);
    ya(1) - p.pin;
    [b.LP zeros(size(b.LP))] * (yb - [p.ur;p.ul]);
    [zeros(size(b.LM)) b.LM] * (yb - [p.ur;p.ul])];
%%%%%%%%%%%%%%%%%%%%%%%%%%%%%%%%%%%%%%%%%%%%%%%%%%%%%%%%%%%
function out = Flinear(U,param)
global p

out = [0 0 1 0;
    0 0 0 1;
    (-p.gamma*(1-2*U(1))./...
            (1+exp(-p.beta*(U(2)-p.alpha)))+1)/p.d(1) ...
     (-p.gamma*p.beta*exp(-p.beta*(U(2)-p.alpha)).*U(1).*(1-U(1))./...
     (1+exp(-p.beta*(U(2)-p.alpha))).^2)/p.d(1) -param/p.d(1) 0;
     (-p.ppar*U(2)./(1+U(1)).^(p.ppar+1))/p.d(2) (1/(1+U(1)).^p.ppar)/p.d(2) ...
```

```
     0 -param/p.d(2)];
%%%%%%%%%%%%%%%%%%%%%%%%%%%%%%%%%%%%%%%%%%%%%%%%%%%%%%%%%%%%
```

A.3.6 double_Fc.m

```
function out = double_Fc(x,y,param)
% out = double_F(x,y)
%
% Returns the split domain for the ode given in the function F.
%
% Input "x" and "y" are provided by the ode solver. Note that s.rarray
% should be [1,2,...,k] and s.larray should be [k+1,k+2,...,2k]. See
% STABLAB documentation for more inforamtion about the structure s.

global s

out = [(s.R/s.I)*Fc(x,y(s.rarray,:),param);...
    (s.L/s.I)*Fc(x,y(s.larray,:),param)];
```

A.3.7 `Fc.m`

```
function out = Fc(x,y,param)
global p

out =  [y(3,:);
       y(4,:);
    (-param*y(3,:)-p.gamma*y(1,:).*(1-y(1,:))./...
            (1+exp(-p.beta*(y(2,:)-p.alpha)))+y(1,:))/p.d(1);
    (-param*y(4,:)+y(2,:)./(1+y(1,:)).^p.ppar-1)/p.d(2)];
```

A.3.8 `riot_solve_end.m`

The following program uses the time evolution method to approximate the wave speed of a traveling wave solution.

```
%%Solve PDE Riot Solve for u: Solves the pde when with
%%discretization of time and space derivatives; sets a delx value,
%%progressively solves for each time step, discarding solutions from
%%previous times.  Stops when calculated wavespeed is within wave.speedeps
%%of previously calculated wave speed.

function [] = riot_solve_end(p)
beep off; close all; clc;

global A u0 xmin xmax vb vstart;

p.d = [1;1];
p.alpha = 1;
p.beta = 70;
p.gamma = 2;
p.ppar = 1;
p.k = 20;

xmin = 0;
xmax = 500;
n = 20000;
% xmax = 1000;
% n = 40000;

% tmin = 0;
% tmax = 20;
% k = 80000;
% T = linspace(tmin,tmax,k+1);

X = linspace(xmin, xmax, n+1)';


delx = (xmax - xmin)/n;
delt = 1/4000;
% delt = 3/5000;

A = 5;

vb = 1;
u0 = 1;
```

```
vstart = 3;

% wave.frac = 0.15*(xmax-xmin);
wave.frac = 0.25*(xmax-xmin);
wave.buoydist = 5;
wave.nbuoy = xmax/wave.buoydist;
wave.markers = (wave.buoydist:wave.buoydist:xmax)/delx+1;
wave.buoy = wave.buoydist:wave.buoydist:xmax;
wave.eps = 0.001;
wave.speedeps = 0.0005;

[u,v,speed,t] = approx(delt,delx,X,@ffun,@gfun,p,wave);
wave.buoylift = speed.data;
wave.wavespeed = speed.wavespeed;
wave.cond = speed.cond;
wave.c = speed.c;
T.end = t;
T.delt = delt;
filename = ['speedruns/p',num2str(p.ppar),'g',num2str(p.gamma),...
    'b',num2str(p.beta),'k',num2str(p.k),'.mat'];
save(filename,'X','T','u','v','wave');

% ----------------------------------------------------------
function [ui,vi] = ic(X,p)
    global A vstart xmin;
    ui = A*(X == xmin);
%     ui = A*exp(-20*X);
%     ui = A*exp(-p.k*X);
    vi = vstart*ones(length(X),1);
% ----------------------------------------------------------
function [f] = ffun(u,v,p)
    global u0;
    f = p.gamma*u.*(u0-u)./(1+exp(-p.beta*(v-p.alpha))) - u;
% ----------------------------------------------------------
function [g] = gfun(u,v,p)
    global vb;
    g = -v./(1+u).^p.ppar+vb;
% ----------------------------------------------------------
function [u,v,speed,t] = approx(delt,delx,X,ffun,gfun,p,wave)
%set coefficient matrices for u and v
d1 = p.d(1);
d2 = p.d(2);
c1 = delt*d1/(delx)^2;
c2 = delt*d2/(delx)^2;

n = length(X)-1;
% k = length(T)-1;
```

```
%used periodic boundary conditions; creates tridiagonal matrix with nonzero
%entries in top right and bottom left corners (for BC)
ec = ones(n+1,1);
ed = ones(n-1,1);
B1 = spdiags([c1*[ed; 2; 2] (1-2*c1)*ec c1*[2; 2; ed]], [-1 0 1], n+1, n+1);
B2 = spdiags([c2*[ed; 2; 2] (1-2*c2)*ec c2*[2; 2; ed]], [-1 0 1], n+1, n+1);

%timesteps
u = zeros(n+1,1);
v = zeros(n+1,1);
speed.data = zeros(wave.nbuoy,2);

[u(:,1),v(:,1)] = ic(X,p);

uprev = u(:,1);
vprev = v(:,1);

speed.wavespeed = zeros(3,1);
lastlift = 0;
lasttime = 0;

i = 1;
speedcount = 1;
wavediff = 1000;
ind = 0;
disttotal = 0;

%calculate time steps:
while(((wavediff > wave.speedeps) || (ind*wave.buoydist < wave.frac))...
        && (disttotal<X(end)))
    unext = B1*uprev + delt*ffun(uprev,vprev,p);
    vnext = B2*vprev + delt*gfun(uprev,vprev,p);
    speed.data(:,2) = (unext(wave.markers)>wave.eps);

%     sum(speed.data(:,2))>lastlift

    if (sum(speed.data(:,2))>lastlift)
        distdiff = (sum(speed.data(:,2))-lastlift)*wave.buoydist;
        lastlift = sum(speed.data(:,2));
        timediff = delt*(i+1)-lasttime;
        lasttime = delt*(i+1);
        speed.wavespeed(:,speedcount+1) = [delt*(i+1); ...
           lastlift*wave.buoydist; distdiff/timediff];
       speed.data(:,1) = speed.data(:,2);
        wavediff = abs(speed.wavespeed(3,speedcount+1)...
                -speed.wavespeed(3,speedcount));
        if (wavediff<wave.speedeps)
            ind = ind + 1;
```

```
        else
            ind = 0;
        end
        speedcount = speedcount + 1;
        disttotal = speed.wavespeed(2,end);

        speed.wavespeed
    end
    uprev = unext;
    vprev = vnext;
    i = i+1;
    speed.cond = (wavediff > wave.speedeps);


end

u = unext;
v = vnext;
t = i*delt;

if (disttotal == X(end))
    speed.c = mode(speed.wavespeed(3,:));
else
    speed.c = speed.wavespeed(3,end);
end
```

A.3.9 `lambda_bounds.m`

The following program calculates the bound for λ that is discussed in Section 6.4.4 for the specified example perturbation and parameter sets.

```
%% Bounds on lambda for Evans function search
% function [out] = findwave()
clear all; clc; close all;
global p s b
% Delta = -1;
% Delta = 0;
Delta = 1;

if (Delta < 0)
    p.gamma = 10;           % Delta < 0
    p.ppar = -4;
    p.beta = 5;
    p.alpha = 1;
    %s.I = 21;               % r = 1000
    %s.I = 21;              % r = 10000
    s.I = 21;              % r = 100000
    r=1000;
elseif (Delta == 0)
    p.gamma = 15.069;       % Delta = 0
    p.ppar = -2;
    p.beta = 5;
    p.alpha = 0.287;
    s.I = 13;               % r = 1000
    %s.I = 14;              % r = 10000
    r=1000;
else
    p.gamma = 20;           % Delta > 0
    p.ppar = -2;
    p.beta = 0.5;
    p.alpha = 0.5;
    s.I = 14;              % r = 10000
    r=1000;
end

p.d = [1;1];
p.c = 2*sqrt(p.d(1)*(p.gamma/(1+exp(-p.beta*(1-p.alpha)))-1));
p.omega = -p.c/2;
p.ul=[null_intersect(p); 0;0];
p.ur=[0;1;0;0];
p.pin = 0.1;
```

```
%structure variables
s.I=21;     % Delta < 0
% s.I=10;     % Delta = 0
% s.I=15;     % Delta > 0
s.larray=[5;6;7;8];
s.rarray=[1;2;3;4];
s.side=1;
s.R=s.I;
s.L=-s.I;

AM = Flinear(p.ul);
PM = projection1(AM,-1);
b.LM = orth(PM.').';

AP = Flinear(p.ur);
PP = projection1(AP,1);
b.LP = orth(PP.').';

s.sol = getprofile2;

X = [-fliplr(s.sol.x) s.sol.x];
U = [fliplr(s.sol.y(5,:)) s.sol.y(1,:)];
V = [fliplr(s.sol.y(6,:)) s.sol.y(2,:)];

Up = [fliplr(s.sol.y(7,:)) s.sol.y(3,:)];
Vp = [fliplr(s.sol.y(8,:)) s.sol.y(4,:)];

%% graphs of U,V and U', V'
figure(1)
plot(X,U,'Color','blue')
hold on
plot(X,V,'Color','red')
xlabel('x')
ylabel('U, V')
legend('U(x,t)','V(x,t)')
titlestring = ['Solution Profiles \Gamma = ',num2str(p.gamma),...
    ', \beta = ',num2str(p.beta),', \alpha = ',num2str(p.alpha), ...
    ', p = ',num2str(-2)];
title(titlestring)
hold off

figure(2)
plot(X,Up,'Color','blue')
hold on
plot(X,Vp,'Color','red')
xlabel('x')
ylabel('dU/dz, dV/dz')
legend('U(x,t)','V(x,t)')
```

```
titlestring = ['Solution Profiles \Gamma = ',num2str(p.gamma),...
    ', \beta = ',num2str(p.beta),', \alpha = ',num2str(p.alpha), ...
    ', p = ',num2str(-2)];
title(titlestring)
hold off

%% Look for maximum of Jacobian and derivative of Jacobian
%define Jacobian elements
J11 = p.gamma*(1-2*U)./(1+exp(-p.beta*(V-p.alpha)))-1;
J12 = p.gamma*p.beta*exp(-p.beta*(V-p.alpha)).*U.*(1-U)./...
    (1+exp(-p.beta*(V-p.alpha))).^2;
J21 = p.ppar*V./(1+U).^(p.ppar+1);
J22 = -(1+U).^(-p.ppar);

figure(3)
plot(X,J11,X,J12,X,J21,X,J22)

%define derivative wrt z of Jacobian elements
DJ11 = (-2*p.gamma*Up.*(1+exp(-p.beta*(V-p.alpha)))+...
    p.gamma*p.beta*Vp.*(1-2*U).*exp(-p.beta*(V-p.alpha)))./...
    (1+exp(-p.beta*(V-p.alpha))).^2;
DJ12 = p.gamma*p.beta*exp(-p.beta*(V-p.alpha)).*...
    ((1+exp(-p.beta*(V-p.alpha))).^(-3)).*((-p.beta*Vp.*U.*(1-U)+...
    Up.*(1-2*U)).*(1+exp(-p.beta*(V-p.alpha)))+2*p.beta*Vp.*...
    exp(-p.beta*(V-p.alpha)).*U.*(1-U));
DJ21 = p.ppar*Vp./(1+U).^(p.ppar+1)-(p.ppar*(p.ppar+1)*Up.*V)./...
    (1+U).^(p.ppar+2);
DJ22 = (p.ppar*Up)./(1+U).^(p.ppar+1);

figure(4)
plot(X,DJ11,X,DJ12,X,DJ21,X,DJ22)

%% Find Infinity norms
%Infinity norm of J (Jacobian)
Jmax = max([max(abs(J11)+abs(J12)) max(abs(J21)+abs(J22))]);

%Infinity norm of J^T (Jacobian transpose)
JTmax = max([max(abs(J11)+abs(J21)) max(abs(J12)+abs(J22))]);

%Infinity norm of J^T + J (Jacobian Transpose + Jacobian)
JTJsum = max([max(abs(2*J11)+abs(J12+J21)) max(abs(J12+J21)+abs(2*J22))]);

%Infinity norm of J^T*J (Jacobian Transpose * Jacobian)
JTJprod = max([max(abs(J11.^2+J21.^2)+abs(J11.*J12+J21.*J22)) ...
    max(abs(J12.*J11+J22.*J21)+abs(J12.^2+J22.^2))]);

%Infinity norm of DJ (derivative of Jacobian)
DJmax = max([max(abs(DJ11)+abs(DJ12)) max(abs(DJ21)+abs(DJ22))]);
```

```
%% Find bound
w = sqrt(2*pi);
dw = sqrt(2*pi);
ddw = 3*sqrt(2*pi);
wddw = 3.79909;
l0 = (ddw+p.c^2/2*dw + (Jmax + JTmax)*wddw + (p.c^4/16 + ...
    p.c^2/4*JTJsum + JTJprod)*w)/w;
```

APPENDIX B

Analytical Determination of Number of Steady States

B.1 Number of Steady States for $p > 0$

Our goal lies in finding the number of non-trivial intersections between the two nullclines:

$$v_1 = -\frac{1}{\beta}\log(\Gamma(1-u)-1)+\alpha \quad \text{and} \quad v_2 = (1+u)^p,$$

where we make the simplification that $\alpha = 1$. We pose this problem in a slightly different way and instead think of finding the roots of the difference of the two functions:

$$v_d = v_2 - v_1.$$

Roots of v_d should exist between or at local extrema, so we can find transitions between regions of Γ, β-space that yield different total numbers of non-trivial intersections by 1) finding the critical points of v_d' and 2) finding where those values are equal to zero in v_d. This method will yield one or more implicit curves in Γ, β-space that show where the number of steady states increases or decreases.

B.1.1 Example: $p = 1$

As an example, we demonstrate the results of this method for $p = 1$. The derivative of v_d is

$$v_d' = 1 - \frac{\Gamma}{\beta(\Gamma(1-u)-1)},$$

and the only critical point is located at $u = 1 - \frac{1}{\Gamma} - \frac{1}{\beta}$. We substitute this value into v_d and set it equal to zero to find the boundary of our steady state region:

$$1 - \frac{1}{\Gamma} - \frac{1}{\beta} + \frac{1}{\beta}\log\left(\frac{\Gamma}{\beta}\right) = 0. \tag{B.1}$$

A contour plot of this curve (plotted using Mathematica) is shown in Figure B.1. Using what we now about the two nullclines, v_1 and v_2, the critical point, and the curve, we can find the number of non-trivial steady states for $p = 1$. We first look at the region to the left of the curve in Figure B.1. In this region, the expression on the left hand side of (B.1) is negative. For $1 < \Gamma < 2$, $v_d(0) < 0$, so

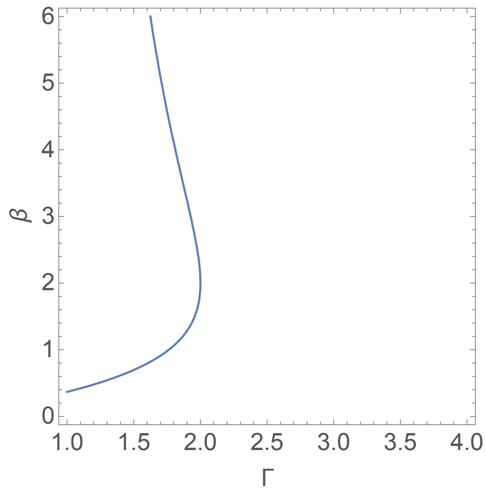

Figure B.1: Curve separating the regions of Γ, β-space that yields different non-trivial steady states for $p = 1$. For values of Γ and β in the region to the left of the curve, the left side of (B.1) is negative; for values located on the curve, the expression is equal to zero; for values to the right of the curve, the expression is positive.

there can be no roots of v_d from $u = 0$ to $u = 1 - \frac{1}{\Gamma} - \frac{1}{\beta}$. For $u > 1 - \frac{1}{\Gamma} - \frac{1}{\beta}$, there are no roots either as v_d remains negative. So we can see that to the **left of the curve**, there are **no non-trivial steady states**, meaning the only steady state is the trivial state of $(u, v) = (0, 1)$, which is due to the intersection of $u = 0$ and $v = (1 + u)^p$.

For values of Γ and β located on the curve, the expression in (B.1) is equal to zero, and we still have that $1 < \Gamma < 2$, so $v_d(0) < 0$. In this case, we see that the intersection of v_1 and v_2 actually occurs at the critical point, and for $u > 1 - \frac{1}{\Gamma} - \frac{1}{\beta}$, $v_d < 0$, so this is the only non-trivial intersection that occurs. We do have to be careful, since certain values of β will push the intersection point into the negative values, in which case we would ignore this intersection, since u must be nonnegative due to its physical interpretation. We therefore require that $\beta > \frac{\Gamma}{\Gamma - 1}$ to insure that this intersection is positive. **Along this curve** (and with the appropriate β value), there will be **one non-trivial steady state**. Overall, this results in two steady states when we also consider the trivial steady state mentioned above.

For values of Γ and β located to the right of the curve, the expression in (B.1) is positive. We need to split up this region into several cases because the value of Γ will change the nature of the relationships between the two curves. For $1 < \Gamma < 2$, $v_d(0) < 0$, so we know there is an intersection between $u = 0$ and $u = 1 - \frac{1}{\Gamma} - \frac{1}{\beta}$. Again, we wish to eliminate the possibility that the intersection is negative, so we require $\beta > \frac{\Gamma}{\Gamma-1}$. Because of the relative domains of v_1 and v_2, and there relationship in this case, we are guaranteed another intersection somewhere in the interval $(1-\frac{1}{\Gamma}-\frac{1}{\beta},1)$. So for $1<\Gamma<2$**,** $\beta>\frac{\Gamma}{\Gamma-1}$ **and** Γ **and** β **values to the right of the curve**, there are **two non-trivial steady states**, resulting in a total of three steady states.

For values of Γ and β to the right of the curve and $\Gamma = 2$, we have the expression in (B.1) is positive and $v_d(0) = 0$. If our critical point is positive, this indicates that there is an intersection between v_1 and v_2 in the trivial location of $(0, 1)$, and then due to the domain and relationship of the curves, we are guaranteed a non-trivial intersection for $u \in (1-\frac{1}{\Gamma}-\frac{1}{\beta},1)$. Again, we place the requirement that $\beta > \frac{\Gamma}{\Gamma-1}$ or $\beta > 2$ since we consider the case $\Gamma = 2$. So for $\Gamma = 2$**,** $\beta > 2$ **and** Γ **and** β **values to the right of the curve**, there is **one non-trivial steady state**, resulting in a total of two steady states.

For values of Γ and β to the right of the curve and $\Gamma > 2$, we have the expression in (B.1) is positive and $v_d(0) > 0$, meaning there are no non-trivial intersections in the interval $(0,1-\frac{1}{\Gamma}-\frac{1}{\beta})$. However, due to the domain and relationship of the curves, we are guaranteed an intersection. Since we are not looking for an intersection in the interval $(0,1-\frac{1}{\Gamma}-\frac{1}{\beta})$, we do not need to place any restrictions on β. So for $\Gamma > 2$ **and** Γ **and** β **values to the right of the curve**, there is **one non-trivial steady state**, resulting in a total of two steady states.

We can utilize this method of analysis to confirm numerical results for whole number p values for which it is possible to find analytic expressions for the critical points of v_d. It is possible to find these critical points by hand for $p = 2$, but for higher order p-values ($p = 3,\ 4$), we utilize Mathematica. Clearly, this method of analysis becomes much more complicated when dealing with implicit plots from four critical points, which is why we present this simple example here.

B.1.2 Results for $p = 1,\ 2,\ 3,$ and 4

As stated in the previous section, the curve separating regions of different numbers of steady states in Γ,β-space for $p = 1$ is

$$1-\frac{1}{\Gamma}-\frac{1}{\beta}+\frac{1}{\beta}\log\left(\frac{\Gamma}{\beta}\right)=0,$$

and this is shown in Figure B.1. We now present the results of this analysis for $p = 2,\ 3,$ and 4.

Remark B.1.1. *Please note that the diagrams of the curves presented in this appendix may differ* *from the parameter space diagrams presented in Section 2.3. This is because these diagrams also include any* ***negative*** *steady states. These negative steady states do not have physical relevance for our system since u and v must both be nonnegative. We are also limiting our analysis here to the non-trivial nullclines, and do not include the nullcline $u = 0$. The addition of this nullcline in Section 2.3 increases the number of nonnegative steady states by one for $\Gamma > 2$.*

For $p = 2$, we define:

$$u_1 = \frac{-2\beta - \sqrt{4\beta^2 - 8\beta\Gamma(2\beta + \Gamma - 2\beta\Gamma)}}{4\beta\Gamma} \quad \text{and}$$
$$u_2 = \frac{-2\beta - \sqrt{4\beta^2 - 8\beta\Gamma(2\beta + \Gamma - 2\beta\Gamma)}}{4\beta\Gamma},$$

and we have the resulting boundary curves:

$$-1 + (1 + u_1)^2 + \frac{1}{\beta}\log[\Gamma(1 - u_1) - 1] = 0,$$
$$-1 + (1 + u_2)^2 + \frac{1}{\beta}\log[\Gamma(1 - u_2) - 1] = 0.$$

These curves are shown in Figure B.2.

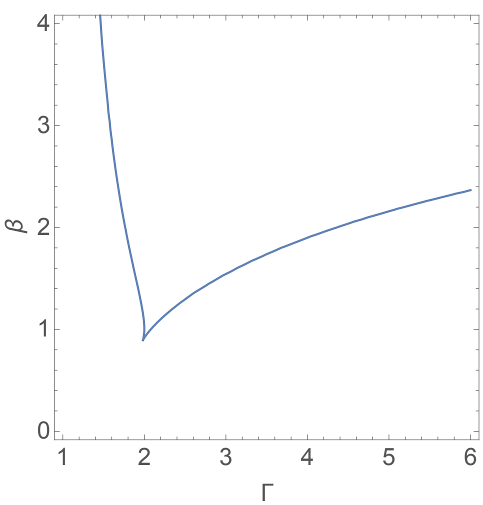

Figure B.2: Curves separating the regions of Γ, β-space, yielding different non-trivial steady states for $p = 2$.

For $p = 3$, we define:

$$
\begin{aligned}
u_1 = &-\frac{\beta+\beta\Gamma}{3\beta\Gamma} \\
&- \frac{\left(2^{1/3}\left(-9\beta^2+36\beta^2\Gamma-36\beta^2\Gamma^2\right)\right)}{\left(27\beta\Gamma\left(-2\beta^3+12\beta^3\Gamma-24\beta^3\Gamma^2-9\beta^2\Gamma^3+16\beta^3\Gamma^3+3\sqrt{4\beta^5\Gamma^3-24\beta^5\Gamma^4+48\beta^5\Gamma^5+9\beta^4\Gamma^6-32\beta^5\Gamma^6}\right)^{1/3}\right)} \\
&+ \frac{1}{3(2^{1/3})\beta\Gamma}\left(-2\beta^3+12\beta^3\Gamma-24\beta^3\Gamma^2-9\beta^2\Gamma^3+16\beta^3\Gamma^3+3\sqrt{4\beta^5\Gamma^3-24\beta^5\Gamma^4+48\beta^5\Gamma^5+9\beta^4\Gamma^6-32\beta^5\Gamma^6}\right)^{1/3}, \\
u_2 = &-\frac{\beta+\beta\Gamma}{3\beta\Gamma} \\
&+ \frac{\left(\left(1+i\sqrt{3}\right)\left(-9\beta^2+36\beta^2\Gamma-36\beta^2\Gamma^2\right)\right)}{\left(27\ 2^{2/3}\beta\Gamma\left(-2\beta^3+12\beta^3\Gamma-24\beta^3\Gamma^2-9\beta^2\Gamma^3+16\beta^3\Gamma^3+3\sqrt{4\beta^5\Gamma^3-24\beta^5\Gamma^4+48\beta^5\Gamma^5+9\beta^4\Gamma^6-32\beta^5\Gamma^6}\right)^{1/3}\right)} \\
&- \frac{1}{6(2^{1/3})\beta\Gamma}\left(1-i\sqrt{3}\right)\left(-2\beta^3+12\beta^3\Gamma-24\beta^3\Gamma^2-9\beta^2\Gamma^3+16\beta^3\Gamma^3+3\sqrt{4\beta^5\Gamma^3-24\beta^5\Gamma^4+48\beta^5\Gamma^5+9\beta^4\Gamma^6-32\beta^5\Gamma^6}\right)^{1/3}, \\
u_3 = &-\frac{\beta+\beta\Gamma}{3\beta\Gamma} \\
&+ \frac{\left(\left(1-i\sqrt{3}\right)\left(-9\beta^2+36\beta^2\Gamma-36\beta^2\Gamma^2\right)\right)}{\left(27(2^{2/3})\beta\Gamma\left(-2\beta^3+12\beta^3\Gamma-24\beta^3\Gamma^2-9\beta^2\Gamma^3+16\beta^3\Gamma^3+3\sqrt{4\beta^5\Gamma^3-24\beta^5\Gamma^4+48\beta^5\Gamma^5+9\beta^4\Gamma^6-32\beta^5\Gamma^6}\right)^{1/3}\right)} \\
&- \frac{1}{6(2^{1/3})\beta\Gamma}\left(1+i\sqrt{3}\right)\left(-2\beta^3+12\beta^3\Gamma-24\beta^3\Gamma^2-9\beta^2\Gamma^3+16\beta^3\Gamma^3+3\sqrt{4\beta^5\Gamma^3-24\beta^5\Gamma^4+48\beta^5\Gamma^5+9\beta^4\Gamma^6-32\beta^5\Gamma^6}\right)^{1/3},
\end{aligned}
$$

and the resulting boundary curves:

$$
\begin{aligned}
&-1+(1+u_1)^2+\frac{1}{\beta}\log[\Gamma(1-u_1)-1]=0, \\
&-1+(1+u_2)^2+\frac{1}{\beta}\log[\Gamma(1-u_2)-1]=0, \quad \text{and} \\
&-1+(1+u_3)^2+\frac{1}{\beta}\log[\Gamma(1-u_3)-1]=0,
\end{aligned}
\tag{B.2}
$$

which respectively yield the labeled curves shown in Figure B.3.

Comparison of the curves shown in the left image of Figure B.3 with those generated in AUTO indicate that Curve 2 is actually extraneous. To understand why this is the case, we use contour plots of the left hand sides of the equations in (B.2). We can see that the left hand sides of the equations (v_d evaluated at the critical points) must be of alternating sign in order to indicate the presence of a zero of v_d. In all regions of Γ, β-space, we see that the sign of the expression corresponding to Curve 2 is either the same as that of the expression corresponding to Curve 1 or Curve 3. Therefore, the critical point represented by u_2 does not indicate the presence of an extra zero of v_d. We can then use the simplified boundaries shown in the image on the right in Figure B.3.

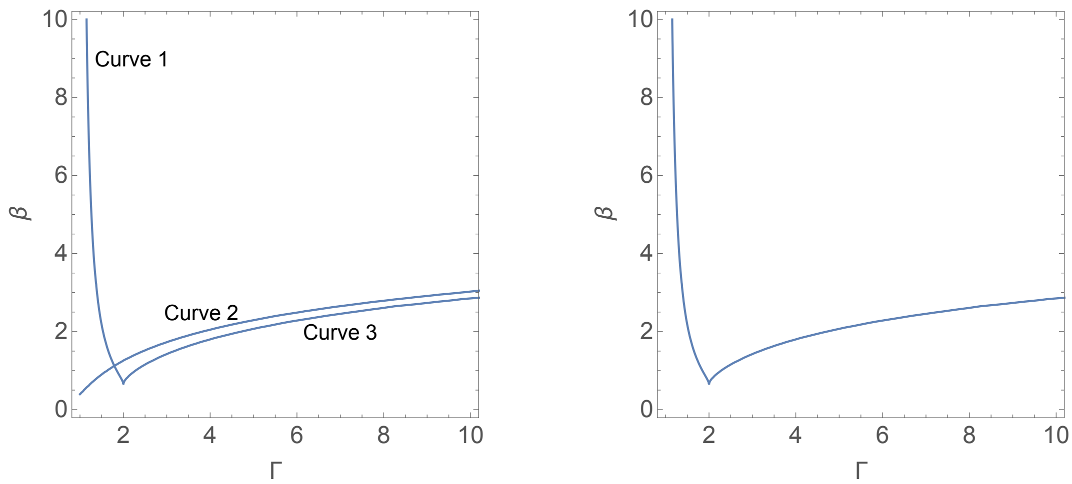

Figure B.3: Curves separating the regions of Γ, β-space, yielding different non-trivial steady states for $p = 3$. Left: We note the presence of Curve 2, which does not appear in the numerical analysis using AUTO. Right: Simplified boundaries; this figure agrees with results from the numerical analysis in AUTO.

For $p = 4$, we let

$$\begin{aligned} R(\Gamma,\beta) &= 432\beta^2\Gamma - 1728\beta^2\Gamma^2 + 1728\beta^2\Gamma^3 \\ &\quad + \sqrt{186624\beta^4\Gamma^2 - 1492992\beta^4\Gamma^3 + 4478976\beta^4\Gamma^4 - 5971968\beta^4\Gamma^5 - 442368\beta^3\Gamma^6 + 2985984\beta^4\Gamma^6} \end{aligned}$$

and define:

$$\begin{aligned} u_1 = &-\frac{1+2\Gamma}{4\Gamma} + \frac{1}{2}\sqrt{1 + \frac{1}{4\Gamma^2} - \frac{1}{\Gamma} + \frac{(4(2^{1/3})\Gamma)}{R(\Gamma,\beta)^{1/3}} + \frac{R(\Gamma,\beta)^{1/3}}{12(2^{1/3})\beta\Gamma}} \\ &- \frac{1}{2}\sqrt{-\frac{4}{\Gamma} + \frac{(1+2\Gamma)^2}{2\Gamma^2} - \frac{(4(2^{1/3})\Gamma)}{R(\Gamma,\beta)^{1/3}} - \frac{R(\Gamma,\beta)^{1/3}}{12(2^{1/3})\beta\Gamma} + \frac{-\frac{8(3-2\Gamma)}{\Gamma} + \frac{12(1+2\Gamma)}{\Gamma^2} - \frac{(1+2\Gamma)^3}{\Gamma^3}}{4\sqrt{1 + \frac{1}{4\Gamma^2} - \frac{1}{\Gamma} + \frac{(4(2^{1/3})\Gamma)}{R(\Gamma,\beta)^{1/3}} + \frac{R(\Gamma,\beta)^{1/3}}{12(2^{1/3})\beta\Gamma}}}}, \\ u_2 = &-\frac{1+2\Gamma}{4\Gamma} + \frac{1}{2}\sqrt{1 + \frac{1}{4\Gamma^2} - \frac{1}{\Gamma} + \frac{(4(2^{1/3})\Gamma)}{R(\Gamma,\beta)^{1/3}} + \frac{R(\Gamma,\beta)^{1/3}}{12(2^{1/3})\beta\Gamma}} \\ &+ \frac{1}{2}\sqrt{-\frac{4}{\Gamma} + \frac{(1+2\Gamma)^2}{2\Gamma^2} - \frac{(4(2^{1/3})\Gamma)}{R(\Gamma,\beta)^{1/3}} - \frac{R(\Gamma,\beta)^{1/3}}{12(2^{1/3})\beta\Gamma} + \frac{-\frac{8(3-2\Gamma)}{\Gamma} + \frac{12(1+2\Gamma)}{\Gamma^2} - \frac{(1+2\Gamma)^3}{\Gamma^3}}{4\sqrt{1 + \frac{1}{4\Gamma^2} - \frac{1}{\Gamma} + \frac{(4(2^{1/3})\Gamma)}{R(\Gamma,\beta)^{1/3}} + \frac{R(\Gamma,\beta)^{1/3}}{12(2^{1/3})\beta\Gamma}}}}, \end{aligned}$$

and the resulting boundary curves:

$$\begin{aligned} -1 + (1+u_1)^2 + \frac{1}{\beta}\log[\Gamma(1-u_1) - 1] = 0 \quad \text{and} \\ -1 + (1+u_2)^2 + \frac{1}{\beta}\log[\Gamma(1-u_2) - 1] = 0, \end{aligned} \tag{B.3}$$

which yield the curves shown in Figure B.4. It is important to note that using the analysis described for the $p = 1$ example, we should have four possible critical points $u_1,\ u_2,\ u_3,\ u_4$ instead of just two,

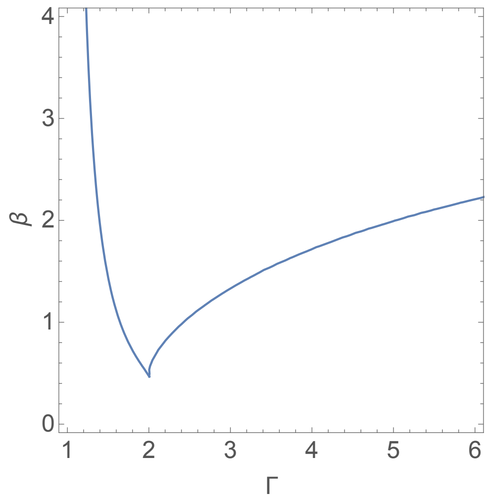

Figure B.4: Curves separating the regions of Γ, β-space, yielding different non-trivial steady states for $p = 4$.

but for $\Gamma > 1$ and $\beta > 0$, two of these points have non-zero imaginary components and therefore do not factor into the creation of the boundary curves.

APPENDIX C

Eigenspace Dimensions

C.1 Dimensions of Unstable Eigenspaces

As discussed in Section 6.1.2, in order to determine the essential spectrum of the linear operator $\mathcal{L} := A\partial_{zz} + C\partial_z + DF(\hat{\mathbf{u}})$, we first look for the boundaries of the essential spectrum. The boundaries consist of four curves in the complex λ plane and are dependent on the value of

$$\Delta = (f_u(u^*, v^*) + g_v(u^*, v^*))^2 - 4f_u(u^*, v^*)g_v(u^*, v^*) + 4f_v(u^*, v^*)g_u(u^*, v^*).$$

Two of the boundaries are

$$\lambda_1^+ = -k^2 + f_u(0, 1) + ikc$$
$$\lambda_2^+ = -k^2 + g_v(0, 1) + ikc,$$

and the remaining two are as follows: for $\Delta < 0$

$$\lambda_1^- = -k^2 + \frac{f_u(u^*, v^*) + g_v(u^*, v^*)}{2} + i\left(kc + \frac{\sqrt{|\Delta|}}{2}\right)$$
$$\lambda_2^- = -k^2 + \frac{f_u(u^*, v^*) + g_v(u^*, v^*)}{2} + i\left(kc - \frac{\sqrt{|\Delta|}}{2}\right),$$

for $\Delta = 0$

$$\lambda_{1,2}^- = -k^2 + \frac{f_u(u^*, v^*) + g_v(u^*, v^*)}{2} + ikc,$$

and for $\Delta > 0$

$$\lambda_1^- = -k^2 + \frac{f_u(u^*, v^*) + g_v(u^*, v^*) + \sqrt{\Delta}}{2} + ikc$$
$$\lambda_2^- = -k^2 + \frac{f_u(u^*, v^*) + g_v(u^*, v^*) - \sqrt{\Delta}}{2} + ikc.$$

To find the regions of the essential spectrum, we find those regions created by these four curves for which the dimensions of the unstable eigenspaces of A_+ and A_- differ. The eigenvalues of A_+ are

$$\begin{aligned}
\mu_1^+ &= \frac{-c+\sqrt{c^2+4(\lambda - f_u(0,1))}}{2}, \quad \mu_2^+ = \frac{-c-\sqrt{c^2+4(\lambda - f_u(0,1))}}{2},\\
\mu_3^+ &= \frac{-c+\sqrt{c^2+4(\lambda - g_v(0,1))}}{2}, \quad \text{and} \quad \mu_4^+ = \frac{-c-\sqrt{c^2+4(\lambda - g_v(0,1))}}{2}.
\end{aligned}$$

The eigenvalues of A_- are

$$\begin{aligned}
\mu_1^- &= \frac{-c+\sqrt{c^2+4\nu_1}}{2}, \quad \mu_2^- = \frac{-c-\sqrt{c^2+4\nu_1}}{2},\\
\mu_3^- &= \frac{-c+\sqrt{c^2+4\nu_2}}{2}, \quad \text{and} \quad \mu_4^- = \frac{-c-\sqrt{c^2+4\nu_2}}{2},
\end{aligned}$$

where

$$\begin{aligned}
\nu_1 &= \frac{2\lambda - g_v - f_u + \sqrt{(g_v+f_u)^2 - 4f_u g_v + 4f_v g_u}}{2} \quad \text{and}\\
\nu_2 &= \frac{2\lambda - g_v - f_u - \sqrt{(g_v+f_u)^2 - 4f_u g_v + 4f_v g_u}}{2}.
\end{aligned} \tag{C.1}$$

and each partial derivative, f_u, f_v, g_u, g_v, is evaluated at (u^*, v^*).

For the region to the right of all the essential spectrum boundaries, where $\mathrm{Re}(\lambda) \to \infty$, we see that the dimensions of the unstable eigenspaces for both A_+ and A_- are two since each matrix has two eigenvalues with negative real part. For the region to the left of all the essential spectrum boundaries, where $\mathrm{Re}(\lambda) \to -\infty$, we see that all four eigenvalues of $A_\pm$ have negative real part, so the unstable eigenspaces both have dimension four. By definition, the essential spectrum boundaries occur when the eigenvalues of either A_+ or A_- are purely imaginary. Therefore, we see that crossing any one of these boundaries increases or decreases the dimension of the unstable eigenspace of either A_+ or A_- by one. We perform several example calculations for the case $\Delta > 0$ to demonstrate that this.

For $\Delta > 0$, the essential spectrum boundaries are four parabolic curves opening to the left with vertices at different points along the $\mathrm{Re}(\lambda)$ axis (see Figure 6.3). Without loss of generality, we choose a parameter set such that

$$\frac{f_u(u^*,v^*) + g_v(u^*,v^*) - \sqrt{\Delta}}{2} < \frac{f_u(u^*,v^*) + g_v(u^*,v^*) + \sqrt{\Delta}}{2} < g_v(0,1) < f_u(0,1), \tag{C.2}$$

and as a result: $\lambda_2^- < \lambda_1^- < \lambda_2^+ < \lambda_1^+$. From Figure 6.3, we can see that the four curves separate the complex λ plane into five regions. In the region between λ_2^+ and λ_1^+, we choose a λ value to test to find the dimension of the unstable eigenspaces, and let $\lambda = 0$ so that $g_v(0,1) < \lambda < f_u(0,1)$. Since $c \geq c_{min} = 2\sqrt{f_u(0,1)}$, the dimension of the unstable eigenspace of A_+ is three. For A_-, we have

$$\begin{aligned} \nu_1 &= \frac{-g_v - f_u + \sqrt{(g_v + f_u)^2 - 4f_u g_v + 4f_v g_u}}{2} \quad \text{and} \\ \nu_2 &= \frac{-g_v - f_u - \sqrt{(g_v + f_u)^2 - 4f_u g_v + 4f_v g_u}}{2}. \end{aligned}$$

Since $\Delta > 0$, $f_u(u^*, v^*), g_u(u^*, v^*), g_v(u^*, v^*) < 0$ and $f_v(u^*) > 0$, both $\nu_1, \nu_2 > 0$, so the dimension of the unstable eigenspace of A_- is still two. We see that traversing a boundary (from right to left) obtained from A_+ increases the dimension of the unstable eigenspace of A_+ by one.

Similarly, if we traverse the boundary λ_2^- from the left and test an eigenvalue, λ, such that $\frac{f_u(u^*,v^*)+g_v(u^*,v^*)-\sqrt{\Delta}}{2} < \lambda < \frac{f_u(u^*,v^*)+g_v(u^*,v^*)+\sqrt{\Delta}}{2}$, then $\lambda - f_u(0,1) < 0$ and $\lambda - g_v(0,1) < 0$, so all four eigenvalues of A_+ have negative real part. For A_-, we have $0 < \nu_1 < \sqrt{\Delta}$ and $\nu_2 < 0$, so the dimension of the unstable eigenspace decreases to three. This example calculation demonstrates that traversing a boundary curve corresponding to A_- either increases or decreases the dimension of the unstable eigenspace of A_- by one.

In the case of $\Delta = 0$, we would also like to demonstrate that crossing coincident boundary curves of the essential spectrum will increase or decrease the dimension of the corresponding unstable eigenspace by two. Again, in the leftmost region of the complex plane for the parameter set in which $\Delta = 0$, $A_\pm$ both have unstable eigenspaces with dimension four. Cross into the region to the right of the coincident curves λ_2^- and λ_1^-, we can test a λ-value such that $\frac{f_u(u^*,v^*)+g_v(u^*,v^*)}{2} < \lambda < g_v(0,1)$ to find the eigenvalues of $A_\pm$. For A_+, both $\lambda - f_u(0,1) < 0$ and $\lambda - g_v(0,1) < 0$, so each of the eigenvalues have real part less than zero, and the dimension of the unstable eigenspace is four. For A_-, with the same restrictions on λ, $\nu_1, \nu_2 > 0$, so the dimension of the unstable eigenspace of A_- is two. We can see from this that crossing the coincident boundaries resulting from A_- decreases (or increases if traveling from right to left) the dimension of the unstable eigenspace by two.

REFERENCES

[1] H. Berestycki, J. P. Nadal, and N. Rodríguez, "A model of riots dynamics: shocks, diffusion, and thresholds," *Networks and Heterogeneous Media*, vol. 10, no. 3, pp. 443–475, 2015.

[2] "Riots in Tottenham after Mark Duggan shooting protest." https://www.bbc.com/news/uk-england-london-14434318, August 2011. From the BBC.

[3] T. P. Davies, H. M. Fry, A. G. Wilson, and S. R. Bishop, "A mathematical model of the London riots and their policing," *Scientific Reports*, vol. 3, no. 1303, 2013.

[4] L. Buchanan, F. Fessenden, K. K. R. Lai, H. Park, A. Parlapiano, A. Tse, T. Wallace, D. Watkins, and K. Yourish, "What happened in Ferguson?," *The New York Times*, August 2015.

[5] C. Tkacik, "Remembering the Baltimore riots after Freddie Gray's death, 3 years later," *The Baltimore Sun*, April 2018.

[6] J. C. Lang and H. De Sterck, "The Arab Spring: A simple compartmental model for the dynamics of a revolution," *Mathematical Social Sciences*, vol. 69, no. 2014, pp. 12–21, 2014.

[7] A. Chrisafis, "The trial that could lay bare France's racial divide," *The Guardian*, March 2015.

[8] J. Eligon and S. G. Stolberg, "Baltimore after Freddie Gray: The "mind-set has changed"," *The New York Times*, April 2016.

[9] M. Edmonds, "How riots work." https://people.howstuffworks.com/riot.htm, July 2011.

[10] L. Bonnasse-Gahot, H. Berestycki, M. Depuiset, M. Gordon, S. Roché, Rodríguez, and J. P. N., Nadal, "Epidemiological modeling of the 2005 French riots: a spreading wave and the role of contagion," *Scientific Reports*, vol. 8, no. 107, 2018.

[11] User:Nilstilar, "France départementale.svg." https://commons.wikimedia.org/wiki/File:France_départementale.svg, July 2010. [Online; accessed March 20, 2015; altered to include department numbers].

[12] P. Baudains, S. D. Johnson, and A. M. Braithwaite, "Geographic patterns of diffusion in the 2011 London riots," *Applied Geography*, vol. 45, pp. 211–219, 2013.

[13] R. A. Fisher, "The wave of advance of advantageous genes," *Annals of Eugenics*, vol. 7, pp. 353–369, 1937.

[14] A. I. Volpert, V. A. Volpert, and V. A. Volpert, *Traveling Wave Solutions of Parabolic Systems*. American Mathematical Society, 1994.

[15] H. Berestycki, L. Rossi, and N. Rodríguez, "Periodic cycles of social outbursts of activity," *Journal of Differential Equations*, vol. 264, no. 1, pp. 163–196, 2018.

[16] H. Berestycki and N. Rodríguez, "Analysis of a heterogeneous model for riot dynamics: the effect of censorship of information," *European Journal of Applied Mathematics*, vol. 27, pp. 554–582, 2016.

[17] H. Berestycki, N. Rodríguez, and L. Ryzhik, "Traveling wave solutions in a reaction-diffusion model for criminal activity," *Multiscale Modeling and Simulation*, vol. 11, no. 4, pp. 1097–1126, 2013.

[18] A. Kolmogorov, I. Petrovskii, and N. Piskunov, "A study of the diffusion equation with increase in the amount of substance, and its application to a biological problem," in *Selected works of A. N. Kolmogorov* (V. M. Tikhomirov, ed.), pp. 242–270, Springer, 1991. Translated by V. M. Volosov.

[19] M. J. Ablowitz and A. Zeppetella, "Explicit solutions of Fisher's equation for a special wave speed," *Bulletin Mathematical Biology*, vol. 41, no. 6, pp. 835–840, 1979.

[20] H. P. McKean, "Application of Brownian motion to the equation of Kolmogorov-Petrovskii-Piskunov," *Communications on pure and applied mathematics*, vol. 28, pp. 323–331, 1975.

[21] D. A. Larson, "Transient bounds and time asymptotic behavior of solutions to nonlinear equations of Fisher type," *SIAM Journal of Applied Mathematics*, vol. 34, pp. 93–103, 1978.

[22] M. R. Booty, R. Haberman, and A. A. Minzoni, "The accommodation of traveling waves of Fisher's type to the dynamics of the leading tail," *SIAM Journal on Applied Mathematics*, vol. 53, no. 4, pp. 1009–1025, 1993.

[23] F. Hamel and L. Roques, "Fast propagation for KPP equations with slowly decaying initial conditions," *Journal of Differential Equations*, vol. 249, no. 7, pp. 1726–1745, 2010.

[24] K. P. Hadeler and F. Rothe, "Traveling fronts in nonlinear diffusion equations," *Journal of Mathematical Biology*, vol. 2, pp. 251–263, 1975.

[25] F. Rothe, "Convergence to traveling fronts in semilinear parabolic equations," *Proceedings of the Royal Society of Edinburgh Section A*, vol. 80, no. 3-4, pp. 213–234, 1978.

[26] P. C. Fife and J. B. McLeod, "The approach of solutions of nonlinear diffusion equations to traveling front solutions," *Archive for Rational Mechanics and Analysis*, vol. 65, p. 335 361, 1977.

[27] N. Bacaër, *A Short History of Mathematical Population Dynamics*. Springer-Verlag, 2011.

[28] E. J. Doedel, B. E. Oldeman, A. R. Champneys, F. Dercole, T. Fairgrieve, Y. Kuznetsov, R. Paffenroth, B. Sandstede, X. Wang, and C. Zhang, "AUTO-07P: Continuation and bifurcation software for ordinary differential equations." http://cmvl.cs.concordia.ca/auto., 2012.

[29] B. Champneys and B. Sandstede, "Numerical computation of coherent structures," in *Numerical Continuation Methods for Dynamical Systems* (B. Krauskopf, H. M. Osinga, and J. Galán-Vioque, eds.), Springer, 2007.

[30] B. Barker, J. Humpherys, and K. Zumbrun, "STABLAB: A MATLAB-based numerical library for Evans function computation (Version 1.0)." http://impact.byu.edu/stablab/, 2009.

[31] J. Venegas-Ortiz, R. J. Allen, and M. R. Evans, "Speed of invasion of an expanding population by a horizontally transmitted trait," *Genetics*, vol. 196, no. 2, pp. 497–507, 2014.

[32] R. Gardner, "Existence and stability of traveling wave solution of competition models: a degree theoretic approach," *Journal of Differential Equations*, vol. 44, pp. 343–364, 1982.

[33] V. A. Volpert and A. I. Volpert, "Application of the leray-schauder method to the proof of the existence of wave solutions of parabolic systems," *Soviet Mathematics Doklady*, vol. 37, pp. 138–141, 1988.

[34] A. Ghazaryan, V. Manukian, and S. Schecter, "Traveling waves in the Holling-Tanner model with weak diffusion," *Proceedings of the Royal Society A: Mathematical, Physical and Engineering Sciences*, vol. 471, no. 2177, 2015.

[35] J. Guo and Y. Morita, "Entire solutions of reaction-diffusion equations and an application to discrete diffusive equations," *Discrete and Continuous Dynamical Systems - A*, vol. 12, no. 2, pp. 193–212, 2005.

[36] Y. Fukao, Y. Morita, and H. Ninomiya, "Some entire solutions of the allen-cahn equation," *Taiwanese Journal of Mathematics*, vol. 8, no. 1, pp. 15–32, 2004.

[37] D. H. Sattinger, "On the stability of waves of nonlinear parabolic systems," *Advances in Mathematics*, vol. 22, pp. 312–355, 1976.

[38] B. Sandstede, "Stability of traveling waves," in *Handbook of Dynamical Systems II* (B. Fiedler, ed.), pp. 983–1055, Elsevier, 2002.

[39] B. Sandstede and A. Scheel, "Spectral stability of modulated travelling waves bifurcating near essential instabilities," *Proceedings of the Royal Society of Edinburgh A*, vol. 130, pp. 419–448, 2000.

[40] B. Sandstede and A. Scheel, "On the structure of spectra of modulated travelling waves," *Mathematische Nachrichten*, vol. 232, no. 1, pp. 39–93, 2001.

[41] W. A. Coppel, *Dichotomies in Stability theory.* No. 629 in Lecture Notes in Mathematics, Springer, 1978.

[42] K. J. Palmer, "Exponential dichotomies and transversal homoclinic points," *Journal of Differential Equations*, vol. 55, pp. 225–256, 1984.

[43] K. J. Palmer, "Exponential dichotomies and fredholm operators," *American Mathematical Society*, vol. 104, pp. 149–156, 1988.

[44] T. Kapitula and K. Promislow, *Spectral and Dynamical Stability of Nonlinear Waves.* Springer, 2013.

[45] J. Evans, "Nerve axon equations (iii): Stability of the nerve impulses," *Indiana University Mathematics Journal*, vol. 22, pp. 577–594, 1972.

[46] J. Alexander, R. A. Gardner, and C. K. R. T. Jones, "A topological invariant arising in the stability analysis of travelling waves," *Journal für die reine und angewandte Mathematik*, vol. 410, pp. 167–212, 1990.

[47] R. A. Gardner and C. K. R. T. Jones, "Traveling waves of a perturbed diffusion equation arising in a phase field model," *Indiana University Mathematics Journal*, vol. 39, pp. 1197–1222, 1990.

[48] R. Pego and M. Weinstein, "Eigenvalues, and instabilities of solitary waves," *Philosophical Transactions of the Royal Society of London A*, vol. 340, pp. 47–94, 1992.

[49] M. J. Ablowitz and A. S. Fokas, *Complex Variables: Introduction and Applications.* Cambridge University Press, 2003.

[50] K. Harley, P. Van Heijster, R. Marangell, G. J. Pettet, and M. Wechselberger, "Numerical computation of an evans function for travelling waves," *Mathematical Biosciences*, vol. 266, no. August 2015, pp. 36–51, 2015.

[51] B. Barker, R. Nguyen, B. Sandstede, N. Ventura, and C. Wahl, "Computing Evans functions numerically via boundary-value problems," *Physica D: Nonlinear Phenomena*, vol. 367, pp. 1–10, 2018.

[52] J. L. Marzuola and G. Simpson, "Spectral analysis for matrix hamiltonian operators," *Nonlinearity*, vol. 24, no. 2, pp. 389–429, 2010.

[53] D. Henry, *Geometric Theory of Semilinear Parabolic Equations.* Springer, 1981.

[54] B. Barker, J. Humpherys, and K. Zumbrun, "STABLAB (version 1.0)." http://impact.byu.edu/stablab/, 2009.